



Society for Pediatric Pathologists

Abstracts of the 2023 Fall Meeting

October 6-8, 2023

Hybrid Meeting

Platform I: Placental Pathology

1

Correlations between Serum Biomarkers of Maternal Inflammation During Pregnancy and Placental Pathology at Delivery

L Ernst ¹, A Freedman ¹, L Singh ¹, L Keenan-Devlin ¹, C Fisher ², A Borders ¹, G Miller ²; ¹ NorthShore University HealthSystem, ² Northwestern University

Background: Systemic inflammation during pregnancy, as measured by cytokines in the maternal serum, has been correlated with preeclampsia and preterm birth, as well as neurodevelopmental impairment in the offspring. However, little is known about the relation between maternal inflammatory cytokines and placental pathology. The purpose of our analysis was to investigate whether second trimester maternal serum inflammatory biomarkers are associated with inflammatory and/or vascular lesions in the placenta at delivery.

Methods: This is a secondary analysis of a prospectively enrolled pregnancy cohort. Study participants had blood drawn in the second trimester and 5 biomarkers of inflammation, CRP, IL-10, IL-1Ra, IL-6, and TNF α , were measured in serum using a multiplex immunoassay. Values were log-transformed and standardized before analysis. Placentas were collected after delivery and evaluated by a perinatal pathologist. Placental lesions were categorized into four types: acute inflammation, chronic inflammation, maternal vascular malperfusion, and fetal vascular malperfusion. Associations between placental pathology types and serum inflammatory biomarkers were estimated using logistic regression. Models were adjusted for gestational age at the blood draw, maternal age, race/ethnicity, body mass index, and infant sex.

Results: Of 605 study participants, 535 (88.4%) completed the blood draw (mean gestational age: 23.7 weeks; SD: 1.7) and had completed placental pathology. The most prevalent placental lesion category was acute inflammation (56.1%), followed by chronic inflammation (54.6%), fetal vascular malperfusion (33.6%), and maternal vascular malperfusion (29.4%). In the adjusted model, a one standard deviation increase in IL-10 was associated with increased odds of chronic inflammation in the placenta (OR: 1.26, 95% CI: 1.05, 1.51; Table 1). IL-10 was also associated with increased odds of maternal vascular malperfusion (OR: 1.30; 95% CI: 1.07, 1.58). TNF α was similarly associated with maternal vascular malperfusion (OR: 1.34; 95% CI: 1.09, 1.64). In an additional adjusted model that included both TNF α and IL-10, associations were consistent in magnitude, indicating these cytokines likely independently contribute to maternal vascular malperfusion. Second trimester serum inflammatory cytokines were not associated with acute inflammation or fetal vascular malperfusion in the delivered placenta.

Conclusion: Increased serum inflammatory biomarkers in the second trimester associate with the presence of chronic inflammation and maternal vascular malperfusion in the placenta at delivery. It is not clear from this study whether IL-10 and TNF α are early markers of these placental diseases or represent upregulated systemic maternal inflammation which

predisposes to these placental diseases. Additional research is needed to clarify the direction of the observed associations.

Platform I: Placental Pathology

2

Patterns of Gene Expression in Chorionic Villous Tissue Based on Placental Pathology

L Ernst ¹, A Freedman ¹, L Keenan-Devlin ¹, A Crockett ², A Borders ¹, G Miller ³, S Cole ⁴;

¹ NorthShore University HealthSystem, ² Prima Health Greenville South Carolina, ³ Northwestern University, ⁴ UCLA

Background: Placental gene expression may provide insight into placental function and identify mechanistic pathways that are correlated with placental pathology. The purpose of our analysis was to investigate gene expression of chorionic villous tissue impacted by the 4 major types of placental injury: acute inflammation (AI), chronic inflammation (CI), fetal vascular malperfusion (FVM), and maternal vascular malperfusion (MVM), as compared to histologically normal placentas.

Methods: We utilized placental tissue prospectively collected from a pregnancy cohort between August 2018 – March 2020. Chorionic villous biopsies were collected following immediately delivery for evaluation of gene expression and additional representative samples from the same placentas were submitted for histologic examination. RNA was extracted from the chorionic villous biopsies and mRNA expression of 15,033 transcripts was profiled. Hematoxylin and eosin-stained placental histology slides were reviewed by a perinatal pathologist. Placentas with ≥ 2 injury patterns were excluded to facilitate interpretation of results. Linear models were used to compare gene expression in each pathology group to the histologically normal placentas. Models were adjusted for gestational age at delivery, mode of delivery, and infant sex, as these may impact gene expression patterns. Differentially expressed genes (DEGs) were identified based on a fold-change of >2 or < 0.5 .

Results: 229/398 (58.9%) of the placentas had more than one type of pathology present and were excluded from the analysis. Amongst the remaining 169, only 5 placentas were identified with FVM, and due to the small sample were excluded from further analysis. Final analysis included 164 placentas: 60 with AI, 25 with CI, 39 with MVM, and 40 histologically normal controls. Based on the fold-change threshold, there were 116 up-regulated and 76 down-regulated genes for AI, 433 up and 95 down-regulated for CI, and 63 up and 564 down-regulated for MVM. 93.3% of the genes downregulated in MVM were unchanged in CI relative to controls and 95.4% of the genes upregulated in CI were unchanged in MVM relative to controls. (Figure 1).

Conclusion: Unique patterns of gene expression emerged for each type of placental injury. This confirms that the constellation of placental findings in MVM, CI and AI represent not only unique histologic patterns, but also have distinct molecular signatures. Further understanding of these molecular differences could assist in finding potential therapeutic targets for these different types of placental pathology.

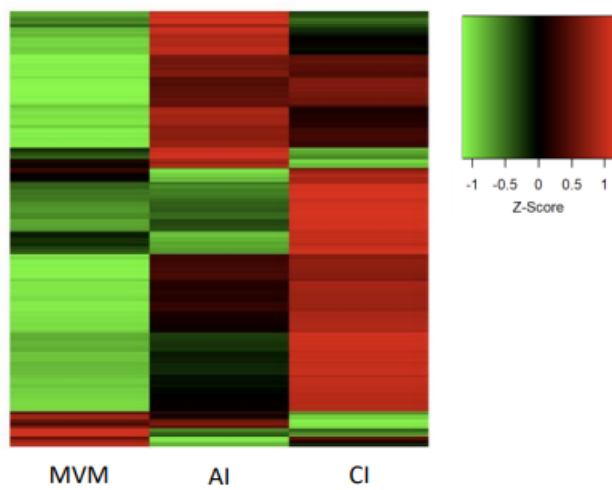


Figure 1. Differentially expressed genes (fold change >2 or <0.5) for maternal vascular malperfusion (MVM), acute inflammation (AI), and chronic inflammation (CI) as compared with healthy controls. Larger z-scores (red) indicate elevated expression relative to controls and smaller z-scores (green) indicate lower expression relative to controls.

A Reassessment of the Incidence of Chronic Inflammatory Lesions in Association with Chorionic Histiocytic Hyperplasia

P Katzman L Metlay; University of Rochester Medical Center

Background: Chorionic histiocytic hyperplasia (CHH) is a chronic inflammatory lesion in which a linear infiltrate of fetal histiocytes is present in the base of the fetal plate or membranous chorion. Our laboratory has been diagnosing this lesion in placentas since its initial description in 2017. CHH has a known association with other chronic inflammatory lesions, including chronic villitis (CV), chronic deciduitis (CD), and chronic chorioamnionitis (CC). We previously reported our experience with CHH between 1/2013 and 10/2015. We performed a retrospective study of placentas diagnosed since that last study period in order to analyze the strength of these associations in a larger cohort of patients.

Methods: Our LIS was queried to find third trimester placentas diagnosed from 11/1/2015 to 7/25/2023 with the CHH diagnosis. Additional queries were performed to identify the total number of third trimester placentas diagnosed and the number of cases with the diagnoses of CV, CD, CC, and eosinophilic/T-cell chorionic vasculitis (ETCV) in this timeframe. CV was further delineated as multifocal (MCV) or basal CV (BCV). Those diagnoses were assigned for this study as MCV with diagnoses of “chronic villitis, multifocal”, “chronic villitis, multifocal, with prominent basal component”, or “foci of chronic villitis”; and as BCV with diagnoses of “basal chronic villitis”, or “basal chronic villitis, multifocal”. Comparisons of incidence of lesions between the prior and current studies were evaluated using the chi square statistic in the online Social Science Statistics calculator with $p < 0.05$ as the threshold for significance.

Results: CHH was present in 2.2% of placentas over the study period, significantly higher than the 1.3% in the prior study period ($p < 0.001$) (Table 1). A majority of CHH cases had accompanying CV of either type (82.3%), which is significantly greater than in the original study (67.5%) ($p = 0.001$). CD was more often associated with CHH in the current study than in the prior study (49.1% vs. 40.0%) ($p < 0.001$). Although, CC was less often associated with CHH in the current study than in the prior study (23.9% vs. 31.2%), this difference was not significant ($p = 0.62$). Almost a third of cases of ETCV seen in this study period had associated CHH (Table 2). (Insert Image)

Conclusion: The greater incidence of CHH in third trimester placentas diagnosed in the past 7.5 years may be due to greater recognition of the lesion by our pathologists. The greater association between CHH and CV over the past 7.5 years and predominance of CHH in MCV cases versus BCV cases (57% vs. 25%) suggests that CHH may be part of the expression of severe fetal inflammatory response in the placenta. This study also showed for the first time an association between the presence of CHH and ETCV.

TABLE 1

	With CHH (%)	Without CHH (%)	Total Placentas	P-value
Placentas in first study	80 (1.3)	6259 (98.7)	6339	0.00001
Placentas in second study	385 (2.2)	16913 (97.8)	17298	

TABLE 2

Lesions other than CHH	Number of Other Lesions with CHH (N=385) (%)	Number of Other Lesions with CHH in Past Study (N=80)(%)	P-value comparing current and prior studies
All chronic villitis	317 (82.3)	54 (67.5)	0.001
Multifocal chronic villitis	220 (57.1)	NE	NE
Basal chronic villitis	97 (25.2)	NE	NE
Chronic deciduitis	189 (49.1)	32 (40.0)	0.00002
Chronic chorioamnionitis	92 (23.9)	25 (31.2)	0.62
Eosinophilic/T-cell chorionic vasculitis	15 (30.6)	NE	NE
NE = not evaluated			

Extravillous trophoblast (EVT) extracellular vesicles (EVs) express PDL-1: Role in T-cell polarization

T Morgan ¹, M Morita ²; ¹ OHSU Center for Developmental Health, ² Oregon Health & Science University

Background: Similar to an invasive cancer, placental extravillous trophoblasts (EVTs) invade the maternal uterus encountering maternal T-cells within the uteroplacental microenvironment. EVTs do not express HLA class 1 -A or -B. Instead, they express HLA-C, which is recognized by maternal uterine natural killer cells, but it does not stimulate an active T-cell response. Interestingly, like an invasive cancer, the uteroplacental microenvironment undergoes T-cell polarization in the first trimester switching from active Th1 cells to immunosuppressive T-regulatory and Th2 phenotypes. The mechanism is uncertain, but likely involves paracrine signals from placental EVTs. We hypothesize that EVTs signal their microenvironment in part by employing extracellular vesicles with HLA-C and PDL-1 on their surface.

Methods: Banked human platelet poor plasma from women at 11-13 weeks gestation was stained for placental alkaline phosphatase (PLAP), HLA-C, CD63, and PDL-1. Immunostained samples were diluted on 200nm-bead spiked 0.1um filtered PBS buffer (1:300) and tested by nanoscale flow cytometry per ISEV guidelines using appropriate sizing and MESF beads for standardization. All experiments were performed on a BD Biosciences FACSAria Fusion normalizing testing volumes by 200nm bead counts yielding EV counts/ul of starting plasma. PLAP+/HLA-C+/CD63+ EVs were evaluated for co-expression of PDL-1. NanoFACS isolated EVT EVs +/- PDL-1 were then incubated with flow sorted T-helper cells for 3 days to test for T-cell polarization. TGF and IL-2 served as positive control reagents while sorted 200nm beads from the plasma and PBS served as negative controls.

Results: First trimester EVT extracellular vesicles co-express PDL-1, similar to many types of invasive cancers. The presence of PDL-1 appears to cause T-cell polarization towards T-regulatory cells by 3 days post exposure.

Conclusion: This exploratory study suggests that invasive placental EVTs may impact the uteroplacental immune microenvironment via extracellular vesicle paracrine effects. The mechanism likely involves PDL-1 surface expression, but a complete analysis of first trimester placental EVT EV cargo remains to be done.

Ascending Pattern of Herpes Simplex Virus Placentitis

J Slack P Charles, L Rabinowitz, A McKenney; Cleveland Clinic

Background: Neonatal herpes simplex virus (HSV) infection is associated with pre-term birth, severe morbidity, and a high rate of mortality. Most (~85 to 90%) transmission occurs during delivery. Rarely, there is postnatal or antenatal intrauterine transmission (~5%, each). Antenatal transmission can be diagnosed on placental exam. The canonical constellation of findings in HSV placentitis includes villous necrosis, fibrosis, mineralization, and chronic villitis with plasma cells. However, these findings, which are consistent with hematogenous transmission, are not frequently seen in the more common cases of ascending infection. Herein, we present a series of four cases with an ascending pattern of HSV placentitis to better describe its associated clinical context, histologic findings, and patient outcomes.

Methods: A search of the laboratory information system was performed to identify recently diagnosed cases of HSV placentitis. Reports, H&E and HSV immunohistochemical paraffin embedded stained slides were reviewed.

Results: The placenta for Case 1 was received following intrauterine fetal demise at 25 gestational weeks, Case 2 following c-section indicated by maternal hypertension at 40+2 gestational weeks, Case 3 following livebirth after preterm premature membrane rupture at 25+1 gestational weeks, and Case 4 with livebirth at 37+1 gestational weeks with clinical concern for abruption. No concern for HSV infection was noted at delivery according to the records. In all cases, placental examination demonstrated spotty amniocyte necrosis, necrotizing funisitis without marked vasculitis, individual eosinophilic stromal cells in the subamniotic stroma of cord and chorionic plate with variably intense subacute inflammation, and rare plasma cells in the cord vessels or stroma. Cowdry inclusions were inconspicuous, but identifiable in 3 cases. Patients 2,3 and 4 were subsequently PCR positive for skin or lesional swabs after results of placental exam were communicated to the pediatrician. Each child received antiviral therapy. Pt 2 remains asymptomatic at 4 years of age, Pt 3 is now 4 years old with chronic kidney disease secondary to unilateral renal vein thrombosis, and Pt 4 developed intracranial hemorrhage with venous infarcts several days after delivery and remains admitted to the NICU at 3 weeks post-delivery.

Conclusion: We report 4 cases of neonatal HSV infections acquired in utero – all of which demonstrated an ascending pattern of infection and no significant villitis. Key findings of this pattern include a peripheral pattern of amniocyte and subamniotic stromal cell necrosis of the cord, extraplacental membranes, and or chorionic plate; mild subacute inflammation (often with plasma cells); and inconspicuous viral inclusions. HSV placentitis was confirmed with strong immunohistochemical staining, most commonly in necrotic stromal cells, in all cases and positive PCR of subsequent patient samples. It is important to recognize the placental findings of ascending HSV infection, as it may be clinically inapparent at birth, and earlier

diagnosis allows earlier treatment which can significantly affect patient outcomes.

Addition of Patient Centered Comments in Placental Pathology Reports Increases Provider Understanding and Comfort

L Ernst A Freedman, S Suresh; NorthShore University HealthSystem

Background: Obstetric providers may not fully understand or feel comfortable with placental pathology report terminology. This problem is further magnified with the advent of the Cures Act which requires all pathology reports be immediately and directly released to the patients, and challenges obstetric providers to explain placental pathology reports to patients. The aim of this study was to determine if additional patient-centered comments appended to the pathology report increase provider comfort and understanding of the report.

Methods: We drafted a priori patient-centered comments explaining the major pathologic findings in the placenta which were then reviewed and refined by health literacy colleagues to reach final versions. Then, to test the acceptability and value of the comments, we designed an anonymous and randomized provider survey aimed to assess understanding of the terminology in the pathology report and comfort with explaining the report to their patients. Survey respondents were randomized to receive 2 hypothetical placental pathology reports, one with and one without patient-centered comments, one primarily with acute inflammation and the other with maternal vascular malperfusion. Respondents were asked to rate their understanding of the report on a scale of 1-5 (1- no understanding, 2- little understanding, 3- some understanding, 4- understanding most of the report, 5 – complete understanding) and comfort level explaining it to their patients (1- Not at all comfortable and would avoid it, 2- I could do it, but only if the patient asked, 3- somewhat comfortable, 4- comfortable, 5 - very comfortable) along with a few other general questions about their practice. Within provider differences in understanding and comfort by report type and pathology type were assessed using repeated measures ANOVA.

Results: A total of 31 providers responded to the survey. A majority of respondents (90.3%) replied that they always or almost always read the placental pathology report and a majority (51.6%) also replied that patients almost never asked them about the results. Providers reported greater complete understanding of the report when reading the report with patient-centered comments as compared to the report without the comments (mean comfort 3.5 for patient centered vs 2.97 original report $p < 0.001$) as well as greater comfort with the report (mean comfort 3.29 for patient centered vs 2.81 for original report, $p = 0.002$). There was no difference in provider understanding or comfort by the pathology findings represented (acute inflammation and maternal vascular malperfusion) ($p = 0.66$).

Conclusion: Our survey results indicate that the inclusion of patient centered comments in addition to the medical language of the placental pathology report can improve provider understanding of the placental findings and therefore improve their comfort when discussing the findings with a patient and considering future treatment options.

Platform II: Autopsy and Pediatric Pathology I

1

The Role of Immunohistochemical Stains in Perinatal Brain Autopsies

A Viaene; Children's Hospital of Philadelphia

Background: The perinatal period is characterized by unique patterns of brain injury not observed outside specific timepoints in development. Identification of injuries is a critical part of perinatal brain autopsies; however, they are not always easily identifiable due to factors such as autolysis and immaturity of the developing nervous system.

Methods: The role of immunohistochemical stains in identification of perinatal brain injury was investigated. Blinded semiquantitative scoring of injury within cortex and white matter was performed on sections of frontal lobe from 75 cases (51 liveborn and 24 stillborn) using the following stains: H&E, GFAP (astrocytic marker), Iba-1 (microglial marker), and bAPP (marker of axonal injury). Digital image analysis was also used to quantify GFAP and Iba-1 stains.

Results: Subject ages ranged from 23-41 weeks gestation (stillborn) and from 22 weeks gestation-36 weeks postnatal (liveborn). Commonly observed pathologies included diffuse white matter gliosis (DWMG), white matter necrosis (WMN), and acute neuronal necrosis. DWMG scores were similar on H&E and GFAP stains for liveborn subjects ($p=.45$). For stillborn subjects, DWMG scores were significantly higher on GFAP stain than H&E ($p<.001$). GFAP DWMG scores were higher in stillborn than liveborn subjects ($p<.01$), and more GFAP staining was present within the white matter on digital image analysis for stillborn than liveborn subjects ($p<.01$). bAPP identified WMN not seen on H&E in 22% of stillborn and 4% of liveborn subjects ($p<.05$). However, frequencies of WMN were similar in liveborn (25.5%) and stillborn subjects (29.2%) ($p=.74$). Diffuse staining for Iba-1 within cortex ($p<.001$) and the white matter ($p<.05$) was positively correlated with age, while GFAP staining was not ($p=.16$). Not surprisingly, more Iba-1 staining was seen in the cortex ($p<.001$) and white matter ($p<.05$) of liveborn than stillborn subjects. Iba-1 staining was occasionally helpful in identifying focal injury not apparent on H&E. Finally, digital image analysis was found to be highly correlated to semiquantitative scoring for GFAP staining within the white matter ($p<.001$) and Iba-1 staining, in both cortex ($p<.001$) and white matter ($p<.001$).

Conclusion: These findings show GFAP and bAPP stains to be most helpful in identifying white matter injury in stillborn subjects. This may be due to high rates of autolysis in stillborn brains, hampering H&E evaluation. Iba-1 staining increases with age but is sometimes useful in highlighting focal lesions. Semiquantitative scoring of immunostains was highly correlated to quantitative image analysis, indicating the reliability of stain interpretation by pathologists. Immunostains may therefore be warranted as a routine part of stillborn brain autopsies.

Defining the Clinical Spectrum of TEK Variants in a Large Cohort of Patients with Venous Malformations

N Nelson ¹, M Gillentine ², S Bhatia ², C Myers ², L Rogge ², L Emery ², J Narayanan ², Z Nelson ², D Jensen ², J Perkins ², C Paschal ², A Wandler ², J Bennett ², N Nelson ²; ¹ Seattle Children's Hospital, ² Seattle Children's Hospital

Background: Venous malformations (VM) most commonly result from somatic or autosomal dominant variants in TEK which encodes the angiopoietin receptor TIE2. Most recurrent somatic variants in TEK are found in the tyrosine kinase domain and cause ligand-independent hyperphosphorylation and result in gain-of-function. We report our experience with TEK variants drawing upon our cohort of 747 individuals with suspected somatic mosaic disorders.

Methods: Extracted DNA was sequenced using a targeted capture panel followed by next-generation sequencing, alignment, and detection of variants using the DRAGEN Somatic bioinformatics pipeline. Samples were sequenced with high depth (~1000x) to identify somatic variants at very low variant allele fractions (limit of detection $\geq 1\%$). Only patients with pathogenic TEK variants were included in this analysis. Available H&E-stained slides from lesions with TEK variants were reviewed to confirm the diagnosis of VM.

Results: We sequenced samples from 747 individuals with suspected somatic mosaic disorders, including predominantly patients with vascular anomalies/overgrowth, and identified pathogenic TEK variants in 65 patients. This includes 19 patients with double TEK variants, two patients with likely germline variants, and one patient with somatic mosaic variants in PIK3CA and TEK. Two patients had somatic TEK variants identified in the blood, the remainder were identified in tissue samples. Variant allele fractions in patients with somatic variants ranged from 1 to 18%. The most common site for TEK mutated lesions was the extremities (n=32), followed by head and neck (n=22). A total of 19 unique variants were identified as detailed in the figure. The most commonly reported TEK variant in VMs, p.Leu914Phe, was found in 32 patients (49%). Thirteen patients (20%) had predicted truncating variants involving the final two exons of TEK, including novel p.T1105Mfs*6 and p.Y1113_A1123del variants. Double TEK variants were enriched in patients with multifocal lesions, as has been previously reported. In 9 patients with double variants the phase of the variants could be determined; 8 were in cis while 1 was in trans. One patient had two biopsy specimens tested which showed the same first hit in TEK but distinct second hits. H&E slides from 30 patients, including the patient with pathogenic somatic PIK3CA and TEK variants, were available for review and all lesions were histologically consistent with VMs.

Conclusion: We describe novel variants in TEK and novel observations including the presence of distinct second hits in TEK within a single patient and the presence of two TEK variants in trans. This is the largest reported cohort of TEK mutated VMs and provides

insight into the genetic spectrum of these lesions within a relatively large population.

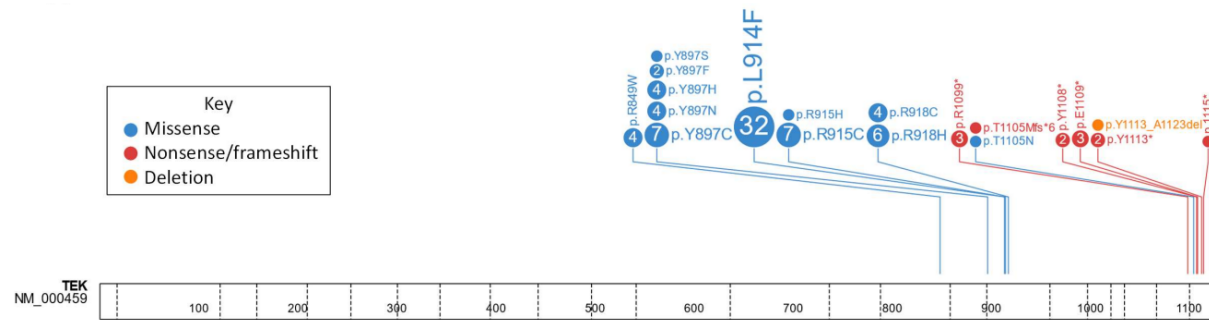


Figure 1. Schematic representation of the pathogenic variants in *TEK* that were identified in this cohort. The number indicates the number of times each variant was observed.

Histologic Activity and Histology-Driven Therapeutic Decisions in Adolescents with Lupus Nephritis: One Academic Center's Experience

K VandenHeuvel ¹, F Flores ²; ¹ Cincinnati Children's Hospital Medical Center, ² Cincinnati Children's Hospital

Background: Lupus nephritis is a significant risk for morbidity and even mortality in patients with systemic lupus erythematosus (SLE), and factors that can improve prognostic accuracy and guide therapeutic decisions are eagerly sought. In the past decade, several studies at adult centers have challenged the use of clinical metrics to determine effectiveness of induction therapy and have shown that there is significant discrepancy between disease activity at the end of induction as determined by clinical parameters and histologic activity on repeat biopsy. As a result, since 2018, we have performed routine repeat biopsies after induction treatment and used histologic activity to guide the timing of transition to maintenance therapy.

Methods: A cohort of patients with SLE was identified who were biopsied from 2018-2023 for new diagnosis of lupus nephritis or suspected flare, and the subset identified who were biopsied after induction by protocol. Biopsy findings, including histologic activity and chronicity indices and ISN/RPS classification were confirmed and information about demographics and outcome were drawn from the medical record. The cohort with protocol repeat biopsies were compared to those with clinically based treatment decisions for flare rate and other long-term outcomes.

Results: 26 patients underwent biopsy from 2018-2023, with an average age at SLE diagnosis of 15.12 +/- 3.46 years (range 8-21 years). 21 patients (80.8%) were female and 12 were African-American (46.1%), 3 Hispanic, 1 Asian, and 1 of mixed background. Of these, 15 patients were biopsied more than one time, and 12 of the 15 underwent protocol rebiopsy after induction therapy with cyclophosphamide or mycophenolate. The initial biopsy for new diagnosis or flare demonstrated proliferative (ISN/RPS class III and IV) or proliferative and membranous (III + V) in 19 patients (73.1%) with an average initial modified NIH activity index of 8.85/24. The repeat biopsy showed activity index > 0 in only 6 of 12, with an average activity index of 1.33/24 in those with activity. New flares took place in 5 patients, 3 in the group which were not rebiopsied after induction and 2 in the rebiopsy group. Of these latter two, one occurred after post-induction activity remained (index = 1/24) and one with no post-induction activity (0/24).

Conclusion: In our institution, induction therapy for lupus nephritis demonstrates significant power to reduce the histologic activity from initial biopsy, though at least minimal (index>0) activity remains in approximately half the biopsies. The flare rate in our 5 year experience has not been sufficient to detect a true difference in flare rate based on residual histologic activity. Further detailed analysis of changes in clinical parameters and laboratory values for nuances

in disease response are being undertaken.

Hepatic Granulomas in North American Children: A Multi-Institutional Analysis of 62 Cases

M Mejia Bautista ¹, A Thaker ², J Liang ³, S Tan ⁴, J Bush ⁵, D El Demellawy ⁶, J Putra ⁷; ¹ Boston Children's Hospital, ² Children's Healthcare of Atlanta, ³ Vanderbilt University Medical Center, ⁴ Stanford University School of Medicine, ⁵ British Columbia Children's Hospital, Vancouver, BC, Canada, ⁶ Children's Hospital of Eastern Ontario, Ottawa, ON, ⁷ Boston Children's Hospital, Boston, MA

Background: Hepatic granulomas, reported in 2-15% of routine biopsies, are associated with a wide range of underlying conditions. In Western adults, common etiologies include sarcoidosis and primary biliary cholangitis. Publications focusing on the pediatric population are limited to case reports and single-institution series. We aimed to perform a contemporary clinicopathologic analysis of pediatric hepatic granulomas in North America.

Methods: A retrospective analysis of pediatric liver cases showing granulomatous process as the primary finding was performed at 6 large academic centers across the U.S. and Canada (2000-2022). Cases with nonspecific microgranulomas and lipogranulomas in the setting of fatty liver disease were excluded. Demographic and clinical information was documented. Histologic data was confirmed by a primary pathologist (JP) using digital slides/photomicrographs of representative sections for each case.

Results: Sixty-two cases (53.3% male; age: 2 months-19 years) consisted of 54 native and 8 allograft liver specimens were included in the study. Two of the native liver specimens were autopsy cases. An underlying cause for hepatic granulomas was noted in 38 cases (61.3%). Infectious etiologies were identified in 17 cases (27.4%), which were mostly fungal organisms (N=9), followed by viruses (N=5), bacteria (N=2), and mycobacterium (1). These cases were seen in association with various risk factors, including hematologic malignancy (N=5), chronic granulomatous disease (N=3), liver transplantation (N=2), Wilms tumor (N=1), and Crohn disease (N=1). In the remaining cases (N=21), non-infectious causes included primary immunodeficiency disorder (PID; N=9), Crohn disease (N=7), and sarcoidosis (N=5). The PIDs in our cohort (N=12) consisted of chronic granulomatous disease (N=5), common variable immunodeficiency (N=2), Kostmann syndrome (N=1), Blau syndrome (N=1), and non-specific PIDs (N=3). Although more frequently seen in infectious cases, necrotizing granulomas were also noted in a subset of PIDs (22.2%) and Crohn cases (14.3%). The location of granulomas (portal, lobular, or both) was not helpful in suggesting etiology. Most cases showed no or mild portal fibrosis; only 1 PID and 1 sarcoidosis case demonstrated bridging fibrosis. The clinical and histologic data of 38 cases with known etiologies are summarized in Table 1. In a significant number of cases (N=24; 38.7%), the cause of hepatic granulomas was unclear despite systematic diagnostic evaluation (including cases with putative causes such as autoimmune hepatitis, sickle cell disease, and medications).

Conclusion: More than half of the children in our cohort (61.3%) have known causes of hepatic granulomas. Infection, in association with either primary or acquired immunodeficiency, remains a frequent cause of hepatic granulomas in North American children. We also identify PIDs as a significant risk factor for hepatic granulomatous disease in children, seen in approximately one-fifth (19.4%) of our patients. Despite the chronic nature of these underlying disorders, advanced fibrosis is extremely uncommon in pediatric hepatic granulomas.

Table 1. Subset of study cases with known cause of hepatic granulomas (N=38 of 62)						
Underlying disease			Infectious (N=17)	Non-infectious (N=21)		
				Primary immunodeficiency (N=9)	Crohn (N=7)	Sarcoidosis (N=5)
Sex	F	%	58.8	44.4	28.6	20
	M	%	41.2	55.6	71.4	80
Age range (years)			0-18	3-17	9-19	4-15
Most common clinical presentations (%)			Transaminitis (29.4); fever (29.4)	Transaminitis (33.3)	Transaminitis (71.4)	Transaminitis (30)
Granuloma type	Necrotizing	%	17.6	0	0	0
	Non-necrotizing	%	53	77.8	85.7	100
	Both	%	29.4	22.2	14.3	0
Granuloma location	Portal	%	17.6	11.1	14.3	20
	Lobular	%	41.2	55.6	28.6	20
	Both	%	41.2	33.3	57.1	60
Portal Inflammation (%)			80 (mild to severe)	85.7 (mild to moderate)	85.7 (mild to severe)	100 (mild)
Lobular activity (%)			80 (mild to severe)	85.7 (mild to moderate)	85.7 (mild to severe)	80 (mild)
Portal fibrosis	None	%	73.3	42.9	57.1	20
	Mild (METAVIR F1-F2)	%	26.7	42.9	42.9	60
	Advanced (METAVIR F3-F4)	%	0	14.2	0	20
Extrahepatic granulomas			17.7	66.7	71.4	0

Atypical Cellular Neurothekeoma in Children: Two Case Reports with Pan-Cancer Targeted Next-Generation Sequencing and Chromosomal Microarray Analysis

M Harrell¹, B Yang², M Bitar², P Zamiara², M Warren², N Shillingford², S Zhou², G Raca², R Schmidt², B Pawel², L Wang²; ¹ Children's Hospital Los Angeles, ² Children's Hospital Los Angeles

Background: Cellular neurothekeoma is a benign skin lesion of uncertain cellular origin. Atypical cellular neurothekeoma (ACN) is a rare variant characterized by large size (up to 6 cm), deep penetration into skeletal muscle and/or subcutaneous fat, diffusely infiltrative borders, vascular invasion, high mitotic rate, and marked cytologic pleomorphism. There is a paucity of data on the molecular changes underlying these exceedingly rare tumors. We report herein two cases of pediatric ACN with extensive molecular genetic investigation.

Methods: We collected two cases of ACN in children, and performed pan-cancer targeted next-generation sequencing (NGS) OncoKids® panel and chromosomal microarray (CMA), to further analyze the clinicopathological features and molecular genetic aberrations.

Results: Case 1. A 6-year-old girl with a left scalp ACN (4.7 cm), which demonstrated marked cytologic pleomorphism, increased mitotic activity (3 mitoses/10HPF), a sclerotic background with thickened collagen bundles, and deep penetration extending into skeletal muscle. Tumor cells were positive for NKI-C3 (diffuse) and CD10 (diffuse), and negative for S100 by immunohistochemistry (IHC). CMA analysis demonstrated a complex pattern of copy number changes, including homozygous loss of CDKN2A/B, and genomic instability in chromosome 1p and 9. Case 2. A 3-year-old girl with a right hand dorsal ACN (1.5 cm), which was characterized by deep and multiple tongue-like extensions, large bizarre pleomorphic cells, frequent mitotic figures (13 mitoses/10HPF) including occasional atypical mitoses. Tumor cells were positive for NKI-C3 (diffuse) and Ki-67 (25%+), and negative for S100. OncoKids® panel revealed a CDH13::STX8 fusion, while CMA analysis demonstrated clonal alterations including homozygous loss of CDKN2A/B, and loss of TP53, NF1 and NF2. Clinical follow-up showed that case 1 had tumor recurrence in the same site 87 months after surgery, and case 2 had no evidence of disease at 9 months.

Conclusion: We have reported two cases of ACN with recurrent homozygous loss of CDKN2A/B and other molecular abnormalities. One case had tumor recurrence. These findings suggest that ACN is a tumor with potentially locally aggressive behavior, and complete surgical excision and long-term postoperative follow-up is essential for ACN. - Dr. Yang B and Dr. Harrell M are co-first authors.

Platform III: Pediatric Pathology II

1

Differential DNA Methylation Profiles in Hepatoblastoma, Hepatocellular Neoplasm, not otherwise specified, and Pediatric Hepatocellular Carcinoma

Z Sandoval ¹, M Li ², S Zhou ³; ¹ Baylor College of Medicine, Children's Hospital Los Angeles, ² University of Southern California, ³ Children's Hospital Los Angeles

Background: Pediatric liver cancers are rare, with hepatoblastoma (HB) being the most common type (about 80%), followed by hepatocellular carcinoma (HCC) and rarely hepatocellular neoplasm, not otherwise specified (HCN-NOS). Distinguishing HCN-NOS from HB or HCC is often challenging due to their overlapping clinical and histopathological features. Epigenetic mechanisms, such as DNA methylation, play a crucial role in the oncogenesis of various cancer types. Previous studies have highlighted the diagnostic and prognostic potential of DNA methylation patterns in common cancers. However, comprehensive studies investigating DNA methylation patterns in pre-treated pediatric liver cancers are currently lacking.

Methods: DNA methylation (EPIC850K array) was conducted on 49 frozen samples, including 42 pre-treated tumor samples from three pediatric liver cancer groups (HB, n=27; HCN-NOS, n=11; and HCC, n=4), as well as 7 normal control samples. The data were analyzed using Partek Genomics Suite software.

Results: The HCN-NOS group exhibited the highest number of differentially methylated (DM) CpG sites (CpGs), approximately 2.1 times that of the HB group and 18.4 times that of the HCC group. Interestingly, both the HCN-NOS and HB groups demonstrated a global hypomethylation pattern, while the HCC group showed a global hypermethylation pattern. Venn diagram analysis revealed a larger overlap in DM CpGs between HB and HCN-NOS compared to HB and HCC or HCN-NOS and HCC. Gene ontology (GO) enrichment analysis on the genes associated with DM CpGs revealed that "developmental process" was a top biological process in all three tumor groups, suggesting developmental processes play a significant role in the pathogenesis of pediatric liver cancers. However, each group had specifically enriched molecular functions and pathways, indicating distinct molecular mechanisms involved in the tumorigenesis of each tumor group. Additionally, HCC exhibited the highest percentage of DM CpGs located within islands (30.2%) compared to HB (12.6%) and HCN (14.4%), with the majority being hypermethylated in all three tumor types (HCC (97.1%), HCN (93.6%), and HB (67.1%)). Furthermore, significant differences were observed in the distribution of DM CpGs across regulatory-region categories among the three tumor groups. Specifically, promoter-located CpGs were predominantly hypermethylated in both HCN-NOS and HCC, but hypomethylated in HB. Nevertheless, enhancer-located CpGs were preferentially hypomethylated in all three tumor groups. Moreover, the study identified 3376 robust DM CpGs that displayed distinct methylation patterns and functional signatures across the three tumor groups.

Conclusion: Distinct methylation patterns were observed among the three tumor types, with

HCN-NOS displaying a closer methylation similarity to HB rather than HCC. The identification of differential DNA methylation patterns and associated functional signatures provides valuable insights for future research aimed at improving diagnosis, prognosis, and treatment strategies for pediatric liver cancers.

Genomic characterization identifies recurrent FGFR2 and PIK3CA abnormalities in sialoblastoma

S Koo ¹, F Malik ²; ¹ St. Jude Children's Research Hospital, ² St. Jude Children's Research Hospital

Background: Sialoblastoma is a rare malignant salivary gland neoplasm that histologically resembles salivary gland anlage structures and presents at birth or in early infancy as painless swelling. Classic histologic features and typical immunoprofile generally permit an accurate diagnosis, with histologic grading dependent on necrosis, mitosis, and Ki-67 proliferation index. The molecular landscape of these tumors is not fully understood.

Methods: Cases diagnosed as sialoblastoma were retrieved from the electronic medical record. Histologic slides were reviewed by 2 pathologists and all pertinent clinical, imaging, and follow-up features were collected. Targeted next-generation sequencing (NGS) was performed on all tumors: 2 tumors with sequencing of FGFR1, FGFR2, FGFR3, and FGFR4, and 1 tumor with sequencing by a large gene panel.

Results: Four specimens from three patients were retrieved (see Table). All tumors presented at birth as a facial lump and were excised. Patient 3 also had a concomitant hepatoblastoma (epithelial type, fetal pattern, PRETEXT III) diagnosed at the same time as the sialoblastoma. Histologically, all salivary gland tumors showed classical histology with solid organoid nests of primitive basaloid epithelial cells, separated by dense fibrous stroma supported by thin-walled branching blood vessels. The tumor cells contained scant cytoplasm with mild nuclear irregularity and few prominent nucleoli. One tumor (Patient 1) showed high-grade features including necrosis and increased Ki-67 proliferation index (~60%); this patient also had multiple local recurrences of her tumor. By immunohistochemistry, the glandular neoplastic cells were positive for cytokeratins, epithelial membrane antigen, and S100 in all cases; smooth muscle actin was negative in all three tumors. Beta-catenin did not show nuclear localization (1 case). In two tumors (Patients 1 and 2), sequencing identified a hotspot mutation in FGFR2 (p.C382R). In addition to the FGFR2 mutation, the tumor from Patient 1 also had a PIK3CA mutation (p.R88Q). The tumor from Patient 3 did not contain mutations in FGFR1, FGFR2, FGFR3, or FGFR4 by targeted NGS; PIK3CA sequencing was not performed.

Conclusion: In our small cohort, we identify hotspot mutations in FGFR2 and PIK3CA in sialoblastoma. These alterations may play a role in the pathogenesis and phenotype of this tumor. Although limited to a single case, the presence of both FGFR2 and PIK3CA mutations in the high-grade case suggests that dual mutations may confer increased proliferative activity and possibly portend worse prognosis in sialoblastomas. Emerging PI3K pathway inhibitors may play a role in disease management. Genetic factors contributing to the development of concurrent sialoblastoma and hepatoblastoma remain unknown.

Table 1. Clinical, histologic, and molecular characteristics of sialoblastoma

Patient	Location	Sex	Age at initial diagnosis	Additional clinical history	Size (cm)	Key histologic features	Molecular testing	Alterations
1	Lip commissure	Female	2 months (detected congenitally)	Multiple local recurrences	1.5	<ul style="list-style-type: none"> • Tumor necrosis present • 16 mitoses per 10 HPF • LVI present • No capsular invasion • Ki67 60% 	Targeted sequencing (302 genes)	<i>FGFR2</i> p.C382R (VAF 97%) <i>PIK3CA</i> p.R88Q (VAF 36%)
							Transcriptome sequencing	No recurrent fusions
2	Parotid gland	Female	6 months	Unknown	Unknown	<ul style="list-style-type: none"> • No tumor necrosis • 8 mitoses per 10 HPF • No LVI • No capsular invasion • Ki-67 40% 	Targeted sequencing (<i>FGFR1</i> , <i>FGFR2</i> , <i>FGFR3</i> , <i>FGFR4</i>)	<i>FGFR2</i> p.C382R (VAF 64%)
3	Submandibular gland	Male	2 months (detected congenitally)	Concurrent hepatoblastoma (fetal type)	4.0	<ul style="list-style-type: none"> • No tumor necrosis • 8 mitoses per 10 HPF • No LVI • No capsular invasion • Ki-67 20% 	Targeted sequencing (<i>FGFR1</i> , <i>FGFR2</i> , <i>FGFR3</i> , <i>FGFR4</i>)	None detected

HPF: high-power fields; LVI: lymphovascular invasion; VAF: variant allele frequency

Platform III: Pediatric Pathology II

3

A Comprehensive Multi-omic Diagnostic Approach of Pediatric Choroid Plexus Tumors

J Suddock¹, A Markowitz², E Castaneda², J Ji², A Margol², B Tamrazi², S Bluml², J Cotter²; ¹ University of Southern California/Los Angeles General Medical Center, Los Angeles, CA, ² Children's Hospital Los Angeles, Los Angeles, CA

Background: Choroid plexus tumors (CPTs) consist of a diverse group of neoplasms, more prevalent in children. They include choroid plexus papillomas (CPPs), atypical choroid plexus papillomas (aCPPs), and choroid plexus carcinomas (CPCs). Traditional grading of CPTs relies on histologic assessment, but evidence suggests incorporation of clinical, radiologic, and molecular characteristics may increase diagnostic accuracy. Here, we investigate the multi-omic associations of CPT subtypes using statistical and machine-learning approaches to develop a computational classification system to aid in the diagnosis of these subtypes.

Methods: The patient cohort consists of 110 CPT samples from a combination of publicly available and in-house sources. Our IRB-approved retrospective study assessed magnetic resonance spectroscopy (MRS) data, whole slide images (i.e., H&E, Ki-67), and DNA methylation profiles to characterize the metabolic, histologic, and molecular heterogeneity of CPTs. We used advanced statistical, machine- and deep-learning tools to test for clinically significant associations and establish detailed multi-omic profiles of CPT subtypes, as well as a machine-learning classifier to predict multi-omic based CPT subtypes.

Results: Using a semi-supervised learning approach, we performed unsupervised clustering of methylation profiles to reveal three distinct subgroups, in line with current literature and understanding of CPT subtypes. Next, a random forest model was developed to classify samples into methylation-based CPT subtypes (OOB error rate = 4.4%, 3-fold cross validation). CPT subtype features showed strong associations with their histologic and metabolic features including Ki-67 labeling index (Spearman's $\rho = 0.60$, $p = 2.3 \times 10^{-2}$) and MRS-based myo-inositol levels (Spearman's $\rho = -0.79$, $p = 3.0 \times 10^{-4}$). Further investigation will include computer vision modeling of whole slide images to associate clinically significant histologic features with their molecular subtype and grade.

Conclusion: Multi-omic analysis reliably separates CPTs by subgroup and grade. This study underscores the significance of integrating multi-omic datasets in refining the diagnosis and prognosis of CPTs. The discovered correlation between Ki-67 values and specific MRS-identified biological factors suggests that MRS is a promising technique to predict CPT grade pre-operatively. Identification of differential metabolic signatures between CPT subgroups can also enable the development of targeted therapeutic strategies. Continued research will focus on a multi-modal approach to improve prediction of aggressive behavior and understanding of inherent metabolic heterogeneity of CPT subtypes.

Malignant High-Grade INI1-Deficient Hematolymphoid Neoplasm: A Series of Three Cases

J Havens ¹, B Hill ², G Li ², V Reddy ¹, J Wicker ²; ¹ The University of Alabama at Birmingham, ² Children's of Alabama

Background: The SMARCB1 gene encodes the protein INI1 that has important functions in transcriptional regulation and tumor suppression. Biallelic SMARCB1 inactivation has been identified in multiple solid tumor types, including malignant rhabdoid tumor, epithelioid sarcoma, and medullary renal carcinoma. Review of the literature revealed only one previously published case of hematopoietic malignancy with biallelic loss of SMARCB1 resulting in loss of nuclear INI1 expression. Biopsy of a mediastinal mass from a fourteen-year-old male with autism spectrum disorder showed an atypical mononuclear cellular infiltrate with expression of CD45, CD2, CD7, CD79a, MPO (dim), and CD13. A diagnosis of malignant hematopoietic neoplasm with myeloid, B-cell, and T/NK-cell differentiation was rendered. We report a series of three malignant high-grade INI1-deficient hematolymphoid neoplasms with T-cell differentiation.

Methods: The clinical history, histology, immunophenotype, and literature are reviewed.

Results: The first patient was a six-year-old male previously diagnosed with distal chromosome 22q11.2 microdeletion syndrome who presented with back pain and multiple bone lesions. Biopsy showed atypical lesional cells that were immunoreactive for CD2, CD3, CD5, CD43, CD45, and focal weak CD4 expression that were negative for nuclear INI1 staining. The second patient was an eleven-year-old female who presented for treatment of a mediastinal mass from an outside institution. Further characterization of diagnostic tissue in addition to a subsequent relapse specimen showed the lesional cells were negative for significant CD2 and CD3 staining but showed diffuse immunoreactivity for CD45, CD4, and CD7 expression with absent nuclear INI1 staining and focal CD30 staining. The third patient was a nine-year-old male who presented with mediastinal mass, dyspnea, and pleural effusion. Cytospin and cell block preparations of the effusion showed pleomorphic neoplastic cells that were diffusely and strongly immunoreactive for CD45, CD43, and CD5 expression with absent nuclear INI1 staining and patchy CD4 and CD30 immunoreactivity. Genomic profiling performed on this specimen showed loss of SMARCB1.

Conclusion: Three cases of INI1-deficient hematolymphoid neoplasms were identified at our institution over a twelve-month period that are characterized by marked cytologic pleomorphism with diffuse CD45 expression and at least some T-cell marker positivity. Significant evidence of myeloid or B-cell differentiation was absent in our cases. Loss of nuclear INI1 expression was consistently seen and can be regarded as a defining oncogenic driver of this entity. INI1-deficient hematolymphoid neoplasms may represent an emerging underrecognized entity and expand the spectrum of SMARCB1/INI1 deficient tumors.

Development of Rhabdoid Tumor Patient-Derived Xenografts Using the Chicken Chorioallantoic Membrane System

Z Zhu ¹, T Bhat ², S An ², C Lim ², J Bush ³; ¹ University of British Columbia, ² BC Children's Hospital Research Institute, ³ BC Children's Hospital

Background: Rhabdoid tumors (RTs) are aggressive tumors that occur throughout the body and share an underlying defect in the SWI/SNF pathway. Obtaining cryopreserved RTs can be difficult as they may not be suspected initially which allows for special cryopreservation procedures, or RTs may have minimal tissue sampled which is submitted for as clinical material only. Research opportunities in RTs could be enhanced if archival frozen tissue could be “revived” for tumor modelling experiments. We developed a unique pipeline for pediatric tumor patient-derived xenograft development using the chick chorioallantoic membrane (CAM) system, and sought to explore the capability of the CAM system for PDX generation of rare tumors from a clinical archival collection of snap frozen tissues.

Methods: Four different snap frozen pediatric RTs were identified from 2016-2022 in our -80C clinical freezer. These tumors were gradually thawed, minced into 1mm³ chunks, and implanted on the CAM using the ex ovo method. Tumor growth over 5 days post implantation were observed using a dissecting microscope and photo macrographs were taken to compare gross morphology on day 1 to day 5 for each CAM-PDX. At day 5 post implantation, CAM tumors were collected and allocated for: (a) serial xenografting onto fresh CAM up to 3 passages; (b) viable cryopreservation in 10% DMSO-media; and (c) formalin-fixed paraffin-embedded (FFPE) tissue specimens for histopathology analysis. The CAM-PDX FFPE specimens were sectioned to perform hematoxylin and eosin (H&E) staining or immunohistochemistry (IHC) using an antibody targeting human LAMP1 (Lysosomal Associated Membrane Protein 1) as a marker for cells of human origin and INI1 as a marker of the original tumor.

Results: H&E staining of first passage implants demonstrated viable cells in 2 of 4 xenografts, and they were confirmed to be human by LAMP1 IHC and tumor cells by INI1 IHC. The two other attempted xenografts demonstrated necrotic tumor cells with no viability. Similar viability was observed in the successful CAMs on subsequent passages.

Conclusion: In this study, we demonstrate that the CAM system can produce viable PDXs from snap frozen tissue without special cryopreservation techniques. The CAM method is ideal for snap frozen samples compared to the mouse model as the CAM xenografts can be macroscopically monitored in real time and early determination of viability is possible. By using the CAM system, opportunities to perform live cell based studies on large archival cohorts becomes possible. For real time patients, the CAM system may allow for frozen tissue to be established as a PDX for personalized medicine approaches such as tumor modelling studies and drug testing.

Resident Recruitment Awards

Resident Recruitment Award

Kaposiform Hemangioendothelioma Masquerading as Juvenile Idiopathic Arthritis

Anh Huynh, Andrea Bakker, Jasmine Steele, Antonio Perez-Atayde

Massachusetts General Hospital

Kaposiform Hemangioendothelioma Masquerading as Juvenile Idiopathic Arthritis

Background: Kaposiform hemangioendothelioma (KHE), first described by Zukerberg et al. in 1993^[1], is a rare and locally aggressive vascular tumor that generally presents in neonates and young children^[2]. In the United States, the estimated incidence rate is less than 1 per 100,000 children with a median age of 2 months at initial presentation^[2,3]. Up to 70% of KHE cases are associated with Kasabach-Merritt phenomenon (KMP), which is characterized by a consumptive coagulopathy and profound thrombocytopenia due to intralesional platelet trapping and carries a mortality rate of 12–30%. KHE classically presents in infancy as a cutaneous lesion; patients without cutaneous lesions tend to be older and exhibit atypical symptoms such as thrombocytopenia, musculoskeletal dysfunction, and pain. Common anatomic locations include the extremities, retroperitoneum, and the cervicofacial region^[3]. In this report we describe a case of delayed diagnosis of KHE masquerading as juvenile idiopathic arthritis.

Case Presentation: A 7-year-old previously healthy male presented to an outside hospital with right hand and wrist pain. Multiple providers attributed his symptoms to trauma. Early X-rays were reportedly normal, but an MRI showed extensive synovitis and erosive disease, prompting a referral to rheumatology. The patient's symptoms continued to progress; even very light touch induced excruciating pain and he developed limited range of motion. He was diagnosed with juvenile idiopathic arthritis (JIA). Over a period of 6 months, the patient was trialed on multiple anti-inflammatory and immunomodulatory medications without significant improvement.

At 9 years of age, he presented to our institution, with continued symptoms despite medical treatment. An X-ray showed diffuse osteoporosis and MRI revealed extensive osseous erosions predominantly affecting the dorsal aspect of the carpometacarpal joints, soft tissue with muscular edema and tenosynovitis. His rheumatological workup was negative for ANA, rheumatoid factor, HLA-B27, CCP, Lyme antibody screening, and his ESR was 13. Given the patient's progressive symptoms and medical refractoriness to multiple JIA treatments, the decision was made to perform a right wrist exploration with debridement and biopsy.

Case Findings: Intraoperatively, the capsule of the wrist joints was noted to be hyperemic and thickened with erosions and synovitis down into the bones of the midcarpal and carpometacarpal joints. Histologic examination of the specimen revealed multiple fragments of fibroadipose and synovial-lined tissue with involvement by an

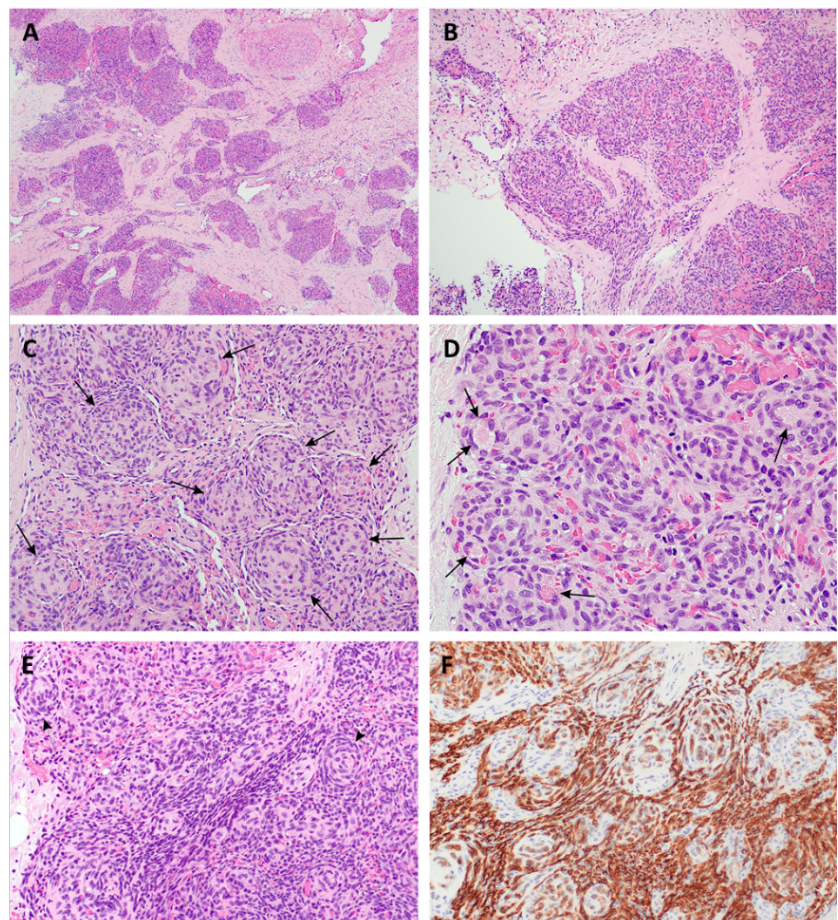


Figure 1. Irregular vascular lobules of KHE infiltrate soft tissue in a characteristic “cannon-ball” pattern of growth (A, B). The lobules consist of Kaposi-like slit-like vessels, glomeruloid structures (C), small vessels with fibrin thrombi (D), and whorls and bundles of spindle cells (E). D240 immunohistochemical stain is intensely positive in slit-like vessels and spindle cells, whereas the glomeruloid structures are negative (F).

infiltrative process arranged in discrete and coalescing nodules and nests. Within the nodules and nests, whorling and glomeruloid structures composed of a proliferation of spindled endothelial cells with slit-like vascular lumina were noted. Hemosiderin deposition and fibrin microthrombi were occasionally seen (Fig 1). By immunohistochemistry, D240 highlighted neoplastic endothelial cells, which were negative for GLUT-1 (not shown). In the vicinity of the lesion, D240 also stained thin-walled malformed lymphatic channels (Fig 2).

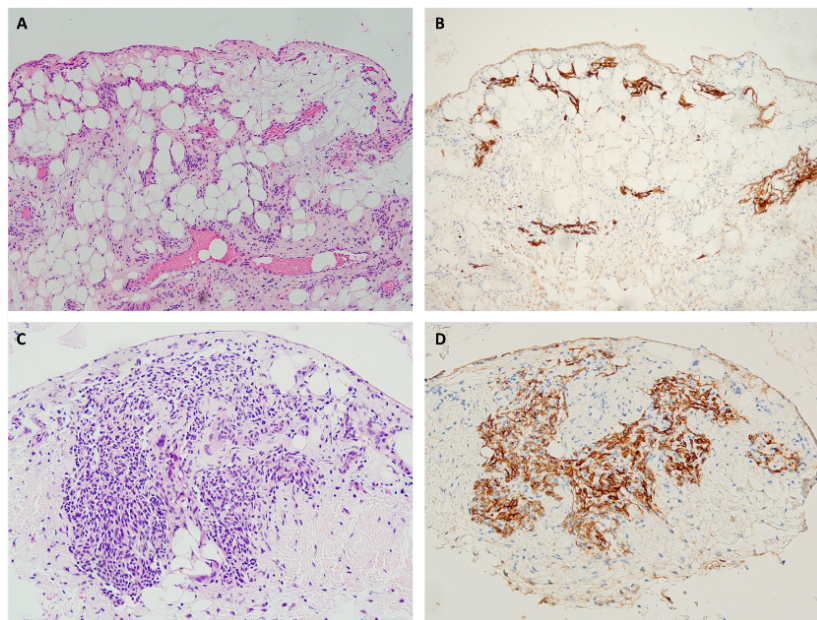


Figure 2. H&E and D240 immunohistochemical stains reveal incipient (A, B) and prominent (C,D) infiltration of the synovial membrane.

Discussion and Conclusion: This case represents a delayed diagnosis of kaposiform hemangioendothelioma due to presumptive clinical diagnosis of JIA. Histologic findings of JIA may include infiltration of synovium by inflammatory cells, synovial lining with reactive and hypertrophic changes, perivascular inflammation, and/or increased vascularity^[4]. However, the histologic findings in this specimen were classic for KHE, as shown in the figures above.

Following this debridement, the patient was started on sirolimus, which has been shown to be efficacious in the management of KHE in recent studies^[1]. Despite initial improvements, his symptoms have recurred with continued limited mobility of the wrist and increasing pain levels. The patient is being followed by vascular anomaly and orthopedic surgery specialists, who feel that there is likely residual or recurrent disease. Genetic testing of the lesion is being considered.

This case demonstrates a considerable delay in diagnosis, which included referrals to multiple providers and culminated in a presumed clinical and radiologic diagnosis of juvenile idiopathic arthritis. The debridement led to a definitive diagnosis nearly two years after onset of symptoms, and appropriate treatment for the patient was initiated. It serves as a reminder that in patients with presumed rheumatological diagnoses refractory to medical therapy, neoplastic diagnoses should be considered, and tissue biopsy may be informative.

References

1. Zukerberg LR, Nickoloff BJ, Weiss SW. Kaposiform hemangioendothelioma of infancy and childhood. An aggressive neoplasm associated with Kasabach-Merritt syndrome and lymphangiomatosis. *Am J Surg Pathol*. 1993 Apr;17(4):321-8. doi: 10.1097/00000478-199304000-00001. PMID: 8494101.
2. Putra J, Gupta A. Kaposiform haemangioendothelioma: a review with emphasis on histological differential diagnosis. *Pathology*. 2017;49(4):356-362. doi:10.1016/j.pathol.2017.03.001
3. Croteau SE, Liang MG, Kozakewich HP, et al. Kaposiform Hemangioendothelioma: Atypical Features and Risks of Kasabach-Merritt Phenomenon in 107 Referrals. *The Journal of Pediatrics*. 2013;162(1):142-147. doi:10.1016/j.jpeds.2012.06.044
4. Thatayatikom A, Modica R, De Leucio A. Juvenile Idiopathic Arthritis. [Updated 2023 Jan 16]. In: StatPearls [Internet]. Treasure Island (FL): StatPearls Publishing; 2023 Jan-. Available from: <https://www.ncbi.nlm.nih.gov/books/NBK554605>.

Resident Recruitment Award

**T-cell Post-Transplant Lymphoproliferative Disorder
Involving a Cardiac Allograft and Masquerading as
High-Grade Acute Cellular Rejection**

**Krupa Merchant, Ian Gelarden, Shunyou Gong, Nicoleta
Arva**

Northwestern University

T-cell Post-Transplant Lymphoproliferative Disorder Involving a Cardiac Allograft and Masquerading as High-Grade Acute Cellular Rejection

Introduction: Allograft rejection is an important cause of morbidity and mortality in pediatric heart transplant patients, and endomyocardial biopsy (EMB) is the gold standard to assess for acute cellular (ACR) and/or antibody-mediated rejection (AMR)¹. Myocardial lymphocytic infiltration seen on EMB raises a differential diagnosis including ACR, Quilty effect, post-operative ischemic changes, and myocarditis. Another important consideration in immunocompromised transplant recipients is post-transplant lymphoproliferative disorder (PTLD). Usually mediated by Epstein-Barr virus (EBV), this disorder occurs in approximately 9% of the pediatric heart transplant population². As PTLD is typically a disorder of B cells, this process is usually easily distinguishable from ACR, a T-cell-dependent process. However, a small subset of PTLD is secondary to clonal T-cell proliferations, reportedly comprising 5% of all PTLD cases³. This report describes a female patient with T-cell PTLD involving the heart allograft and masquerading as ACR.

Clinical History: This is a 12-year-old female with a history of histiocytoid cardiomyopathy and intractable arrhythmias. She received an orthotopic heart transplant at 9 months old in 2011. From 2011-2022, the post-transplant EMBs exhibited multiple instances of ACR, up to ISHLT grade 3R/3B, with clinical response to titrated immunosuppressive therapy. In February 2023, the patient presented with intermittent abdominal pain, tachycardia, and a new gallop. Although the echocardiogram demonstrated preserved graft function, a right pleural effusion was identified, and lab testing revealed an elevated natriuretic peptide. Chest X-ray showed a right lower lobe pneumonia. The patient was treated with a full course of antibiotic therapy prior to undergoing an urgent cardiac catheterization, EMB, and thoracentesis.

Case Findings: The EMB was initially diagnosed as ISHLT ACR grade 3R/3B. Ancillary testing at the time of biopsy were also supportive of ACR (donor-derived cell-free DNA fraction elevated at 0.32% [normal value: <0.2%] and molecular gene expression profile also positive for ACR). Additionally, there was a focal lymphocytic infiltration within the endocardium, interpreted as invasive Quilty effect. A concurrent pleural fluid cytology sample exhibited numerous monomorphic, medium to large lymphocytes with basophilic cytoplasm, oval to irregular nuclei, clumped chromatin, and small nucleoli, raising concern for a lymphoproliferative process (Figure 1A). Flow cytometry of the pleural fluid showed a large population of atypical CD4+ T cells (48% of total cellular events) that were aberrantly negative for CD7 (Figure 1B-D). These findings were suspicious for a T-cell PTLD, prompting further clinical evaluation. Whole body PET-CT revealed diffuse lymphadenopathy, and core needle biopsy of a perisplenic lymph node was performed. Histology of this sample showed effacement of nodal architecture by sheets of atypical, medium to large lymphoid cells with pale cytoplasm, irregular nuclei, and clumped chromatin. Of note, the Ki-67 index by immunohistochemistry was approximately 10%. Next-generation sequencing performed on the perisplenic lymph node revealed variants of potential clinical significance (tier 2) of the *KRAS* and *DICER1* genes. The pleural fluid also demonstrated clonal T-cell receptor gene rearrangement. This in turn led to additional workup of the concurrent EMB, which showed a diffusely CD3+ T-lymphocytic infiltrate with multifocal myocyte damage (Figure 2A-B). Immunohistochemical stains were positive for CD4, negative for CD8, and aberrantly negative for CD7. These findings, along with T-cell receptor gene rearrangement molecular studies, confirmed allograft involvement by monomorphic T-cell PTLD, consistent with peripheral T-cell lymphoma, not otherwise specified (PTCL, NOS).

Discussion: This report describes a rare case of T-cell PTLD involving the cardiac allograft more than a decade after transplant and mimicking ACR (initially considered due to heavy infiltration by CD3+ T cells). T-cell PTLD is an exceedingly infrequent diagnosis, and its clinical behavior compared to *de novo* cases in immunocompetent individuals is not well known⁴. In particular, the low Ki-67 index is unusual for this entity and raises other differential diagnoses of low-grade T-cell lymphomas, such as T-cell prolymphocytic leukemia and T-cell large granular lymphocytic leukemia⁵. Besides rejection (which, as opposed to T-cell PTLD, is mediated by CD8+ lymphocytes), differential diagnosis of lymphocytic infiltration within the allograft myocardium also includes lymphocytic myocarditis. Viral infection is the most common cause of the latter, and a transplant recipient's immunocompromised status should lower the threshold for this diagnosis⁶. However, routine serum surveillance testing for common viral agents can provide insight into making this diagnosis¹. It is crucial to rule out these mimicking entities that require less intensive treatment. T-cell PTLD is an aggressive entity and generally does not respond to reduction of immunotherapy⁷. This patient is currently being evaluated for a hematopoietic stem cell transplant due to the lack of response to immunomodulation and ongoing chemotherapy. More studies are required to better understand the biology, clinicopathologic characteristics, and optimal therapy for this entity.

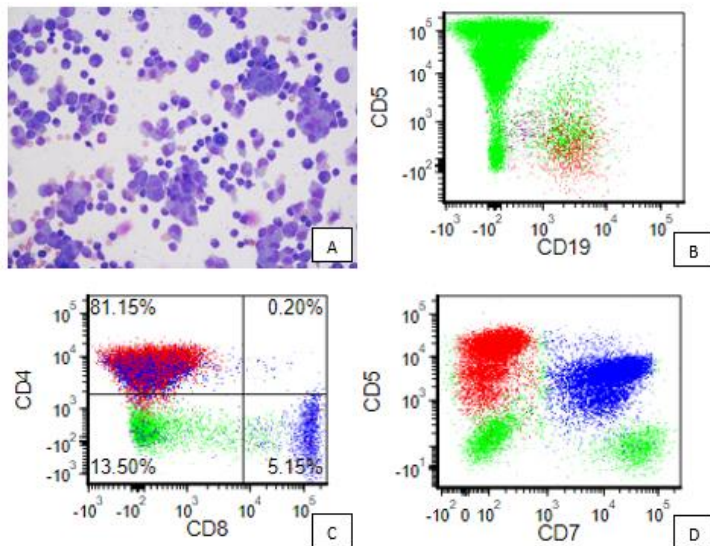


Figure 1. Wright stain of the pleural fluid shows several medium- to large-sized lymphocytes with basophilic cytoplasm, irregular nuclei, clumped chromatin, and small nucleoli with frequent mitotic figures and small mature lymphoid and myeloid cells in the background (A). Flow cytometric immunophenotyping of the pleural fluid identified a population of T cells that are bright CD5+ (B and D), CD4+ (C), and aberrantly CD7- (D).

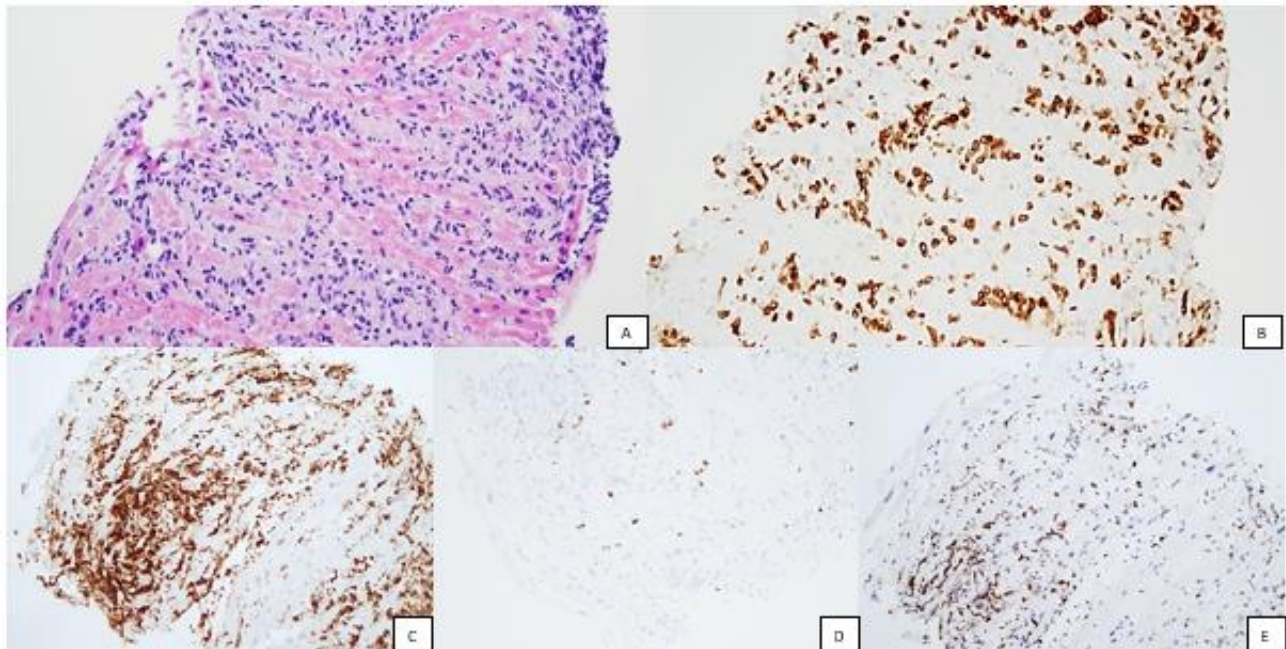


Figure 2. H&E section showing endomyocardium with a diffuse infiltrate composed of small- to medium-sized lymphoid cells with interstitial edema and multifocal myocyte damage (A). Immunohistochemical stain for CD3 demonstrates that the infiltrate is composed predominantly of T cells (B). Further evaluation confirmed the lymphocytic infiltrate is positive for CD4 (C), negative for CD8 (D), and shows aberrant decreased expression of CD7 (E).

References:

1. Zinn MD, Wallendorf MJ, Simpson KE, Osborne AD, Kirklin JK, Canter CE. Impact of routine surveillance biopsy intensity on the diagnosis of moderate to severe cellular rejection and survival after pediatric heart transplantation. *Pediatr Transplant*. 2018 May;22(3):e13131.
2. Liu Y, Wang BC, Zuppan CW, Chau P, Fitts J, Chinnock R, Wang J. Relationship of Post-Transplant Lymphoproliferative Disorders (PTLD) Subtypes and Clinical Outcome in Pediatric Heart Transplant Recipients: A Retrospective Single Institutional Analysis/Experience of 558 Patients. *Cancers (Basel)*. 2023 Feb 3;15(3):976.
3. Kuno M, Ito A, Maeshima AM, Taniguchi H, Tanaka T, Inamoto Y, Kurosawa S, Kim SW, Fukuda T. T-cell posttransplant lymphoproliferative disorders after allogeneic hematopoietic cell transplantation. *Int J Hematol*. 2020 Aug;112(2):193-199.
4. Lee, M., Abousaud, A., Harkins, R.A. et al. Important Considerations in the Diagnosis and Management of Post-transplant Lymphoproliferative Disorder. *Curr Oncol Rep* 25, 883–895 (2023).
5. Stefano A, Pileri, Dennis D, Weisenburger, Ivy SNG, et al. Peripheral T-cell lymphoma, NOS. In: Steven H. Serdlow, Elias Campo, Nancy Lee Harris, et al., editors. *WHO Classification of Tumours of Haematopoietic and Lymphoid tissues: International Agency for Research on Cancer (IARC) Lyon, France; 2017*. 403-7.
6. Winter, MP., Sulzgruber, P., Koller, L. et al. Immunomodulatory treatment for lymphocytic myocarditis—a systematic review and meta-analysis. *Heart Fail Rev* 23, 573–581 (2018).
7. Herreman A, Dierickx D, Morscio J, et al. Clinicopathological characteristics of posttransplant lymphoproliferative disorders of T-cell origin: single-center series of nine cases and meta-analysis of 147 reported cases. *Leuk Lymphoma*. 2013 Oct;54(10):2190-9.

Resident Recruitment Award

Multiple intestinal atresias and combined immune deficiency in a patient with TTC7A mutations

Eunice Chou, Sam Sirotnikov, Heather Rytting, Ahmed Aljudi

Emory University School of Medicine

Title: Multiple intestinal atresias and combined immune deficiency in a patient with TTC7A mutations.

Brief Clinical Synopsis:

A normal weight male infant was born at term with marked abdominal distension, colonic atresia, and abdominal calcifications (Figure 1). Laparotomy on the fourth day of life revealed numerous atresias within the ileum, ileocecal valve, and ascending colon. The affected bowel was resected, followed by ileostomy placement. The post-operative course was complicated by episodic fevers and gastric outlet obstruction. Laparotomy at 6 weeks of life revealed a stenotic pylorus and more atresias involving the entire colon. Additional ascending colon was resected and a pyloroplasty was performed. However, pyloric obstruction recurred along with increased watery, blood-tinged ileostomy output. Ileoscopy at 8 weeks of life revealed friable, bleeding mucosa, which was biopsied and diagnosed as apoptotic ileitis suggestive of immune dysregulation. Altogether, these findings triggered a clinical work-up for immunodeficiency and targeted sequencing analysis for early onset inflammatory bowel disease (IBD). Newborn screening results were negative, including normal levels of T-cell receptor excision circles (TREC). Testing for human immunodeficiency virus was also negative. Further work-up revealed a combined immunodeficiency with markedly reduced T-cells (absolute CD3+ T-cell count of 195 cells/ μ L [reference range is 2500-5500 cells/ μ L]), normal B-cell and NK-cell counts, and markedly reduced immunoglobulin levels (IgG, IgA, IgE, and IgM all below limit of quantification). T- and B-cell proliferative responses to mitogen stimulation were also severely diminished. At this point, the patient began immune modulatory therapy and immunoglobulin infusions. Genetic testing finally returned a complex set of heterozygous mutations classified as variants of unknown significance. These include a single mutation in nucleotide-binding oligomerization domain-containing protein 2 (NOD2) and three biallelic mutations in the tetratricopeptide repeat domain 7A (TTC7A). A diagnosis of TTC7A deficiency associated with multiple intestinal atresia-severe combined immunodeficiency (MIA-SCID) was thus confirmed and the patient underwent bone marrow transplant at 10 months of age.



Figure 1 Pre-surgical x-ray showing marked abdominal distention and small punctate calcifications (red asterisk).

Surgical Pathology Findings:

Resected ileum and colon segments on the fourth day of life demonstrated atretic lumen with multiple small channels present in granulation tissue and aggregates of smooth muscle (Figure 2A). Extensive erosions with exudate, apoptotic debris, eosinophils, and few neutrophils and macrophages were also present (Figure 2B). The small intestine epithelium was stratified and disorganized, exhibiting loss of polarity as well as misplaced goblet cells and Paneth cells. Numerous apoptotic cells and clumps of sloughed off epithelium were also present. The large bowel mucosa had decreased, irregularly spaced glands (Figure 2C) surrounded by lamina propria containing abundant eosinophils and macrophages, few lymphocytes, and noticeably absent plasma cells (Figure 2D). Lymph nodes were severely atrophic, including one showing only the nodal reticular stromal framework and essentially absent lymphocytes. Colonic resections at 7 weeks of life and ileal biopsy at 8 weeks of life redemonstrated previous findings, in addition to prominent lymphoid depletion in a hypocellular lamina propria containing eosinophils and macrophages as well as apoptotic ileitis.

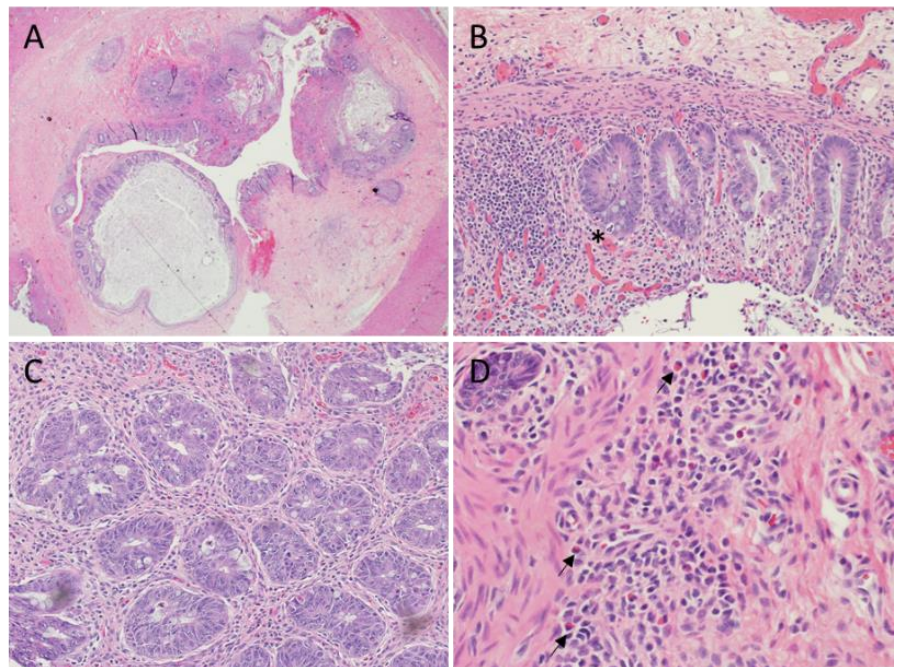


Figure 2 Colonic mucosa with multiple small channels surrounded by granulation tissue (A, 2X), epithelial erosion with exudate and increased apoptotic bodies (asterisk) (B, 10X), architectural distortion with irregular glands (C, 10X), and inflammation with abundant macrophages and eosinophils (arrows) (D, 40X).

Discussion:

This report aims to increase recognition and awareness of a relatively new and rare entity that can present as multiple intestinal atresias of unknown etiology. TTC7A deficiency is an autosomal recessive disorder first reported in 2013¹, and is now included in the expanding list of monogenic forms of IBD. Approximately 50 cases have been reported to date.² There is phenotypic variability depending on the severity of mutation. This case is the severe congenital form with both intestinal atresias and immunodeficiency that meets criteria for SCID (CD3+ T-cell count <300/ μ L).¹⁻³ The disease can affect the stomach and intestines with atresias beginning at the pylorus as in our case. Milder forms can present in older patients, lack immunodeficiency, and present as IBD.⁴⁻⁶ The differential may include congenital malformation syndrome (e.g. VACTERL syndrome) or ischemic injury (e.g. volvulus), Crohn's disease, and infectious enterocolitis.^{2,7}

Histopathologic findings of MIA-SCID can be heterogenous, but some combination of the following is frequently seen: intestinal fibrosis at sites of atresia, apoptotic enterocolitis with mucosal ulceration and regenerative changes, crypt drop-out and distortion, villous blunting of the small bowel, neutrophilic and eosinophilic infiltration of the lamina propria, and decreased plasma cells.^{2,8-11} Thickened fibrotic bowel wall with calcifications and reduced lymphoid follicle size may also be seen.¹² A recent study comparing the gastrointestinal histopathology of patients with TTC7A germline mutations to a control group of patients with intestinal atresia and clinicopathologic findings incompatible with TTC7A mutation noted several of these findings.¹¹ Moreover, the authors reported that all four patients with the SCID phenotype demonstrated a lack of plasma cells.

In our case, sequential intestinal specimens from birth to 8 weeks of life permit detailed pathologic analysis of histopathologic patterns. Recognizing apoptotic ileitis in the final biopsy specimen was key to initiating the correct diagnostic work-up. In hindsight, the earlier resection specimens also held diagnostic clues, including epithelial disorganization and apoptosis. Lymphoid depletion was challenging to assess initially as normal neonates are immunologically naïve and have incomplete lymphoid development. However, at least one lymph node appeared virtually empty. This gastrointestinal lymphopenia persisted to 7 weeks of life, along with absent plasma cells, which is altogether abnormal given this is an area with high antigenic stimulation. Notably, these findings are uncharacteristic of IBD associated with lymphoplasmacytosis.¹³ The lamina propria is hypocellular with focally cellular areas demonstrating eosinophilic cryptitis and eosinophilic exudates.¹⁴

Another interesting feature of this case is that the biopsy findings drove work-up for immunodeficiency, while in the vast majority of typical SCID cases it is driven by the newborn screen, which was negative in this patient.³ One possible explanation may be that T-cell numbers were not low enough to trigger an abnormal TREC result or the cutoff value used is not low enough. It is important to emphasize that immunodeficiency in the TTC7A deficiency setting is markedly variable ranging from absent or negligible immune defects to typical SCID.

Mutated variants of the TTC7A associated with severe congenital bowel obstruction was first reported in a study of French-Canadian family members.^{1,15} Over 20 pathogenic TTC7A mutations leading to deficiency in the encoded protein have been identified since then.² The TTC7A protein serves multiple functions including cell cycle regulation, cellular organization, and epithelial cell polarity.^{9,10,16} Its dysfunction or deficiency causes inflammation leading to stenotic segments of bowel that is refractory to surgical resection, as well as T-cell lymphopenia leading to either CID or SCID.^{9,16} Mutations causing protein truncation or deletion (i.e. nonsense mutations) have been associated with MIA-SCID phenotype, as well as greater morbidity and mortality.^{17,18} Other mutations may lead to milder hypomorphic presentations.^{4,6} However, the dichotomous framework between truncated and hypomorphic mutations may be incomplete as discrepancies between genotype and phenotype in TTC7A patients have been reported.⁴ The patient in this case had three heterozygous mutations on the gene: c.1373G>A (p.Cys458Tyr), c1817A>G (p.Lys606Arg), and c.2086T>C (p.Ser696Pro or p.Ser672Pro). The first variant is novel and of unknown significance, whereas the latter two variants are missense mutations that have been associated with multiple gastrointestinal atresia ± immunodeficiency syndrome.^{17,19}

No standard treatment for TTC7A mutant intestinal disease exists currently, as surgical resections do not prevent recurrent atresia and immunosuppressants traditionally used to treat inflammatory bowel disease are ineffective here.^{2,15} Patients typically experience severe chronic diarrhea and infection risks from multiple surgeries. Patients with atresia, IBD, and combined immunodeficiency have a mean survival of 24 months², although few reported cases have been shown to live beyond infancy with aggressive surgical and medical management including bone marrow transplantation.²⁰ Other than symptomatic management with surgery and nutritional support, the drug Leflunomide may be a potential therapy for patients with TTC7A deficiency, as it has been shown to reduce mucosal apoptosis and restore gut function in a zebrafish model and in primary patient-derived colonoids.²¹

To summarize, TTC7A has a role in cellular processes and epithelial organization, where its deficiency has been associated with mucosal sloughing and apoptosis in the gastrointestinal tract. Patients may present with early inflammatory bowel disease, multiple gastrointestinal atresias, and combined immunodeficiency. Treatment depends on prompt clinicopathologic diagnosis and early surgical and medical intervention. This case reminds us that young children with aggressive intestinal disease, especially with increased bowel mucosal apoptosis on microscopy, may be candidates for TTC7A genetic testing. If pathogenic mutations of TTC7A are found, the presence of combined immunodeficiency should be promptly investigated as these patients are at heightened risk of morbidity and mortality from infection and susceptibility to graft-versus-host disease after transplantation.

- Samuels, M. E. *et al.* Exome sequencing identifies mutations in the gene TTC7A in French-Canadian cases with hereditary multiple intestinal atresia. *J Med Genet* **50**, 324–329 (2013).
- Jardine, S., Dhangani, N. & Muise, A. M. TTC7A: Steward of Intestinal Health. *CMGH* vol. 7 555–570 Preprint at <https://doi.org/10.1016/j.jcmgh.2018.12.001> (2019).
- van der Spek, J., Groenwold, R. H. H., van der Burg, M. & van Montfrans, J. M. TREC Based Newborn Screening for Severe Combined Immunodeficiency Disease: A Systematic Review. *J Clin Immunol* **35**, 416–430 (2015).
- Woutsas, S. *et al.* Hypomorphic mutation in TTC7A causes combined immunodeficiency with mild structural intestinal defects. *Blood* **125**, 1674–1676 (2015).
- Avitzur, Y. *et al.* Mutations in tetratricopeptide repeat domain 7A result in a severe form of very early onset inflammatory bowel disease. *Gastroenterology* **146**, 1028–1039 (2014).
- Neves, J. F. *et al.* Missense mutation of TTC7A mimicking tricho-hepato-enteric (SD/THE) syndrome in a patient with very-early onset inflammatory bowel disease. *Eur J Med Genet* **61**, 185–188 (2018).
- Al-Zaiem, M. M., Alsamli, R. S., Alsulami, E. A., Mohammed, R. F. & Almatrafi, M. I. Hereditary Multiple Intestinal Atresia: A Case Report and Review of the Literature. *Cureus* (2022) doi:10.7759/cureus.30870.
- Avitzur, Y. *et al.* Mutations in tetratricopeptide repeat domain 7A result in a severe form of very early onset inflammatory bowel disease. *Gastroenterology* **146**, 1028–1039 (2014).
- Bigorgne, A. E. *et al.* TTC7A mutations disrupt intestinal epithelial apicobasal polarity. *Journal of Clinical Investigation* **124**, 328–337 (2014).
- Lien, R. *et al.* novel Mutations of the Tetratricopeptide Repeat Domain 7A gene and Phenotype/genotype comparison. *Front Immunol* **8**, (2017).
- Dannheim, K. *et al.* Pediatric Gastrointestinal Histopathology in Patients with Tetratricopeptide Repeat Domain 7A (TTC7A) Germline Mutations A Rare Condition Leading to Multiple Intestinal Atresias, Severe Combined Immunodeficiency, and Congenital Enteropathy. *American Journal of Surgical Pathology* (2022)
- Fayard, J. *et al.* TTC7A mutation must be considered in patients with repeated intestinal atresia associated with early inflammatory bowel disease: Two new case reports and a literature review. *Archives de Pédiatrie* **25**, 334–339 (2018).
- Skinner, J. M. & Whitehead, R. *The plasma cells in inflammatory disease of the colon: A quantitative study.* *J. clin. Path* vol. 27 (1974).
- Alhmod, T. *et al.* Outcomes of inflammatory bowel disease in patients with eosinophil-predominant colonic inflammation. *BMJ Open Gastroenterol* **7**, (2020).
- Fernandez, I. *et al.* Multiple intestinal atresia with combined immune deficiency related to TTC7A defect is a multiorgan pathology: Study of a French-Canadian-Based cohort. *Medicine (United States)* **93**, e327 (2014).
- Culbreath, K. *et al.* Intestinal atresias and intestinal failure in patients with TTC7A mutations. *J Pediatr Surg Case Rep* **80**, (2022).
- Chen, R. *et al.* Whole-exome sequencing identifies tetratricopeptide repeat domain 7A (TTC7A) mutations for combined immunodeficiency with intestinal atresias. *Journal of Allergy and Clinical Immunology* **132**, (2013).
- Mou, W. *et al.* A Novel Homozygous TTC7A Missense Mutation Results in Familial Multiple Intestinal Atresia and Combined Immunodeficiency. *Front Immunol* **12**, (2021).
- Kammermeier, J. *et al.* Stem cell transplantation for tetratricopeptide repeat domain 7A deficiency: Long-term follow-up. *Blood* vol. 128 1306–1308 Preprint at <https://doi.org/10.1182/blood-2016-01-696385> (2016).
- Buckley, S. *et al.* Patients with TTC7A Deficiency Causing Multiple Intestinal Atresia with Combined Immunodeficiency (MIA-CID) Can Survive Well Beyond Infancy. *Transplantation* **101**, S34 (2017).
- Jardine, S. *et al.* Drug Screen Identifies Leflunomide for Treatment of Inflammatory Bowel Disease Caused by TTC7A Deficiency. *Gastroenterology* **158**, 1000–1015 (2020).

Posters

No System Left Untouched: A Case of Diffuse Alveolar Hemorrhage and Waterhouse-Friderichsen Syndrome in the Setting of Juvenile-Onset Systemic Lupus Erythematosus

P Jafari G Venkataraman, P Pytel, R Katkhuda, A Chang, A Husain; University of Chicago Medicine

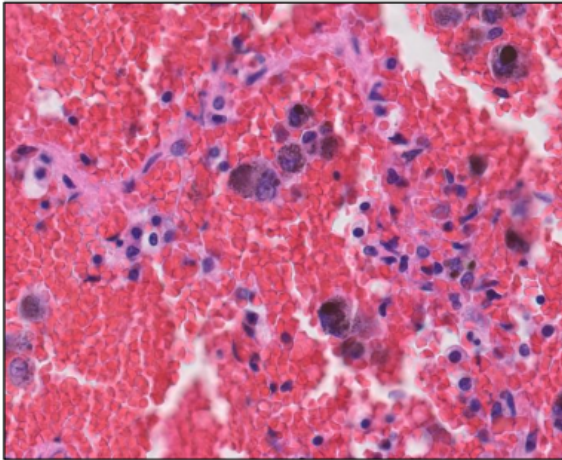
Background: Though rare, juvenile-onset systemic lupus erythematosus (jSLE) is associated with an aggressive natural history as compared to adult-onset SLE. Pediatric patients experience higher rates of disease activity and more rapid progression to organ damage, often necessitating intensive immunosuppression. These features are illustrated in the case of a 12-year-old male with jSLE, managed on multiple immune suppressants, who presented with sepsis and disseminated intravascular coagulopathy (DIC). The patient died within 24 hours of presentation despite broad-spectrum antibiotics and extracorporeal membrane oxygenation (ECMO) support.

Methods: A complete autopsy was performed per family request. Blood cultures drawn upon admission grew *S. pneumoniae*. Postmortem cultures of peritoneal fluid and all 5 lung lobes were negative.

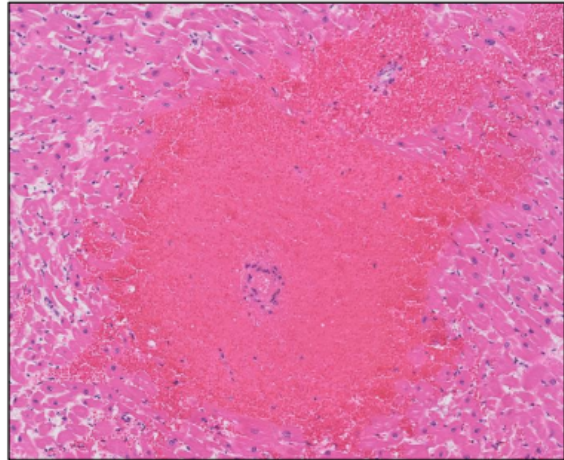
Results: The lungs exhibited striking hemorrhage and hemosiderosis (Figure 1A), consistent with diffuse alveolar hemorrhage, a well-recognized complication of SLE associated with high mortality rates. The myocardium exhibited small vessels surrounded by lake-like collections of extravasated erythrocytes (Figure 1B), an exceedingly unusual finding outside of the transplant setting. Other findings reflecting the clinical history of sepsis and coagulopathy included diffuse hemorrhagic necrosis of the bilateral adrenal glands (Waterhouse-Friderichsen syndrome; Figures 1C-D); a 6 cm subcapsular hematoma of the left kidney; multifocal hemorrhage involving the subendocardium, right renal pelvis, and bladder and gastrointestinal mucosa; diffuse left-sided subgaleal hemorrhage; and patchy bilateral subarachnoid hemorrhages. The kidneys (Figure 1E) exhibited thrombotic microangiopathy in a background of crowded, sclerotic glomeruli, marked interstitial fibrosis, and tubular atrophy. Cortical microinfarcts were noted in the left frontal and right parietal lobes of the brain. The hematolymphoid system was notable for hemophagocytosis in the bone marrow, suggestive of evolving hemophagocytic lymphohistiocytosis (Figure 1F); diffuse lupus lymphadenitis; and scattered calcifications in the thymus. < insert image>

Conclusion: As exemplified here, the diverse and striking histopathologic manifestations of jSLE can be traced across multiple organ systems. The aggressive immunosuppression required for disease management, coupled with reduced physiologic reserve due to chronic SLE-related organ damage, may leave patients vulnerable to devastating infections.

Figure 1. Gross and histologic autopsy findings.



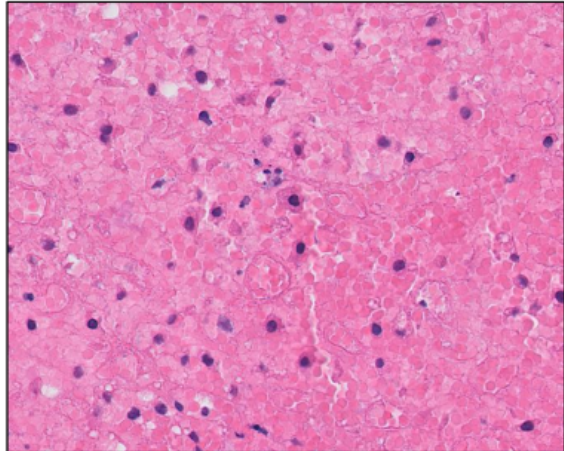
A. Lung with diffuse alveolar hemorrhage, including hemosiderin-laden macrophages.



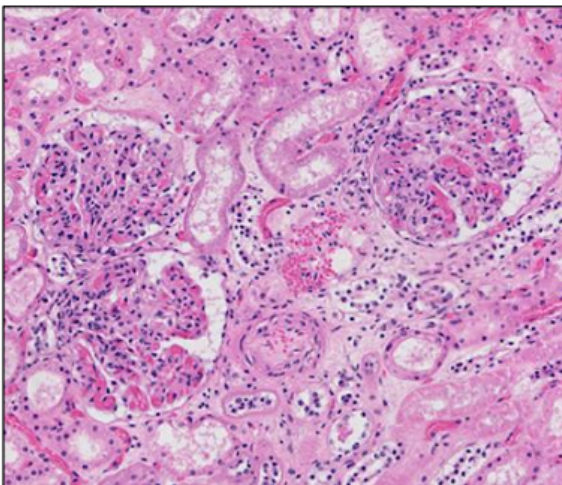
B. Myocardium with small vessel surrounded by lake-like collection of extravasated erythrocytes.



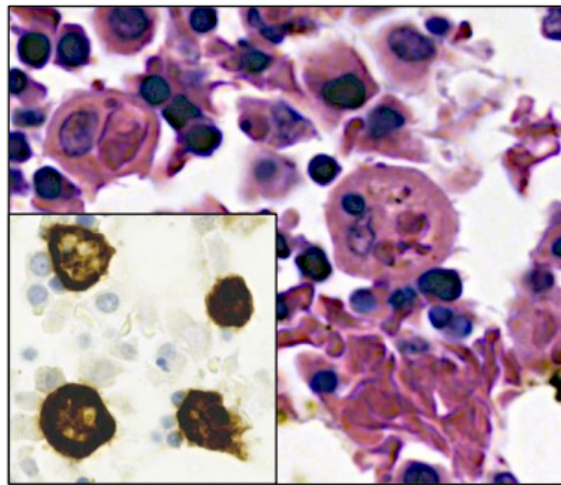
C. Bilateral kidneys and enlarged, hemorrhagic adrenal glands.



D. Diffuse hemorrhagic necrosis of adrenal glands (Waterhouse-Friderichsen syndrome).



E. Kidney with glomerular crowding, suggestive of marked interstitial fibrosis and tubular atrophy.



F. Bone marrow with erythrophagocytosis, highlighted by CD68 immunostain (inset).

Neonatal Hemochromatosis in a Newborn with Trisomy 21: an Autopsy Case Report and Literature Review

M Harrell ¹, J Suddock ², P Zamiara ², C Guardado-Salazar ³, D Hawes ², L Wang ²; ¹ Children's Hospital Los Angeles, ² Children's Hospital Los Angeles, ³ Valley Children's Healthcare

Background: Neonatal hemochromatosis (NH) is a rare, severe liver condition which affects newborns and is characterized by liver failure and significant iron deposition in extra-hepatic tissues, often within the initial weeks of life. While NH is frequently attributed to gestational alloimmune liver disease (GALD), a process mediated by maternal antibodies, etiologies of non-GALD mediated NH remain unclear. Rare cases of NH associated with trisomy 21 have previously been reported.

Methods: A consented, unlimited autopsy, including external and internal examination, neuropathology consultation, and histological evaluation, was performed at our hospital.

Results: The decedent was a 9-week-old female with a history of trisomy 21, transient myelodysplastic disorder, liver failure, and hypoxic-ischemic encephalopathy. Treatment was initiated for suspected GALD and liver failure, ultimately proving unsuccessful. Autopsy revealed an infant smaller than expected for gestational age (< 5th percentile for weight and < 1st percentile for height), displaying pronounced jaundice and dysmorphic facial features, including low-set ears, high-arched palate, and a flattened nasal bridge. On internal examination, the liver demonstrated significant yellow-green discoloration, with nodular and firm cut surface. Histologic sections of the liver revealed diffuse hepatocyte necrosis, multinucleated hepatocytes, and bile ductular reaction. There was severe portal and bridging fibrosis, highlighted by Masson's trichrome stain. In addition, numerous foci of siderosis were identified across multiple organ systems by hematoxylin and eosin and Prussian blue staining, including involvement of the myocardium, pancreas, thyroid, liver, respiratory glands, and focally in peri-renal soft tissue. Other findings included non-specific lung congestion and splenomegaly. Evaluation of bone marrow was limited by autolysis, but demonstrated a mild increase in megakaryocytes, with hypolobated and hyperchromatic forms. A dedicated neuropathology examination revealed a markedly yellow discoloration of brain parenchyma and localized iron deposits in the adenohypophysis by Prussian blue staining.

Conclusion: The autopsy findings confirmed a diagnosis of neonatal hemochromatosis in a 9-week-old female infant, highlighted by hepatic cirrhosis and pronounced multi-organ siderosis. While GALD is the most common cause of fetal liver injury leading to NH, the NH phenotype has been associated with non-GALD disease states such as trisomy 21, perinatal infection, deoxyguanosine kinase (DGUOK) deficiency, infantile myofibromatosis, tricho-hepato-enteric syndrome, and GRACILE syndrome, among others.

Colonic Malakoplakia in a Child with Activated PI3K-delta Syndrome

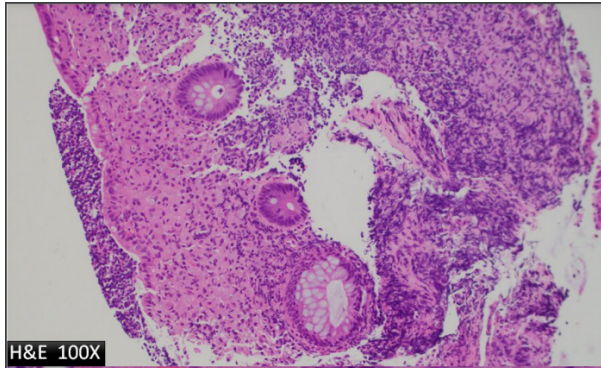
M Harrell ¹, M Hook ², M Bitar ², N Joseph ², C Costales ², L Wang ², N Shillingford ²; ¹ Children's Hospital Los Angeles, ² Children's Hospital Los Angeles

Background: Malakoplakia is a rare and complex inflammatory condition with an unclear etiology, predominantly seen in immunocompromised individuals. Thought to stem from a bactericidal defect in macrophages, malakoplakia most often involves the genitourinary system. A less commonly described site is the gastrointestinal tract, with the highest frequency in the distal colon and rectum. In the pediatric population, literature regarding colonic malakoplakia is scant. PI3K-delta syndrome is an immunodeficiency disorder caused by a gain of function mutation in the PIK3CD gene leading to constitutional activation of phosphoinositide 3-kinase delta. Its association with colonic malakoplakia has not been previously established. This abstract delineates the first reported case of colonic malakoplakia manifesting in a child with PI3K-delta syndrome.

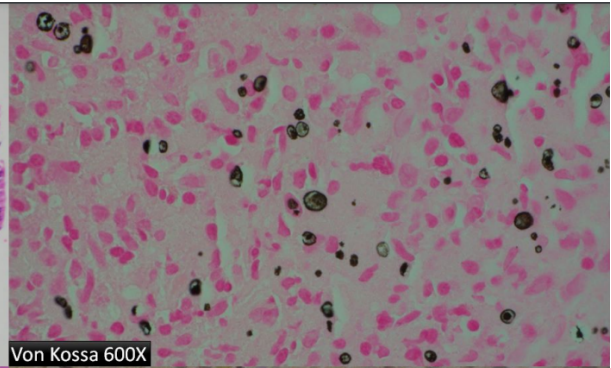
Methods: Esophagogastroduodenoscopy and colonoscopy were performed and endoscopic biopsies were obtained from multiple locations. The specimens were processed routinely and stained with hematoxylin and eosin. Special stains, such as Grocott's methenamine silver (GMS), Periodic Acid-Schiff (PAS), mucicarmine, and Von Kossa were performed.

Results: The patient is a 10-year-old male with history of PI3K-delta syndrome and very early onset inflammatory bowel disease (VEO-IBD) that presented for interval evaluation due to undetected sirolimus levels and intermittent bloody stools while on sirolimus treatment. Colonoscopy showed multifocal patchy erythema and friability throughout the colon, and mucosal ulcerations from the transverse colon to rectum. Histologic sections revealed chronic, severely active colitis with mucosal ulceration in the descending colon and sigmoid colon. The lamina propria deep to these ulcerations was involved by sheets of foamy epithelioid histiocytes which contained numerous layered, basophilic concentric structures, ranging in size from approximately 3-10 um. The structures were negative by GMS, PAS, and mucicarmine, eliminating a fungal etiology, including cryptococcus. These calcified, concentric structures were highlighted Von Kossa stain, confirming our suspicion for Michaelis-Gutmann bodies. The remaining biopsy sites, including the esophagus, stomach, ascending colon, and rectum were uninvolved.

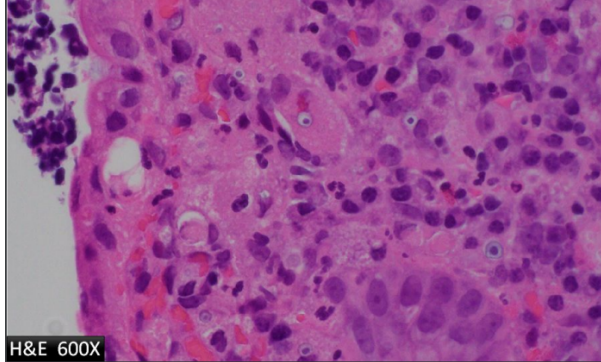
Conclusion: The presence of Michaelis-Gutmann bodies, histiocytic inflammation, and the absence of fungal organisms confirm the diagnosis of malakoplakia. This is the first reported occurrence of colonic malakoplakia in a child with PI3K-delta syndrome, highlighting a potential association between these two rare conditions. Given the link between malakoplakia and immunodeficiency syndromes, this case accentuates the need for both clinicians and pathologists to include malakoplakia in their working differential diagnosis, especially in the setting of VEO-IBD, where malakoplakia may mimic malignancy.



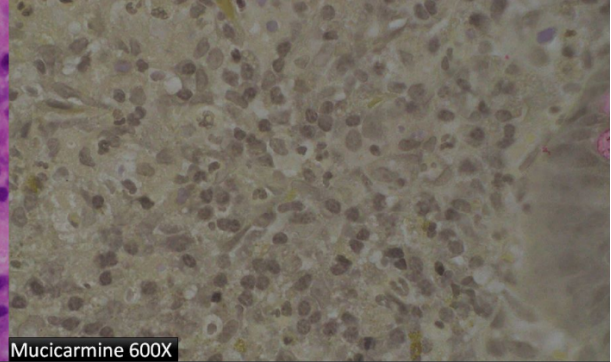
H&E 100X



Von Kossa 600X



H&E 600X



Mucicarmine 600X

Regenerative Nodule As Diagnostic Pitfall in the Neonate With Acute Liver Failure and a Liver Lesion

C Castaneda ¹, S Ranganathan ², K Furuya ¹, J Gulliver ¹; ¹ University of Wisconsin School of Medicine and Public Health, ² Cincinnati Children's Hospital

Background: Acute liver failure in the neonate generates a broad differential diagnosis of varying etiology including inborn errors of metabolism, infections, cholestatic disorders, iron storage disease, alpha-1 antitrypsin deficiency, total parenteral nutrition-related injury, malignancy, and others. We present a case of a neonate born at 39 weeks' gestational age who presented on day 5 of life with coxsackievirus encephalitis and COVID-19 infection and subsequently found to be in acute liver failure (AST 1,864 IU/L, ALT 535 IU/L) with increasing alpha-fetoprotein. Evaluation for possible liver transplantation included an abdominal MRI, which showed a 2.4 x 1.7 x 2.1 cm round mass-like lesion in segment 2 of the liver, raising a differential diagnosis which included hepatoblastoma. This lesion and the background liver were biopsied. The severity of liver injury and histologic findings in the setting of dual coxsackievirus and COVID-19 infections were also questioned by the clinical team.

Methods: Microscopic examination of H&E-stained sections of 5 liver core biopsies from the mass lesion and the background liver. Trichrome and reticulin special stains were performed on the lesional biopsy, as well as immunohistochemistry for glypican-3 (GPC3), glutamine synthetase, beta-catenin, and CD34. Prussian blue and copper stains were performed on the background liver. Slides were also reviewed in consultation at Cincinnati Children's Hospital Medical Center, where SARS-CoV-2 immunohistochemistry was performed.

Results: H&E-stained sections of the mass-like lesion showed liver parenchyma with a nonspecific hepatitic pattern of injury including prominent canalicular cholestasis, pseudo-acinar transformation, focal giant cell transformation, and ballooned hepatocytes, while the background liver was nodular with post-necrotic changes and collapse of the lobular architecture. SARS-CoV-2 immunohistochemistry was negative. Glypican-3 staining was noted in sections of the lesion with the background liver also showing positive glypican-3 staining to the same intensity.

Conclusion: Our case highlights a potential diagnostic pitfall in the usage of glypican-3 staining when considering the diagnosis of hepatoblastoma in a neonate with recent liver injury. This neonate was known to have been infected with COVID-19 at the time of initial presentation as well as coxsackievirus. Fulminant hepatitis associated with coxsackievirus is known to occur in the neonatal period. The pattern of liver injury when neonates present with viral co-infections is not frequently described. While clinical case reports exist of acute hepatitis in neonates with COVID-19, the role dual infection may play in causing severe liver injury is unique to our case and provides territory for continued investigation.

Micronodular PEComa of the Appendix in an Infant

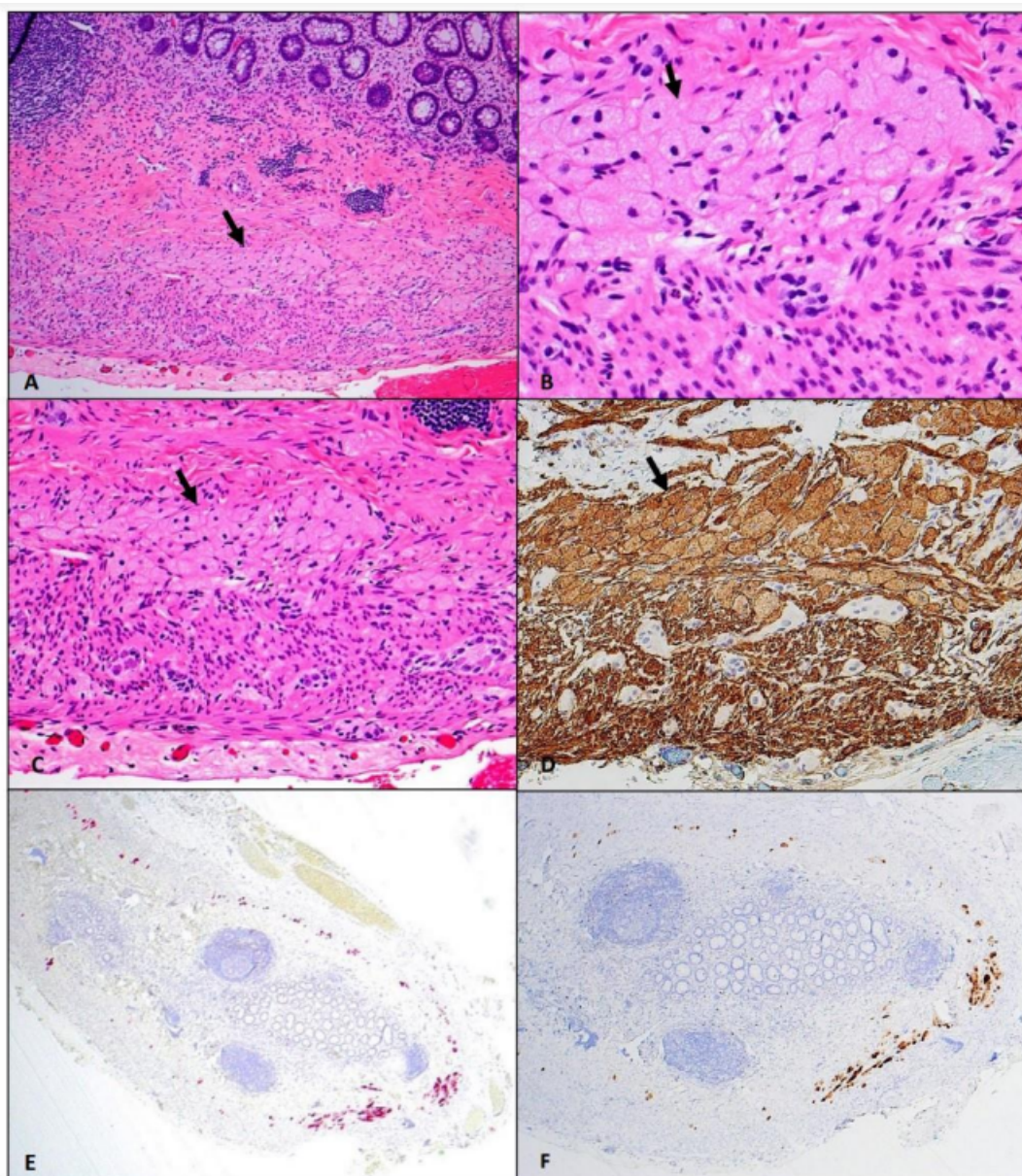
P Sylvestre ¹, R Gonzales ¹, J Velazquez Vega ²; ¹ Department of Pathology and Laboratory Medicine, Emory University School of Medicine, Atlanta, Georgia, USA, ² Department of Pathology, Children's Healthcare of Atlanta, Atlanta, Georgia, USA

Background: Perivascular epithelioid cell tumor (PEComa) is a rare mesenchymal neoplasm with myomelanocytic differentiation that is thought to arise from perivascular epithelioid cells. PEComa of the appendix has rarely been reported and is even rarer in the pediatric population. Historically, the cells of interest in micronodular PEComa of the appendix (also known as local PEComatosis) were believed to be degenerated smooth muscle cells and, as such, was previously known as “granular degeneration of smooth muscle.” The terminology of “micronodular PEComa of the appendix” was recently proposed to describe lesions that, by definition, are not grossly seen, have uniformly low-grade histologic features, and show coexpression by immunohistochemistry of muscle and melanocytic markers with most arising within the inner smooth muscle layer of the appendiceal muscularis propria.

Methods: Presented herein is a case of a micronodular PEComa of the appendix in an infant. The female patient was born at 27 weeks' gestation and developed necrotizing enterocolitis requiring segmental small intestinal resection with ileostomy. At three months of age an ileocectomy with ileostomy takedown was performed. The grossly unremarkable appendix measured 3.4 cm in length and 0.4 cm in diameter and was entirely submitted for microscopic examination.

Results: H&E-stained sections of the appendix revealed multiple nests of plump, polygonal cells with pale-pink eosinophilic granular cytoplasm located predominantly within the inner layer of the muscularis propria in the distal aspect of the appendix (Figures A & B) with occasional smaller nests and isolated cells trailing off proximally from the tip. No significant stroma was present between the smooth muscle and granular cells (Figure C). By immunohistochemistry, the granular cells were positive for smooth muscle actin, HMB45, and cathepsin K (Figures D, E, and F) as well as for MiTF and desmin. TFE3 IHC showed rare weak nuclear positivity. S100 and Melan-A immunostains were negative. The remainder of the appendix was histologically unremarkable.

Conclusion: Given the subtle histologic appearance of this microscopic finding, micronodular PEComa of the appendix may easily go unrecognized and therefore underreported. While the nature of the cells forming this appendiceal lesion has not been completely elucidated, micronodular PEComas of the appendix appear to be unassociated with tuberous sclerosis and follow an indolent course. References: 1. Sobel HJ, Marquet E, Schwarz R. Granular degeneration of appendiceal smooth muscle. Arch Pathol. 1971 Dec;92(6):427-32. PMID: 4330583. 2. Anderson WJ, Kojc N, Fletcher CDM, Hornick JL. Micronodular PEComas of the appendix. Histopathology. 2021 Jun;78(7):1047-1050. PMID: 33502031. 3. Tran TAN, Fanaian N. Local PEComatosis of the Appendix: New Insights Into the Histogenesis of Nodular Granular Muscle Degeneration and Granular Cells/Granular Cell



Adenomyoma of the Small Intestine: A Rare Cause of Pediatric Ileocolic Intussusception

K Teehera ¹, J Bodmer ², P Jedlicka ², L Westbrook ¹; ¹ University of Colorado, ² Children's Hospital Colorado

Background: Adenomyoma is a rare, benign, polypoid lesion that occurs in various sites of the GI tract, but rarely in the ileum. While the etiology is unknown, adenomyomas are likely the result of a hamartomatous or heterotopic pancreatic process. Histologically, the submucosa is expanded by cystic glands surrounded by smooth muscle. Due to submucosal growth, the resulting mass lesion has the potential to be a lead point for intussusception.

Methods: Two cases of pediatric intussusception were identified in 2013-2023. Clinical presentation, medical history, and histology were compared between the cases.

Results: The patients were a 38-day-old male and a 3-year-old female who presented with ileocolic intussusception. One patient had an ultrasound that revealed a sub-centimeter, eccentric, multi-cystic, ovoid structure at the distal ileum. Intraoperatively, both patients were discovered to have a polypoid ileal mass; partial small bowel resections were performed. Microscopic examination of both lesions showed multiple cystically dilated lumens within the submucosa, lined by pseudostratified columnar epithelium and surrounded by disorganized smooth muscle fibers. Ganglion cells were absent within the smooth muscle walls. One case additionally showed focal ectopic pancreatic acinar glands. Immunohistochemistry performed on one of the adenomyomas showed diffuse positive CK7 staining of the epithelial lining of the glands, positive SMA staining of the smooth muscle fibers, and weak positive CK20 staining (Figure 1).

Conclusion: Here, we report two unusual cases of ileal adenomyoma causing ileocolic intussusception. Histologically, adenomyomas have characteristic submucosal, cystically dilated glands lined by columnar epithelium and surrounding irregular smooth muscle expansion. Ectopic pancreatic acini or islets can be seen. Given their relative rarity and benign appearance, these lesions are likely under-recognized and underreported. The differential diagnoses include enteritis cystic profunda and well-differentiated adenocarcinoma. While the pathogenesis is unclear, adenomyoma may arise from a hamartoma or pancreatic heterotopia. The latter theory is supported by the immunophenotype of one case: strong positive CK7 and weak positive CK20 of the cyst epithelium, in contrast to the background intestine, which was strongly positive for CK20. Heterotopic pancreatic acinar tissue was also seen, further suggesting a pancreaticobiliary origin of the adenomyomatous glandular component. The tumor-like nature of the adenomyoma lends to the possibility of intussusception. Most cases of intussusception due to adenomyoma occur in infancy to early childhood, but most cases of pediatric intussusception have no identified lead point. Thus, adenomyoma should be high on the differential diagnosis.

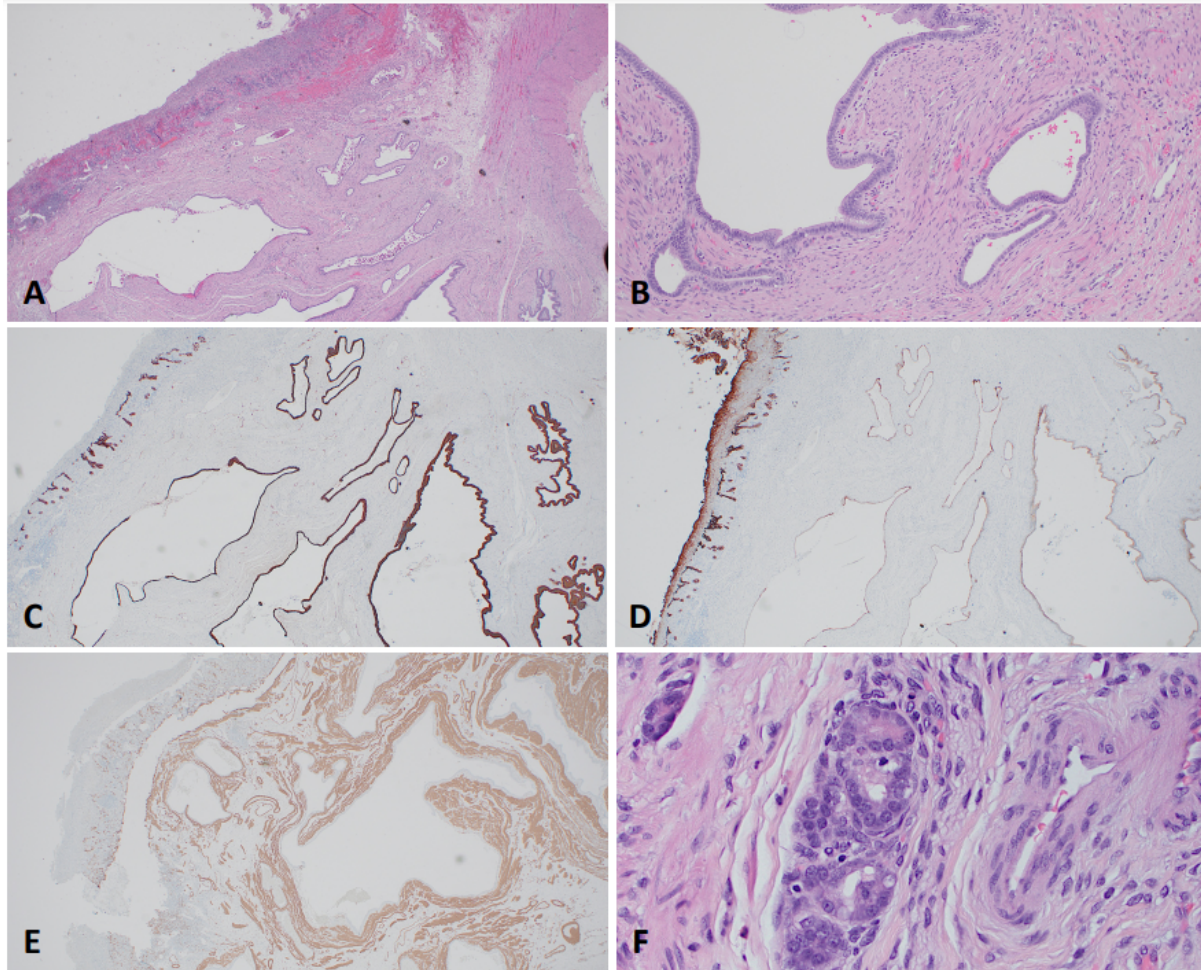


Figure 1: Adenomyoma of the ileum. A. Cystically dilated glands with disorganized smooth muscle (H&E, 2X). B. Columnar epithelium lining the glands (H&E, 10X). C. Diffusely positive CK7 staining of cystic gland epithelium (2X), with comparatively weak staining of overlying ileal epithelium. D. Weakly positive CK20 staining of cystic gland epithelium (2X), with comparatively strong staining of overlying ileal epithelium. E. Positive SMA staining of disorganized smooth muscle surrounding cystic glandular epithelium (2X). F. Heterotopic pancreatic acini (H&E, 40X).

Multifocal Hepatocellular Carcinoma with DROSHA Mutation in a Patient on Long-Term Cholic Acid Treatment for Zellweger Spectrum Disorder

J Salise ¹, L Berklite ², A Bondoc ², K Bove ², K Campbell ², D Leino ², S Ranganathan ², S Roy ², K Somers ²; ¹ Cincinnati Children's Hospital Medical Center, ² Cincinnati Children's Hospital Medical Center

Background: Zellweger spectrum disorders (ZSD) are a group of peroxisome biogenesis disorders (PBD) due to defects in PEX genes required in normal peroxisomes. Liver disease occurs due to impaired fatty acid β -oxidation and bile acid synthesis with accumulation of hepatotoxic intermediates. Rare cases of hepatocellular carcinoma (HCC) in the context of ZSD have been reported. Oral cholic acid (CA) is given to reduce hepatotoxic C27-bile acid intermediates. Data is limited regarding the impact of disease severity on its effectiveness. We present an 11-year-old female with ZSD on long term CA therapy who developed multifocal HCC requiring liver transplantation, highlighting the unique histologic, ultrastructural, and molecular features of the case.

Methods: All relevant clinical and pathologic data was obtained retrospectively from the electronic medical record and surgical pathology reports with IRB approval.

Results: The patient presented with neonatal cholestasis at 33 days of life. Mass spectrometry showed increased long-chain bile acids. PEX1 molecular testing revealed heterozygous mutations including frameshift mutation (c.2097-2098insT) and missense mutation (c.2528G>A) consistent with ZSD. She started CA in her first year of life. Her course was marked by seizures, hypotonia, failure to thrive, gastroesophageal reflux disease, gastric tube dependence, hearing and visual impairment, and chronic liver disease. At 10 years of age, she was diagnosed with hepatocellular carcinoma (HCC). (Insert image#1) Microscopically, the background liver showed moderate portal inflammation with intraportal macrophages, nonuniform periportal fibrosis with occasional thin septa/bridges, and a variegated appearance of the hepatocytes reminiscent of glycogen storage disease (GSD). (Insert image #2 and #3) Electron microscopy showed no normal peroxisomes with rare smaller membrane bound structures and accumulation of macrophages containing dysmorphic residual bodies with crystal configuration consistent with fatty acids. (Insert image #4 and #5) She underwent thermal microwave ablation of a large single lesion, but developed additional lesions on imaging, ultimately requiring liver transplant, with findings of multifocal HCC. Molecular testing identified a DROSHA p.R279C mutation. The background liver was notable for areas of cirrhosis and widespread PAS-negative GSD-like changes.

Conclusion: Limited studies are available on ZSD patients with HCC and even less is known on the histologic changes following long term CA treatment. We present a unique case of multifocal HCC arising in a patient with ZSD which harbored a DROSHA mutation not previously reported in HCC. In addition, her background liver showed both fibrosis and a pattern reminiscent of GSD not previously described in ZSD liver disease. Whether this pattern is typical of CA therapy requires further investigation.

Image #1 HCC:

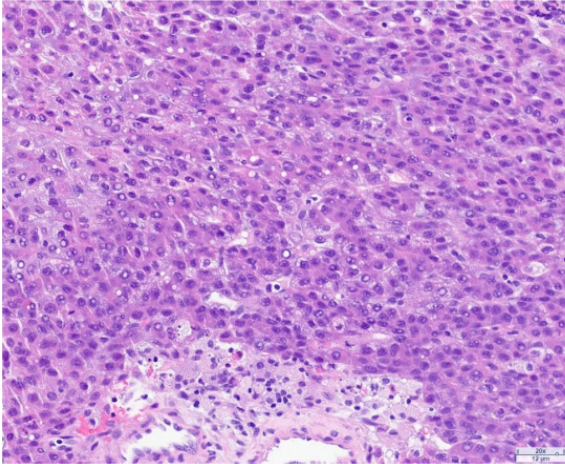


Image #4 No normal peroxisomes:

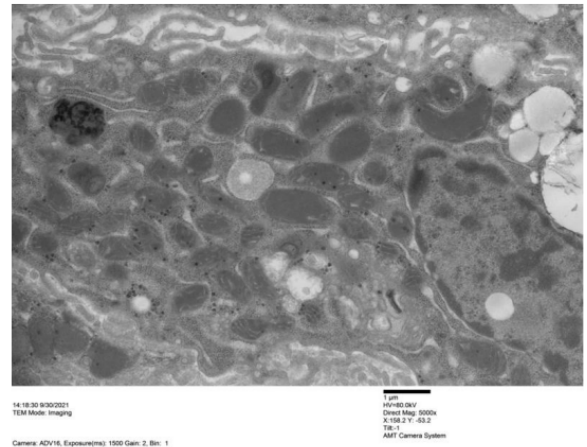


Image #2 Background liver H&E:

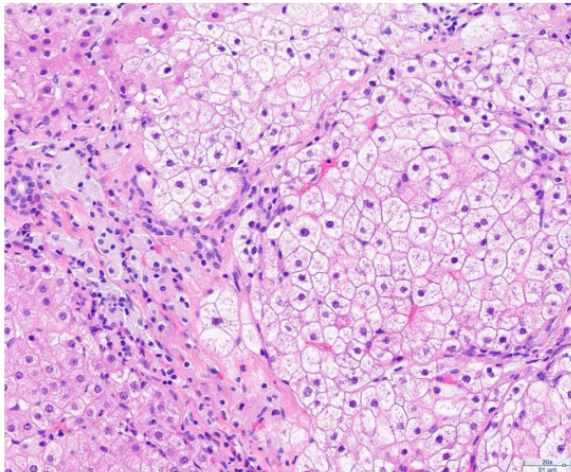


Image #5 HCC EM macrophage crystals:

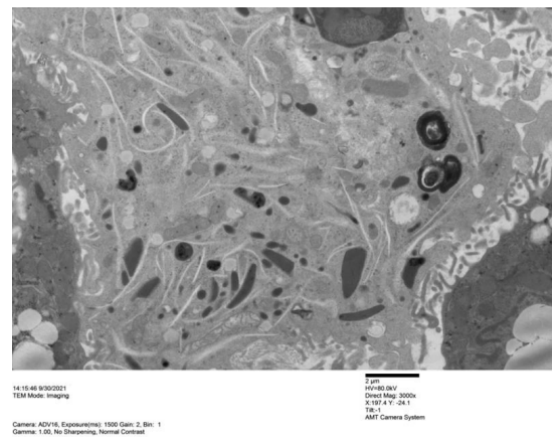
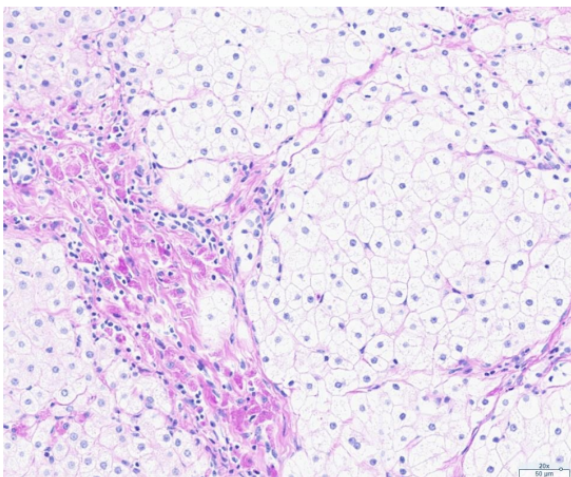


Image #3 Background liver PASD:



Genome-Wide Paternal Uniparental Isodisomy: Adding Pancreatic Well-Differentiated Neuroendocrine Neoplasms to the Spectrum of Associated Pathologies

K Grenier ¹, T Bhatti ², B Wilkins ², J Kalish ²; ¹ Children's hospital of Philadelphia, ² Children's hospital of Philadelphia

Background: Mosaic paternal uniparental isodisomy (pUPD) is a genetic phenomenon where part of the maternal contribution of a chromosomal region or the entire genome (GWpUPD) is lost and replaced by the paternal contribution, with various clinical presentations depending on the specific pUPD chromosomal region involved and the level of pUPD mosaicism in different tissues. pUPD including chromosome 11p15 (pUPD11) presents as a phenotypic spectrum between isolated hemihyperplasia and Beckwith-Wiedemann Syndrome (BWS). Affected patients can develop congenital endocrine abnormalities and are susceptible to developing embryonal tumors including pancreatoblastoma. While the congenital features of GWpUPD have been described, their evolution over time and the spectrum of findings at later ages are not well defined.

Methods: N/A

Results: Our patient is a 13 year old girl previously reported to have GWpUPD with findings of hemihyperplasia, bile duct hamartomas, and congenital hyperinsulinism, consistent with pUPD11. At 11 years old, she was diagnosed with breast fibroadenomas and pancreatoblastoma. Surgical resection included a lymph node showing a low-grade acinar proliferation, interpreted as differentiated metastatic pancreatoblastoma. In addition, a histopathological spectrum ranging from enlarged trabecular islets, to microscopic endocrine overgrowth into surrounding acinar tissue, and exaggerated ductulo-insular complexes containing nested endocrine proliferations was seen in the pancreatic parenchyma. The largest lesions showed circumscribed purely endocrine proliferations with nested, trabecular, glandular and microcystic growth with mitotic activity consistent with grade 2 pancreatic neuroendocrine tumor (panNET). At birth, GWpUPD mosaicism levels were reported at 30% in the peripheral blood. At 11 years of age, GWpUPD mosaicism levels were 98% in the peripheral blood and in the pancreatoblastoma.

Conclusion: Here, we add a case of pancreatoblastoma with differentiated lymph node metastasis and panNET arising in the background of islet cell adenomatosis to a previously reported GW pUPD case. To our knowledge, panNET represents a novel tumor association with GWpUPD and BWS. However, it remains unclear if this tumor represents the end-spectrum of GWpUPD/BWS-associated pancreatic neuroendocrine overgrowth or an independent neoplasm. Interestingly, this case also demonstrates an enrichment in GWpUPD mosaicism levels within peripheral blood and almost complete GWpUPD in the pancreatoblastoma. This suggests that GWpUPD clones may have a selective advantage and might increase the risk of developing pancreatic tumors, thereby supporting the recommendation of continued abdominal tumor screening in GWpUPD patients beyond 7

years.

A Rare Case of an Infant With TFE3 Mutation Presenting With Direct Hyperbilirubinemia and Hepatomegaly

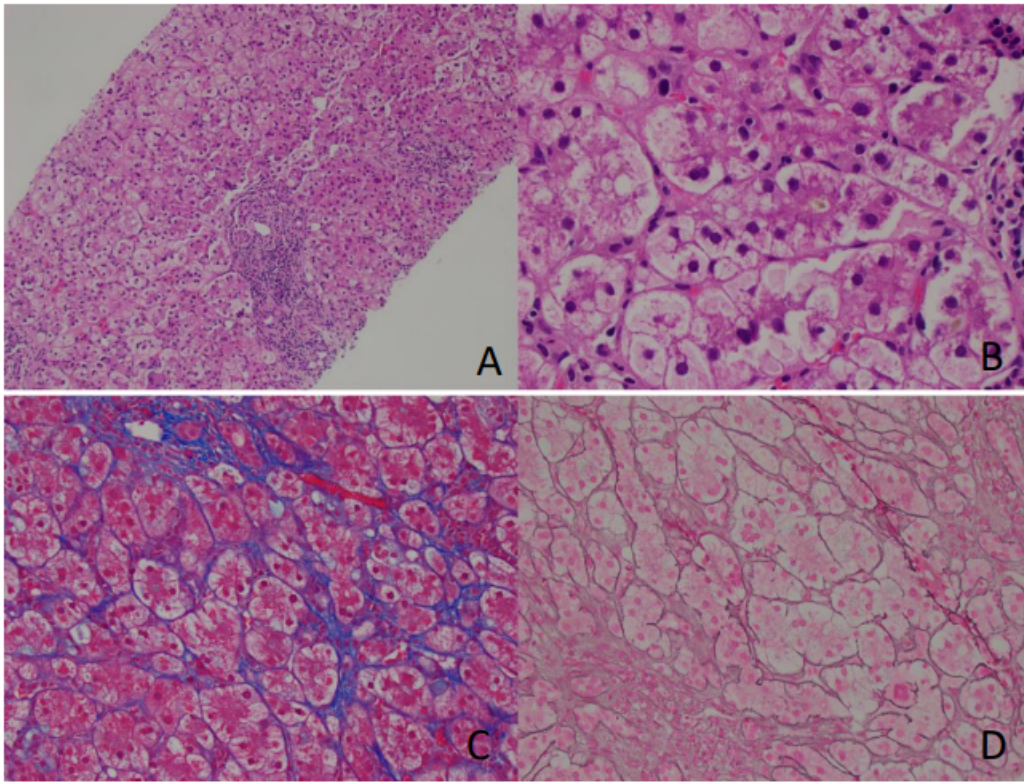
Q Zhang ¹, Y Haw ², A Axellbaum ¹, K Furuya ¹, J Gulliver ¹; ¹ University of Wisconsin Hospitals and Clinics, ² University of Wisconsin Hospital and Clinics

Background: TFE3 encodes a transcription factor with a basic helix-loop-helix (bHLH) domain. TFE3 gene mutation has been associated with multiple neoplasms including renal cell carcinoma, alveolar soft part sarcoma, perivascular epithelioid cell tumor, epithelioid hemangioendothelioma and others. Here we report a case of a 3-month-old male with an identified TFE3 mutation. The patient presented with worsening jaundice, direct hyperbilirubinemia, and hepatomegaly. The patient subsequently had two liver biopsies. The morphology of the second liver biopsy is detailed here, though both showed similar findings. The histologic pattern of liver injury associated with TFE3 mutation has not previously been described.

Methods: Light microscopic and electron microscopic examination were performed. Immunohistochemical staining for trichrome, reticulin, CK7, copper, iron, PAS, and PAS-D was performed.

Results: Microscopic sections of the liver biopsy showed liver parenchyma with extensive pseudo-rosette formation with severe canalicular cholestasis and giant cell reaction (Figures 1, Panel A and B). Trichrome staining demonstrated perisinusoidal fibrosis and reticulin stain highlighted the giant cell transformation (Panel C and D). CK7 showed bile ducts which were normal in size and number. Immunohistochemical staining for BSEP, MYO5B, and MDR3 showed retained canalicular staining, a normal pattern. Electron microscopy did not show evidence of a lysosomal storage disorder or mitochondrial disorder.

Conclusion: The MiT-TFE family of transcription factors plays a critical role in regulating various cellular metabolic processes. Organs such as the liver and muscles, which exhibit high metabolic activity, possess high expression of the TFE3 gene. This gene plays a critical role in regulating various metabolic processes, including lipid and glucose metabolism. Disruption of TFE3 gene expression in the liver could cause lipid and glucose metabolism disorders, resulting in serious consequences. In our case, the infant was confirmed to have a TFE3 mutation and presented with worsening jaundice, direct hyperbilirubinemia and hepatomegaly. Histologically, the main findings were a giant cell hepatitis pattern of injury with severe cholestasis and focal perisinusoidal fibrosis. Electron microscopy did not show any abnormal storage material. Neonatal liver abnormalities such as hepatomegaly and cholestasis have been described in association with TFE3 mutation. To the best of our knowledge, histologic findings in neonates with TFE3 mutation have not previously been described and represent an area for further study to provide prognostic and therapeutic guidance for future patients.



Figures 1 Panel A and B: Liver parenchyma with extensive pseudorosette formation with severe canalicular cholestasis and giant cell reaction. Panel C: Trichrome stain showing perisinusoidal fibrosis. Panel D: Reticulin stain highlighting giant cell reaction

A Case of Rare Kidney Tumor Harboring YWHAE-NUTM2 Infusion in a 3-Month-Old Male

Q Zhang G Zhang, P Kubica, C Bockoven, S Cook; University of Wisconsin Hospitals and Clinics

Background: Clear cell sarcoma of the kidney (CCSK) is the second most common malignant renal tumor in children after Wilms tumor. CCSK commonly accounts for 3% - 5% of all pediatric renal tumors and approximately 20 new cases are diagnosed annually in the United States. The National Wilms Tumor Study Group has reported that the morphology of CCSK exhibits diverse histologic variants, often making it difficult to distinguish CCSK from Wilms tumor. Here, we present the case of a 3-month-old male with progressive abdominal distention and a palpable abdominal mass, who was diagnosed with CCSK.

Methods: Microscopic examination, immunohistochemical (IHC) staining, and chromosomal analysis were performed.

Results: Light microscopy revealed tumor that is composed of sheets of uniform small round cells with clear cytoplasm and fine-to-open chromatin arranged in a delicate vascular network. Immunohistochemistry staining was employed and showed the cells were positive for Cyclin D1, BCOR, and SATB2 (Figure 1B, C, and D), had patchy positivity for PAX-8, were negative for WT-1, EMA, AE1/AE3, PHOX2B, and P53, and retained staining for INI-1 and BRG-1. Chromosomal analysis revealed a reciprocal translocation between chromosomes 10 and 17.

Conclusion: CCSK is the most frequently misdiagnosed renal tumor in children and there are no reliable imaging features to distinguish CCSK from Wilms tumor. Common clinical presentations include a large unilateral abdominal mass, abdominal pain, gross hematuria, and hypertension. In our case, the border between tumor and normal kidney parenchyma appears sharply demarcated on gross examination. At high magnification on light microscopy, subtle infiltration of tumor cells into the normal parenchyma at the periphery becomes apparent (Figure 1A). In addition, isolated native renal tubules are often entrapped throughout the tumor's peripheral regions due to the insidious expansion of cord cells in CCSK. This growth pattern serves as a crucial distinction from Wilms tumor, which typically exhibits a sharply defined pushing border with a capsule. Tandem duplication of the BCOR gene or YWHAE-NUTM2 fusion are two important biological abnormalities in CCSK. For our case, the IHC staining of BCOR is positive and the translocation between chromosome 10 and 17 results in fusion of YWHAE-NUTM2. Overall, CCSK is rare and often misdiagnosed. To avoid diagnostic pitfalls, it is crucial to recognize key histologic features such as trapping of normal tubules within the tumor and the lack of a well-defined capsule. The diagnosis should then be confirmed with appropriate IHC staining and molecular identification of YWHAE-NUTM2 fusion. In pediatric patients who present with a large solitary unilateral eccentric kidney mass, CCSK should always be considered in the differential diagnosis.

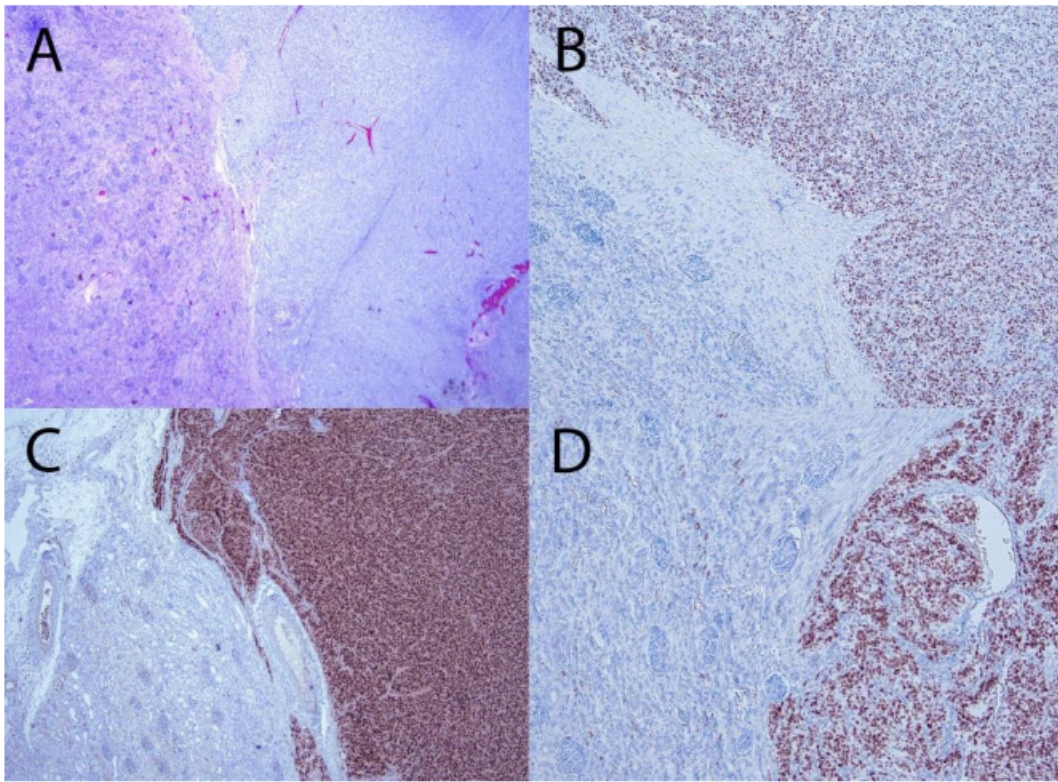


Figure 1: Light microscopy (2x) of CCSK showing characteristic subtle infiltration of tumor cells into the normal parenchyma at the periphery. (A) Immunohistochemistry staining is positive for (B) BCOR, (C) Cyclin D1, and (D) SATB2

Beyond Wilms Tumor: Case of Wilms Tumor Leading to Discovery of an Undiagnosed Genetic Syndrome

E Alston ¹, S Vargas ²; ¹ Boston Children's Hospital, ² Boston Children's Hospital

Background: Osteopathia striata with cranial sclerosis (OSCS) is a rare developmental syndrome caused by a germline mutation in WTX. It is an X-linked dominant disorder characterized by sclerosis of the long bones and skull with longitudinal striations of the long bones, pelvis, and scapulae. Other common features include macrocephaly, cleft palate, hearing loss, and distinct facies. Somatic WTX mutations are present in up to one third of Wilms tumors. At the time the tumor described herein was diagnosed, Wilms tumor had not been previously reported in OSCS.

Methods: We present a case of OSCS recognized at the time of pathologic evaluation of a renal mass, when pathologists were prompted by the finding of Wilms tumor to undertake medical review to evaluate a previously undiagnosed constellation of medical and phenotypic abnormalities.

Results: The patient was a 6-year-old female with a history of cleft palate who presented with flank pain and dark urine. An 8.9 cm renal mass was discovered, and a radical nephrectomy was performed. Histopathologic evaluation of the mass revealed a triphasic Wilms tumor without anaplasia or nephrogenic rests. Intrigued by the history of cleft palate, the pathology team combed the medical record and found that the patient had been evaluated by multiple services since birth for an apparent syndromic condition. Careful examination by the patient's geneticist over the years had revealed short stature, right postaxial polydactyly, macrocephaly with frontal bossing and bitemporal narrowing, slight pectus excavatum, nasal speech and distinct facial features including micrognathia, mildly low-set ears, crowded and small teeth, prominent nasal root, epicanthal folds, telecanthus, and facial asymmetry. Additional medical history included Pierre Robin sequence (with repaired cleft palate), conductive hearing loss, nasolacrimal duct obstruction, ventriculoseptal defect, and patent ductus arteriosus. Prior to presenting with Wilms tumor, no definitive underlying syndrome had been established. However, with the additional knowledge of the Wilms tumor and an understanding of its genetic features the diagnosis of OSCS was brought up in the pathology report as a unifying diagnosis. Follow-up showed that the patient indeed harbored a germline pathogenic variant in WTX, c.1057C>T (p.R353*). Since the time of this patient's diagnosis, Wilms tumor arising in OSCS has been reported in a handful of instances.

Conclusion: Together with recently reported cases, our case helps establish OSCS as a syndrome predisposing to Wilms tumor. Furthermore, our case demonstrates how the pediatric pathologist may be in a unique position to diagnose rare genetic syndromes at the time of tumor diagnosis based on knowledge of established--or potential--syndromic associations.

Müllerian-type Adenosarcoma With A Distinct Somatic Mutation Arising As The Fifth Neoplasm In A Pediatric Patient With DICER1 Syndrome

N SHILLINGFORD ¹, M Bitar ², M Harrell ², N Joseph ², A Minja ³, R Schmidt ², L Wang ², M Warren ², P Zamiara ², S Zhou ²; ¹ Children's Hospital Los Angeles, ² Children's Hospital Los Angeles, ³ Harbor-UCLA

Background: DICER1 syndrome is a relatively recently recognized familial tumor predisposition syndrome characterized by benign and malignant neoplasms. The most frequently reported malignancy is pleuropulmonary blastoma, however, an increasing number of neoplasms are being reported. Other neoplasms associated with DICER1 syndrome include embryonal rhabdomyosarcoma (ERMS), ovarian Sertoli-Leydig cell tumor (OSLCT), papillary thyroid carcinoma (PTC), cystic nephroma, Wilms' tumor, pituitary blastoma, pineoblastoma, sinonasal chondromesenchymal hamartoma, medulloepithelioma and others. We present a case of a 19 year old girl with DICER1 syndrome who developed a fifth neoplasm before age 20.

Methods: A 19-year-old girl with DICER1 syndrome presented because of heavy bleeding per vagina (PV). At 13 years of age, with a history of multinodular goiter (MNG) and pulmonary blebs, she expelled a fleshy tissue fragment per vagina which was diagnosis as ERMS. A CT scan detected a mass originating from the left ovary. Salpingo-oophorectomy was performed and a diagnosis of OSLCT was rendered. A month later she underwent a thyroidectomy for MNG. A 1.5 cm PTC nodule was found. Four years later a 4.3 cm right serous cystadenoma (SCA) was detected on surveillance. During workup for this new onset of PV bleeding a CT revealed a tubular structure within the vaginal vault. A biopsy was performed.

Results: Prior Sanger sequencing of the patient's blood revealed a DICER1 c.5504_5507delATCC (p.Tyr1835Serfs*2) germline mutation. Samples from the ERMS, OSLCT and PTC also showed the germline mutation. Additionally, somatic mutations c.5428G>C (p.Asp1810His), c.5439G>T (p.Glu1813Asp) and c.5113G>A (p.Glu1705Lys) were detected in the ERMS, OSLCT and PTC respectively. The SCA was not tested. Her mother, who has no history of neoplasms, also had the germline mutation. Two brothers did not have mutations (Table 1). Histologic sections from the vaginal mass show a biphasic neoplasm with a malignant mesenchymal component in association with benign glandular structures (Figure 1A) and increased mitotic activity (Figure 1B). The cells are strongly and diffusely positive for CD10 (Figure 1C) and desmin (Figure 1D) and negative for myogenin and MyoD1. NGS revealed the germline DICER1 mutation and a c.5425G>A (p.Gly1809Arg) somatic DICER1 mutation.

Conclusion: DICER1 syndrome is a tumor predisposing syndrome in which patients develop a host of malignant and benign tumors. It exhibits variable expressivity as evidenced in this case where the patient has developed 5 tumors before the age of 20 while her mother has not had a neoplasm. To our knowledge there has not been a report of child with five neoplasms in

the English literature. This case serves to highlight the importance of surveillance in patients with DICER1 syndrome.

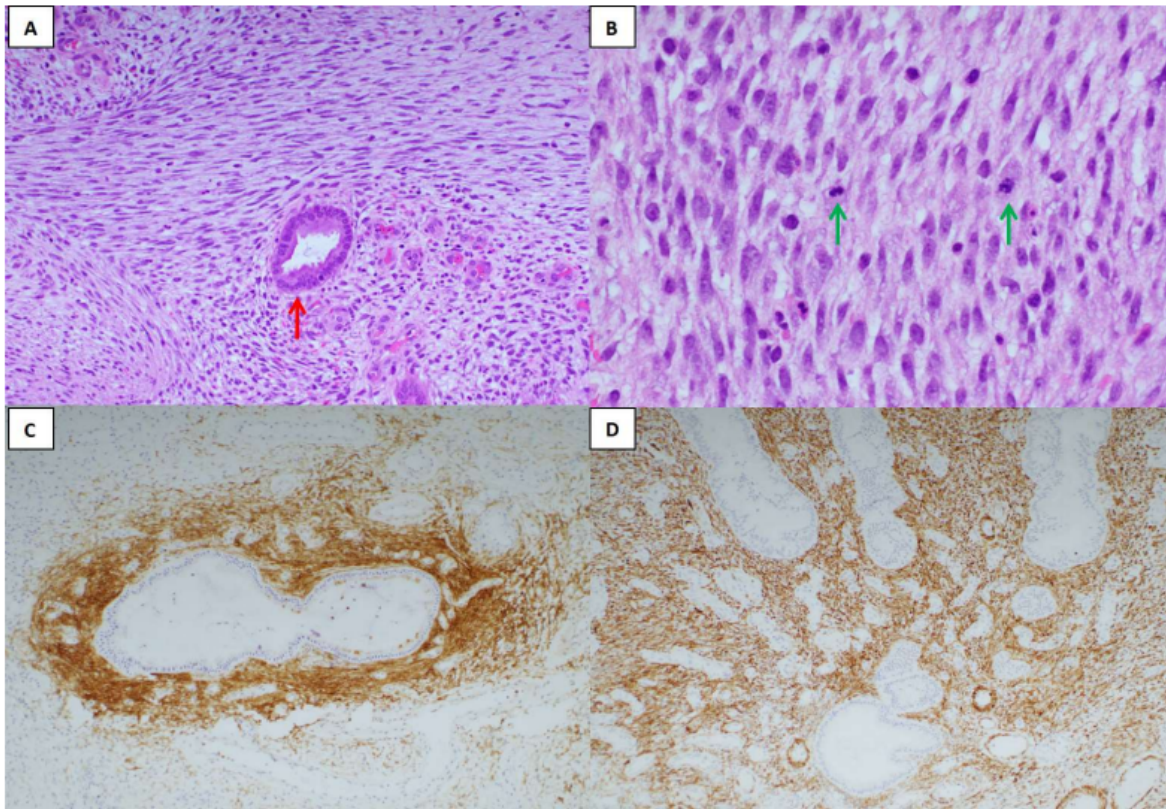


Figure 1. Uterine adenosarcoma. Histologic sections show a low grade malignant mesenchymal neoplasm composed of spindle cells accompanied by benign glandular structures (1A). The stromal component demonstrates increased mitotic activity (1B). Immunohistochemical stain for CD10 (1C) shows strong cytoplasmic positivity in the areas of periductal condensation of malignant cells while desmin (1C) is diffusely positive.

DICER1-Associated Sarcoma Arising in Retroperitoneal Mature Cystic Teratoma: A case report and literature review

A Oren ¹, C Guardado Salazar ², N Shillingford ³, B Pawel ³, L Wang ³, M Warren ³, S Zhou ³, R Schmidt ³, P Zamiara ³; ¹ Children's Hospital Los Angeles, ² Valley Children's Hospital, ³ Children's Hospital Los Angeles

Background: DICER1, located on chromosome 14q, encodes an enzyme critical for microRNA maturation, which regulates post-transcriptional gene activity. Biallelic inactivation of DICER1 can occur through either two somatic events or a combination of somatic and germline inactivation, leading to impaired production of mature miRNAs. When a tumor is found to have biallelic DICER1 mutations without a prior diagnosis of DICER1 syndrome, it is essential to conduct germline testing. A positive result would warrant further screening for additional tumors and genetic counseling for family members. Teratomas are not considered part of the spectrum of tumors arising in DICER1 syndrome and the identification of biallelic DICER1 somatic mutations therein is very rare. Malignant transformation of teratomas occurs in approximately 2% of all cases, with squamous cell carcinoma being the most common. Pure sarcomas rarely arise from teratomas.

Methods: Microscopic examination with H&E and immunohistochemical stains was performed. Ancillary techniques included targeted next generation sequencing (NGS), chromosomal microarray, and Sanger sequencing.

Results: A 2-year-old girl without any significant family history presented to medical attention with abdominal distension and firmness. An abdominal MRI revealed a multi-cystic retroperitoneal mass, suspected to represent lymphatic malformation, prompting serial doxycycline sclerotherapy. However, the mass persisted and demonstrated increased complexity on repeat imaging. Ultimately, the patient underwent exploratory laparotomy and resection of the mass. Gross examination demonstrated a 19.3 cm mass with cystic (expressive of serous fluid) and solid (tan and fleshy) components. Microscopic evaluation of the cystic component revealed mature teratoma, with tissue derived from endoderm, mesoderm, and ectoderm (Fig.1 A-C). The solid component, meanwhile, revealed hypercellular foci of so-called “small round blue cells”, showing a herringbone and fascicular architecture, abundant mitotic figures, and intimate association with hyaline cartilage (Fig.1 D-F). An immunohistochemical panel including myogenin, myoD1, NKX2.2, WT1, SSX, and TdT was negative in the sarcomatous cells of interest. INI1 and BRG1 staining were retained. Targeted NGS (OncoKids® pan-cancer panel) showed biallelic inactivating DICER1 mutations (NM_177438.3: c.5439G>T and c.4405_4406delCT). Follow-up Sanger sequencing of peripheral blood was negative for germline DICER1 mutations. Insert image.

Conclusion: We report a retroperitoneal mature cystic teratoma harboring DICER1-associated malignant sarcomatous transformation in a 2-year-old girl. Sanger sequencing confirmed the somatic origin of both DICER1 mutations, representing an exceedingly rare

somatic malignancy arising in teratoma.

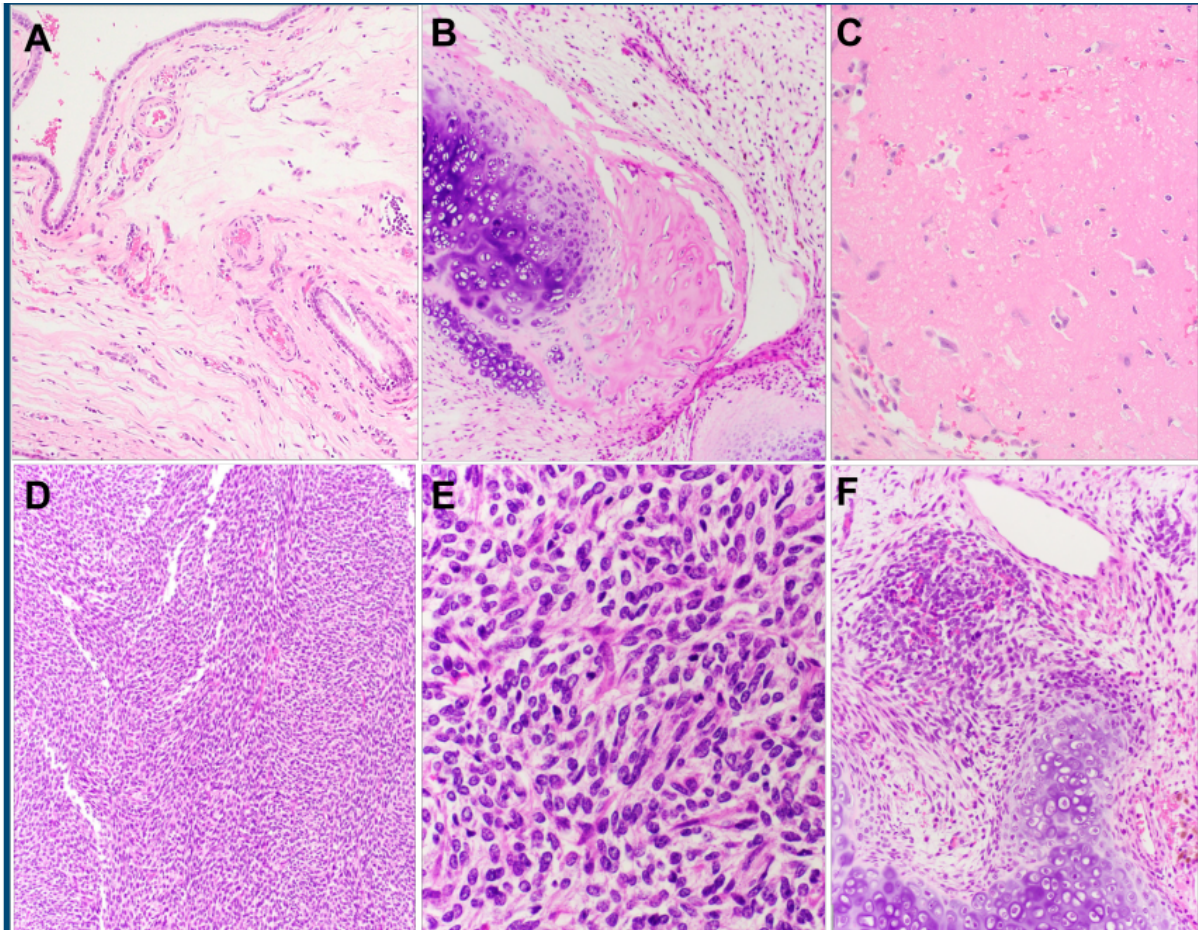


Figure 1, microscopic H&E: Cyst lined by simple columnar epithelium; gastric foveolar epithelium is also apparent - endoderm component, 200x (A). Hyaline cartilage and focal bone, mesoderm component, 200x (B). Mature neuroglial tissue, ectoderm component, 200x (C). Solid component shows foci of herringbone and fascicular architecture with scattered thin-walled vessels, 100x (D). Multiple mitotic figures identified in the solid component; up to 22 per 10 high-power fields 400x (E). Primitive blastema-like cells emanating from hyaline cartilage, 200x (F).

Highly Unusual Pure Squamous Malignant Transformation of Childhood Giant Cell Tumor of Bone

A Oren ¹, W Shon ², E Vail ², B Balzer ², H Maluf ², L Wang ³, X Fan ²; ¹ Children's Hospital Los Angeles, ² Cedar Sinai, ³ Children's Hospital Los Angeles

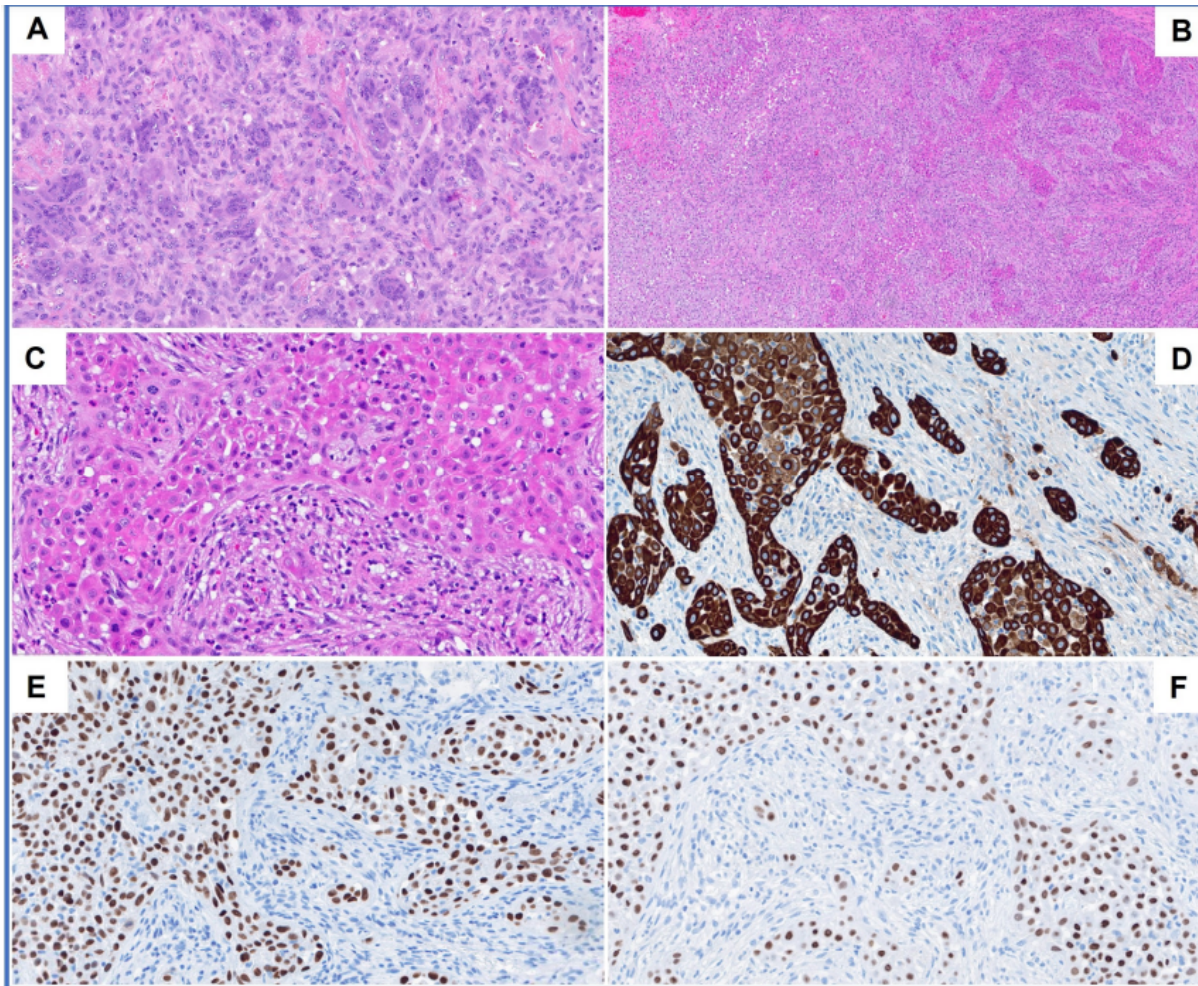
Background: Giant cell tumor of the bone (GCTB) is a benign tumor, mostly occurring in skeletally mature individuals, with a low incidence in children. Despite their benign nature, GCTBs can display locally aggressive behavior, high recurrence rates, and infrequent malignant transformation, typically to sarcomas. Children with GCTB have a higher incidence of multicentric disease and local recurrence compared to adults. Malignant transformation of GCTB can be either primary, arising adjacent to the benign tumor, or secondary, arising at the site of previously documented GCTB. Secondary malignant transformation is more common after radiotherapy rather than surgery alone. More than 95% of both conventional and malignant GCTBs exhibit a mutation in the H3F3A gene. Histone H3.3 G34W is expressed in the nuclei of the mononuclear cell population of H3F3A-altered GCTB, and IHC can provide valuable support for diagnosis. A comprehensive literature search yielded only one previous case of GCTB malignant transformation into a carcinosarcoma with osteogenic sarcoma and squamous cell carcinoma components.

Methods: Microscopic examination with H&E and immunohistochemical stains was performed. Ancillary techniques included 500 gene panel next-generation sequencing (NGS).

Results: A 34-year-old male with a history of GCTB in the lumbar spine, treated with resection and instrumentation at 13 years of age at a local Children's Hospital, presented with worsening back pain. He had no history of radiation therapy. Imaging revealed a large osteolytic lesion involving the T1 and T2 vertebral body. Resection revealed a poorly differentiated carcinoma involving bone. The tumor exhibited histopathologic and immunophenotypic features (positive for AE1/AE3, P63, and P40, and negative for TTF-1, Napsin A, and P16) compatible with a squamous cell carcinoma (SCC) of unknown origin (Fig. B-E). Further molecular characterization via next-generation sequencing (NGS) surprisingly revealed the presence of a H3F3A p.G35W mutation, not characteristic of SCC but of GCTB. IHC for H3F3A G34W was performed and demonstrated positive nuclear staining in the squamous cell carcinoma while background reactive-appearing spindle cells were negative (Fig. F). The original pathology of the L4 tumor resected 21 years prior was obtained and reviewed with additional studies performed. A giant cell tumor of bone was confirmed histologically (Fig. A). This was further supported by positive H3F3A G34W immunostaining and the presence of H3F3A p.G35W mutation by NGS. Insert image.

Conclusion: We present a unique case of malignant SCC transformation in a recurrent GCTB of the thoracic spine, 21 years after the initial resection during childhood. The squamous cell carcinoma in this case exhibits characteristic immunophenotypic and molecular features of GCTB, confirming a malignant transformation from a GCTB into a SCC. A malignant transformation from GCTB to a pure SCC has not been previously reported in the English

literature.



Original L4 tumor demonstrating typical features of a giant cell tumor of bone with numerous osteoclast-like giant cells embedded in mononuclear and neoplastic spindled stromal cells (A). T1 lesion demonstrating infiltrative poorly differentiated squamous cell carcinoma in spindled cell stroma at lower power (B) and higher power (C). Positive staining for AE1/AE3 (D), P40 (E), and H3F3A G34W (F) identified in carcinoma while surrounding nonneoplastic stromal cells are negative for these immunostains.

Pediatric Malignant Mesothelioma In A Patient With A History Of Marfan's Syndrome

S Fitzlaff H Correa, C Hughes; Vanderbilt University Medical Center

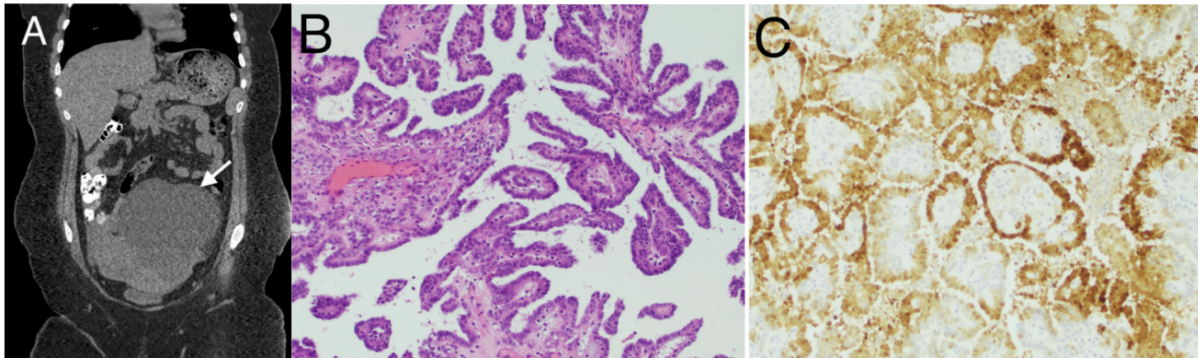
Background: Malignant mesothelioma (MM) is an aggressive tumor that arises from the serosal membranes that line the body cavities. MM is exceedingly rare in the pediatric population and it is not uncommon for it to be initially misdiagnosed. In children, the most common primary site is the peritoneum, in contrast to the pleura in adults. Treatment strategies vary, however most patients receive cytoreductive surgery with hyperthermic intraperitoneal chemotherapy (HIPEC) and adjuvant chemotherapy. Pediatric MM has a less aggressive behavior than that observed in adults, though there is a high rate of recurrence. In this case report, we describe a case of a 16-year-old female with Marfan's syndrome diagnosed with MM of the pelvic peritoneum. We aim to expand awareness of this rare tumor in the pediatric population and discuss the possibility of Marfan's syndrome as a predisposing factor for the development of malignancy, especially MM.

Methods: Hematoxylin and eosin (H&E) staining and immunohistochemistry (IHC) were performed routinely per standard practice.

Results: A 16-year-old female with Marfan's syndrome (MFS) presented with abdominal pain and nausea. A CT scan revealed a complex pelvic mass measuring 24 cm in greatest dimension (Figure A). Laboratory workup was notable for a mildly elevated CA-125. An exploratory laparotomy was performed with a moderate amount of ascites within the abdomen, a 12 cm multicystic and solid cul-de-sac mass with dense adhesions, and small implants on the bladder peritoneum. A sub-optimal debulking was performed with grossly visible residual disease. H&E-stained sections showed sheets of epithelioid cells forming papillae and tubular structures surrounded by reactive spindled cells (Figure B). The tumor cells were cytologically bland and mitoses were infrequent. Ovarian neoplasms considered in the differential diagnosis included serous carcinoma, malignant germ cell tumors, especially yolk sac tumor, malignancy arising from a teratoma, amongst others. Tumor cells were positive for calretinin (Figure C), CK5/6, EMA, WT1, D2-40, and CK7, with patchy expression of PAX8 and p16. p53 showed wild type expression and BAP-1 was retained. The patient was diagnosed with MM, epithelioid type, tubule-papillary subtype with involvement of the cul-de-sac, peritoneum, and the omentum with prominent lymphovascular involvement. Neoadjuvant chemotherapy with cisplatin and paclitaxel was initiated. She then returned to the OR for resection of the remainder of the tumor and HIPEC. This operation was followed by cycle 4 of chemotherapy, and the patient is currently stable.

Conclusion: In conclusion, we present an incredibly rare diagnosis in pediatric pathology that poses unique diagnostic and therapeutic challenges. Many reports suggest an association between MFS and hematologic and solid malignancies with one study showing patients with MFS have a higher risk of malignancy compared to the general population. Furthermore, it has been proposed that connective tissue disorders such as MFS could be a predisposing factor for MM specifically due to the abnormal collagen produced in both connective tissue

syndromes and MM. As such, this is the first pediatric patient and third reported patient with MFS diagnosed with MM.



A Case Of Chorangiomas And Chronic Histiocytic Intervillositis In The Setting Of Acute COVID-19 Infection And HELLP Syndrome

S Fitzlaff C Hughes, S Schauwecker; Vanderbilt University Medical Center

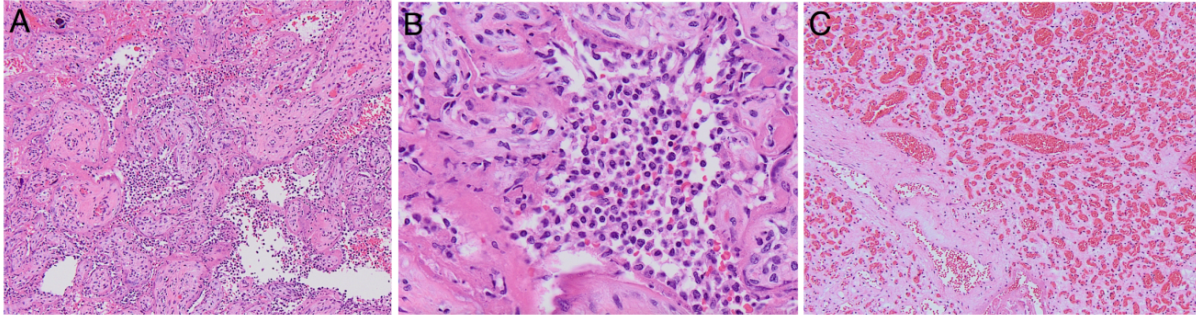
Background: The COVID-19 pandemic has resulted in millions of infections worldwide and is a risk factor for multiple adverse pregnancy outcomes. Histopathologic evaluation of the placenta is critical to characterize changes that may occur in the setting of maternal COVID-19 infection, and what, if any, adverse outcomes result. The placental findings in COVID-19 infection are variable with some reports describing no significant change; however, the most commonly reported pathologic findings are related to maternal vascular malperfusion although evidence of fetal malperfusion and inflammation have also been described. In this case report we present a case of IUFD in the setting of COVID-19 infection and HELLP syndrome with histopathologic findings of chronic histiocytic intervillositis (CHI) and chorangiomas (CM). CM has not been previously described in association with COVID-19 infection.

Methods: Hematoxylin and eosin (H&E) staining and immunohistochemistry (IHC) were performed routinely per standard protocol. Over-the-counter, at home, COVID-19 antigen diagnostic test.

Results: A 22-year-old primigravida presented at 32 weeks gestation with preterm uterine contractions. She was diagnosed with COVID-19 four days prior to presentation via an at-home, rapid antigen test, and was symptomatic with diarrhea and loss of taste and smell. Her pregnancy was otherwise complicated by chronic hypertension, glucose intolerance, and anxiety. An anatomy scan at 20 weeks was normal. On initial assessment, fetal heart tones were absent and ultrasound confirmed fetal demise. Her blood pressure was elevated and she had thrombocytopenia, hypofibrinogenemia, and transaminitis, concerning for HELLP syndrome versus abnormalities related to COVID-19. Labor was induced, and she delivered a stillborn phenotypically normal female infant. Gross examination of the placenta revealed an intact basal plate, semi-opaque fetal membranes, and a hypocoiled (1 coil per 10 cm) three-vessel umbilical cord. H&E stained sections of the placental disc revealed maturing villi with acute subchorionitis, diffuse perivillous fibrin deposition (Figure A), diffuse CHI (Figure B), and CM (Figure C). A CD168 immunostain highlighted increased macrophages.

Conclusion: The pathology in this case, including diffuse CHI and perivillous fibrin deposition, have been reported in cases of IUFD associated with COVID-19 infection; however, CM has not. CM is a villous capillary lesion believed to be related to hypoxia, though the pathogenesis is incompletely understood. CM has been associated with pre-eclampsia, extreme prematurity, congenital malformations, and IUGR. This patient also had clinical features of HELLP syndrome which has been observed to overlap with COVID-19 infection throughout the pandemic. The multitude of clinical and histologic factors in this case, including HELLP syndrome, COVID-19 infection, diffuse CHI, and CM ultimately led to fetal demise, though the sequence and association of these diagnoses is unclear. As this is

the first case reported of CM in association with maternal COVID-19 infection, further research is needed to understand the relationship between the two and its impact for mother and neonate.



MULTIFOCAL CHORANGIOMATOSIS, MOLECULAR INVESTIGATION OF A RARE ENTITY

P Charles ¹, E Azzato ², M Jakubowski ², A Heerema-McKenney ²; ¹ Cleveland Clinic Pathology and Laboratory Medicine Institute, ² Cleveland Clinic

Background: Multifocal Chorangiomas (MC) is a rare placental pathology characterized by multiple, large, tumor-like vascular proliferations in the villous parenchyma that are grossly evident. The clinical presentation of MC ranges from uneventful peripartum courses to poor fetal outcomes such as hydrops fetalis and fetal death. The precise etiology is unclear, however recurrence of MC in some families and the pathology of multiple benign "tumorlets" suggests a genetic abnormality. A recent study suggests possible associations between MC and TP53 mutations. To date, we are aware of no reported case of MC with extensive molecular genetic investigation for known cancer-causing genes. We present a recent case of this rare entity with associated molecular investigations.

Methods: With consent from the patient, lesional (chorangioma) and control (umbilical cord) paraffin embedded tissue was utilized for molecular analysis. Extracted nucleic acid from the specimens, both DNA and RNA, were subjected to separate targeted amplification reactions, using AmpliSeq custom primers designed by Thermo Fisher Scientific (Thermo Fisher Scientific, Waltham, MA). DNA hotspots and selected fusions in 59 genes were sequenced using Illumina (San Diego, CA) 2x150 paired-end cycle chemistry. A customized bioinformatics analytical platform was used for read alignment (Genome Build GRCh37/hg19), variant identification and annotation. In addition, P53 (1:50 dilution, DO-7 mouse monoclonal, Ventana) immunohistochemical staining was performed.

Results: Review of clinical history revealed a family history of sporadic cancers and a history of small for gestational age in a previous gestation (placenta not evaluated). This was an uncomplicated pregnancy that ended at 37 weeks and 6 days via spontaneous vaginal delivery. A 2.7kg live neonate with Apgar's 9(1) and 9(5) was delivered. The gross placental examination was significant for a hyper-coiled 3-vessel umbilical cord and a fixed placental weight of 369g, (less than the 3rd percentile). Sectioning of the placenta revealed approximately 20 gray-white rubbery nodules distributed throughout the dark-red spongy parenchyma, ranging from 0.5 to 2.0 cm. Microscopically, the nodules were comprised of chorangiomas at the cellular (early) stage. The remaining placenta showed mature third trimester villous maturation with a small peripheral infarct. The molecular assay showed no abnormalities in the queried genes. Immunohistochemistry for p53 showed a wild-type pattern of nuclear staining. The child has normal development at 1 year of age.

Conclusion: We report a classic case of multifocal chorangiomas of the placenta associated with normal fetal growth and development. No genetic abnormalities were found on comprehensive analysis. Immunohistochemistry for p53 shows a wild-type pattern of staining.

Intravillous Bizarre Cytologic Changes in a Premature Infant with Coats Plus syndrome

J Slack L Rabinowitz; Cleveland Clinic

Background: CTC1 (CST Telomere Replication Complex Component 1) is a component of the CST complex essential in telomere replication. Defects in CTC1 are implicated in the autosomal recessive disorder Coats Plus (cerebroretinal microangiopathy with calcifications and cysts) characterized by retinal telangiectasia and exudates, intracranial calcification with leukoencephalopathy and brain cysts, osteopenia/fracture predisposition, bone marrow suppression, gastrointestinal bleeding, and portal hypertension. To our knowledge, there have been no previous reports of specific cytologic placental abnormalities associated with Coats Plus disorder.

Methods: H&E-stained paraffin embedded sections were evaluated. Immunohistochemical staining was performed using standard immunostaining procedures.

Results: A 30-week female newborn with fetal growth restriction was delivered by emergent c-section for decreased fetal movement and category 2 tracing, with Apgars of 1 (1 min) and 7 (5 min). The mother had a history of mild Von Willebrand disease and HSV positivity. Evaluation revealed a small for gestational age newborn (birth weight 817 g) with exudative retinopathy, mineralizing lenticulostriate vasculopathy in the left thalamus, persistent pulmonary hypertension, and other issues related to prematurity. Urine CMV was negative. A vitreoretinopathy panel established the diagnosis of Coats Plus disorder with the detection of two pathogenic heterozygous mutations for CTC1 {c.2954_2956del, p. (Cys985del); c.724_727del, p. (Lys242Leufs*41)}. The placenta showed numerous intravillous vascular and stromal cells displaying striking cytologic abnormalities and high grade chronic villitis of unknown etiology. These cells showed marked variable karyomegaly, with polylobate nuclei, hyperchromasia and prominent nucleoli. The bizarre cytology raised concern for viral infection. Similarly, the vasculocentric location raised the possibility of intravascular tumor. Stains for CMV, HSV and EBV were negative. Many bizarre cells were immunoreactive for ERG, CD34, CD31, desmin and vimentin, supporting a vascular differentiation, and negative for HCG, Sox10, epithelial and lymphohistiocytic markers.

Conclusion: We document the first description of an unusual placental pathology for a neonate born with Coats Plus syndrome. The awareness of this finding could inform future pathologic workup of similarly affected placentas, where the degree of cytologic atypia might suggest infection or neoplasm. This pathology can also prompt more specific investigation for Coats Plus syndrome in the infant. The mechanism whereby CTC1 mutations may induce cytologic atypia is unclear, however the resemblance of these cells to degenerative atypia (“ancient change”) in a variety of neoplasms may provide a pathway for future investigation.

Transplacental Hematogenous Spread of Congenital Sarcoma between Monochorionic Triplets.

J D'Ardis ¹, T Boyd ², C Kim ², K Patel ², N Quintanilla ², E Taylor ³; ¹ CAP, USCAP, TSP, SPP, ² Texas Childrens, ³ Baylor College of Medicine

Background: A G2P1001 female with no significant medical history delivered triamniotic dichorionic triplets at 32 weeks 6 days via Cesarean section due to a large obstructive neck mass in triplet B.

Methods: The submitted placenta showed a triamniotic dichorionic triplet placenta with diamniotic monochorionic dividing membranes between triplets A and B. The vasculature of placenta A was injected with ink, however, the vasculature of placenta B could not be injected due to a disrupted umbilical cord at the insertion site. Nevertheless, inked grossly appeared to extend across the dividing zone and was visualized at the base of umbilical cord B, consistent with vascular anastomoses. Triplet C had a triamniotic dichorionic placenta and did not share circulation with triplets A and B.

Results: Microscopically, triplet B had rare hypercellular chorionic villi mimicking stromal hypercellularity seen in preterm placentas. No similar foci were identified in Triplet A or C. Subsequently, biopsy of the neck mass in Triplet B revealed a small round blue cell tumor with diffuse membranous staining for CD99 and CD56. The tumor was negative for NKX2.2, desmin, myogenin, MPO, CD43, Phox2B, WT1, calretinin, Sat2B, S100, CD45 LCA, synaptophysin, chromogranin, and ERG. It had retained nuclear expression of INI-1 and BRG1 with strong to moderate nuclear expression for H3K27. BCOR internal tandem duplication test was negative. Molecular analysis revealed HNF1A loss within the tumor that was not reported in the germline constitutional microarray, suggesting a somatic origin. Triplet B died at 5 weeks of age due to widely metastatic disease. A few weeks after the diagnosis of triplet B, a growing mass was noted in the antecubital fossa of triplet A. Resection of the mass revealed a high-grade small round blue cell sarcoma, morphologically resembling his identical twin's tumor, with a similar immunoprofile and similar loss of HNF1A by molecular testing, suggesting a common clonal origin. Triplet A has received 2 cycles of chemotherapy followed by re-resection (due to a positive margin) and is alive to date. Triplet C is healthy with no evidence of disease. This case illustrates placental metastasis of a congenital sarcoma in triplet B with evidence strongly supportive of hematogenous metastatic spread to triplet A via inter-placental vascular anastomoses.

Conclusion: This theory is supported by the similar immunophenotypic and molecular profiles between the tumors and the sparing of Triplet C, who did not have a shared circulation. Although cases of intraplacental metastases have been previously reported, their occurrence is rare.

A Novel Case of Atypical Ductal Proliferation Involving a Papillary-Cystic Salivary Gland Neoplasm

K Jorgenson ¹, C Griffith ², A Israel ¹; ¹ University of Rochester Medical Center, ² Cleveland Clinic

Background: According to the National Cancer Institute's SEER Program, in 2020 the incidence of oral cavity and pharynx cancers was 0.2/100,000 children. We report a case of a papillary-cystic neoplasm of the lip with features resembling multiple salivary gland neoplasms, but not fitting precisely into one specific diagnosis.

Methods: A 4-year-old male presented with a slowly enlarging, 1 cm, firm, nontender submucosal lower lip mass, clinically thought to be a mucocele or pyogenic granuloma.

Results: Sections reveal a nested salivary gland neoplasm with focal connection to the surface mucosa. Tumor cells are uniform with round nuclei and occasional mitotic figures. The tumor nests show rounded borders and demonstrate cribriform, papillary and solid architecture, reminiscent of intermediate grade ductal carcinoma in situ (DCIS) of the breast. While there is a degree of sclerotic stroma surrounding the tumor nests, invasion is not identified. The un-oriented specimen was not processed as a marginal resection, limiting assessment of tumor distance to tissue edges. However, where evaluable, a rim of normal tissue surrounds the tumor nests, with a closest distance of < 0.1 cm from the specimen edges. Immunohistochemistry highlights that the lesional cells express CK7, Cam 5.2, S100 and mammaglobin (patchy). SOX10 expression is equivocal. Calponin, SMA, p40 and p63 highlight a peripheral myoepithelial layer surrounding the tumor nests, as well as lining the fibrovascular cores of papillae. AR and pan-TRK are negative. Ki-67 proliferative index is variable and overall low (< 5%). Mucicarmine highlights intra- and extracellular mucin. A next generation sequencing panel to detect common salivary gland/head and neck tumor rearrangements was performed and did not identify a rearrangement. The morphologic features of this tumor are unusual and not characteristic of any typical salivary gland neoplasm. While intraductal carcinoma is a differential consideration, lack of a gene rearrangement, equivocal SOX10 and patchy mammoglobin expression, round rather than oval nuclei (intercalated duct subtype), lack of snouting (apocrine subtype) and inconspicuous nucleoli (oncocytic subtype), preclude this diagnosis. Based on the presence of intraductal papillary growth, connection to the surface mucosa and lack of identifiable chromosomal rearrangements, we think this tumor is best classified as an atypical ductal proliferation involving a papillary-cystic salivary gland neoplasm. Insert image

Conclusion: We are not aware of similar prior reported cases, which makes it difficult to predict clinical behavior. However, due to its low-grade appearance, limited mitotic activity and nested architecture, we believe the tumor is likely indolent and recommend close clinical follow-up after complete excision.

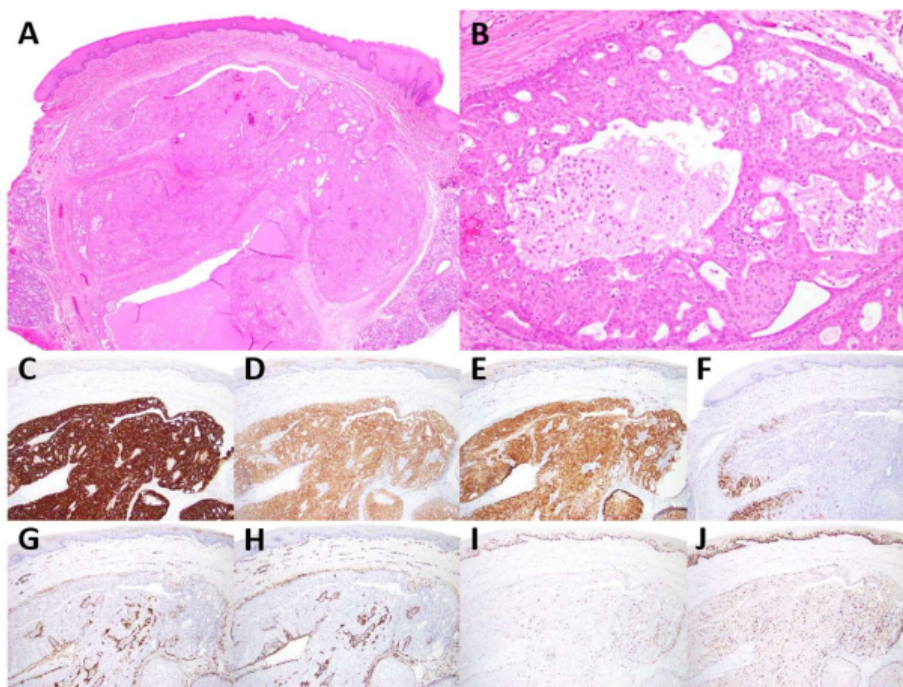


Figure 1. Papillary-cystic salivary gland neoplasm, (A) H&E, x20; (B) H&E, x100; (C) CK7, x40; (D) Cam 5.2, x40; (E) S100, x40; (F) Mammaglobin, x40; (G) Calponin, x40; (H) SMA, x40; (I) p40, x40; (J) p63, x40.

Neonatal Head and Neck Tumors with Multiphasic Differentiation: A Differential Diagnosis

K Jorgenson ¹, A Israel ², P Katzman ¹; ¹ University of Rochester Medical Center, ² University of Rochester

Background: Nasopharyngeal masses pose issues for neonates in breathing and for pathologists to diagnose due to sampling limitations. The presence of both epithelial and mesenchymal cell proliferations can help narrow a differential diagnosis, but if all components necessary for a diagnosis are not identified, a relevant diagnosis may be erroneously omitted or undervalued.

Methods: We review two cases of midline nasopharyngeal tumors in neonates who presented with respiratory distress since birth and discuss the differential diagnosis of bi- and ‘multi’ phasic tumors in this setting.

Results: Case 1: Laryngoscopy of a 3-day-old female identified a polypoid mass on the left nasal cavity floor extending into the nasopharynx. Histology showed sheets of round to spindle pleomorphic cells with vesicular nuclei, gland formation, and foci of squamous differentiation (A – D). Due to necrosis and Ki-67 proliferation up to 20%, a malignant neoplasm was initially favored, however, upon further review the most likely diagnosis was determined to be a salivary gland anlage tumor (SGAT). Case 2: A biopsy was obtained from a 4-day-old female with a mass filling the nasopharynx. Sections revealed a myxoid stroma with low cellularity, skeletal muscle fibers, fragments of squamous and glandular epithelium thought to be due to entrapment (E & F), and a focus of small round blue cells. A diagnosis favoring rhabdomyoma was rendered. Subsequent resection of the tumor revealed mature elements of all three germ layers (G & H), leading to the diagnosis of a mature teratoma.

Insert image

Conclusion: SGATs exhibit mesenchymal spindle cell stroma around squamous nests and duct networks. They are typically located in the posterior nasopharynx and have been suggested to be best classified as hamartomas. Intranasal pleomorphic adenomas (PA) are uncommon in neonates, usually appearing during the third to sixth decades of life, and exhibit a higher proportion of epithelial to stromal components than their equivalent in the major salivary glands. Synovial sarcomas can be monophasic or biphasic with glandular or solid epithelial cells, occur rarely in the sinonasal tract and skull, and are more likely to be seen in older children in the soft tissue of the neck or elsewhere. While not strictly ‘phasic,’ teratomas involve tissues from all three germ layers, resembling biphasic tumors. Head and neck teratomas are rare but are most frequently reported in the sinonasal tract and nasopharynx. Diagnostic challenges arise in biopsy when only one or two components are sampled, as seen in Case 2. When faced with a biphasic midline tumor of the nasopharynx in a neonate, one should consider SGAT, PA, and synovial sarcomas. However, even when only two components are visible, the possibility of a teratoma should not be dismissed.

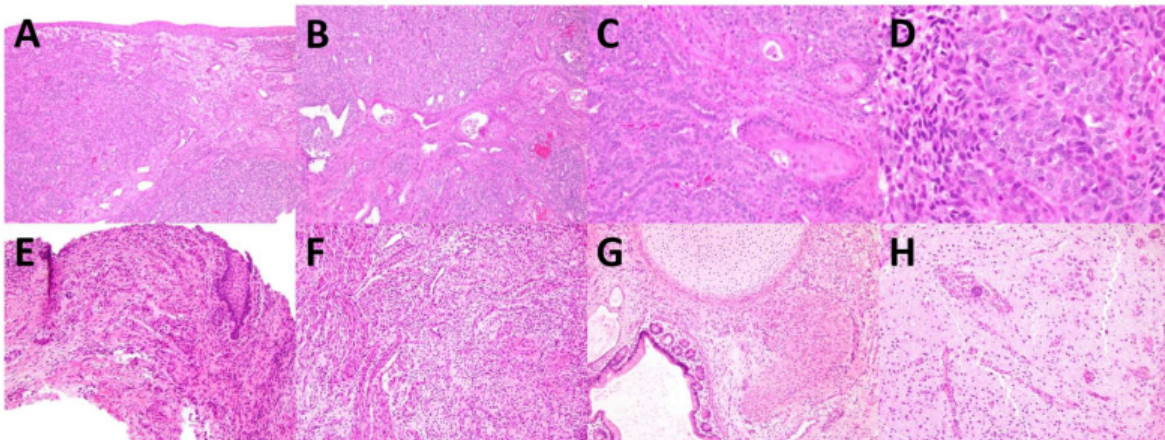


Figure 1. H&E of Case 1: Salivary gland anlage tumor, (A) x100, (B) x100, (C) x200, (D) x400; Case 2: biopsy favoring Rhabdomyoma, (E) x100, (F) x100; Case 2: resection of mature teratoma (G) x100, (H) x100.

A Case of Oculo-Auriculo-Vertebral Spectrum (OAVS) with Multiple Midline Duplications and a Lesion of the Ocular Surface: Relationships to Etiology of Twinning?

E Cochran B Zoshchuk; Penn State Health

Background: Oculo-auriculo-vertebral spectrum (OAVS) is a condition characterized by hemifacial microsomia, cleft lip/palate, hearing impairment, vertebral anomalies, and ocular lesions. Twinning has been shown to occur in higher incidence among individuals with Oculo-Auriculo-Vertebral Spectrum in several studies. Wieczorek et al. reported a twin rate of 7.46%, Lawson et al. reported a twin rate of 6.9%, and Werler et al. reported a twin rate that was higher than expected. The etiology of OAVS is unknown, but thought to be multifactorial with interactions of multiple genes and epigenetic factors. Theories as to the relationship between OAVS and twinning include 1) that the environment of twinning could predispose to OAVS, and 2) that OAVS and twinning share a common genetic developmental etiology.

Methods: We review a case of OAVS in which a lesion was excised from the ocular / orbital surface and correlate some of the features with some known associations of twins and congenital anomalies to support the common genetic developmental etiology theory of OAVS and twinning.

Results: An 8 year old girl with OAVS presented for excision of an ocular lesion. The excised tissue consisted of fibroadipose tissue, lacrimal glands, sebaceous glands, and stratified squamous epithelium consistent with a dermoid cyst. Interestingly, this patient had a history of several midline duplications, including double outlet right ventricle, nasal duplication, and a bifid tongue. The clinical history was also significant for facial asymmetry, cleft lip/palate, vertebral anomalies, and autism. Hearing was intact. No germline genetic variants were identified by karyotype or microarray analysis.

Conclusion: The presence of duplications of several midline tissues in this case argues for the common etiology theory of twinning and OAVS. Although the etiology of OAVS is unknown and is likely to be multifactorial (genes + epigenetic factors) there may be some predisposition to a developmental process that leads to midline duplications. This is particularly intriguing as there is a strong association with OAVS and twinning. Could it be possible that a similar process that leads to the duplication of structures in OAVS is responsible for an etiology of twinning? Furthermore, the ocular lesions in OAVS include dermoid cysts. These are neuroectodermal / ectodermal lesions in a neuroectodermal / ectodermal condition. Sacrococcygeal teratomas are an example of a somewhat similar lesion that already have an association with twinning, thus the presence of dermoid cysts in OAVS may be significant in regard to this discussion of an association with etiology of twinning, given that an association with OAVS and twinning already exists.

Two Cases of Rhabdomyomatous Mesenchymal Hamartoma: A Rare Entity

A Grover K Klement, J Jensen, L Lalor, K Wanat, K Young; Medical College of Wisconsin

Background: Rhabdomyomatous mesenchymal hamartoma (RMH) is a rare congenital tumor of the dermal and subcutaneous tissues, presenting as a midline, often pedunculated or sessile, papule on the head and neck. It was first described as “striated muscle hamartoma” by Hendrick et al. (1986) and there are only 67 cases reported in literature.

Methods: We report two cases of RMH here: one in a child with neurofibromatosis type 1 (NF1) and another as an isolated lesion in an infant.

Results: The first case is a 12-year-old male with autism and NF1 who presented with a 5-6 mm, slightly pink papule on his nose that was gradually increasing in size over 10 years. He underwent excision and histopathological examination showed skeletal muscle fibers admixed with mature adipose tissue, adnexal structures and neurovascular bundles in a haphazard manner compatible with a diagnosis of RMH. The other case is a 48-day-old male who presented with a 4 mm firm, solitary, non-tender, smooth, mobile nodule on the upper cutaneous lip lateral to the philtrum which was first noticed at birth. He underwent excision at 9 months of age with histopathology consistent with RMH. While RMH is a benign neoplasm, it may be associated with other congenital anomalies. The histologic differential diagnosis includes neuromuscular choristoma (also known as benign triton tumor), fetal rhabdomyoma, rhabdomyosarcoma, nevus lipomatosus superficialis and fibrous hamartoma of infancy.

Conclusion: Our cases highlight the importance of considering RMH in the differential diagnosis of congenital midline facial lesions with skeletal muscle differentiation.

Benign CTNNB1-Mutated Skeletal Muscle Tumor in a Male Infant

S Allen-Winters¹, S Koo²; ¹ University of Tennessee Health and Science Center, ² St. Jude Children's Research Hospital

Background: Benign tumors with skeletal muscle differentiation are rare, and their molecular features and immunohistochemical profile are poorly characterized. The Wnt/beta-catenin signaling pathway may play an important role in tumor development. Mutations in CTNNB1 have been previously implicated in the development of neoplasms with skeletal muscle differentiation, such as benign triton tumor/neuromuscular choristoma and fusion-negative rhabdomyosarcoma. We describe a case of a benign-appearing soft tissue tumor with skeletal muscle differentiation in an infant male, which was subsequently found to have a CTNNB1 mutation.

Methods: The patient presented with a palpable left foot soft tissue mass at one day of age. Magnetic resonance imaging was performed and showed a bilobed 3.1 x 2.5 x 2.7 cm mass that involved the lateral aspect of the foot, involving plantar and dorsal aspects and extending between metatarsals. Biopsies and subsequent debulking of the mass were performed over the course of the subsequent 6 months. Paired analysis of the tumor and comparator sample by whole genome, whole exome, and transcriptome sequencing was performed for the identification of germline and somatic variants.

Results: Histologically, the mass was composed of relatively mature-appearing skeletal muscle fibers with centrally located nuclei and prominent fibrous stroma, with occasional interspersed small nerve fascicles. There was no marked atypia, necrosis, or obvious histological features of malignancy. By immunohistochemistry, the tumor was diffusely positive for desmin and largely positive for myogenin and myoD1. Beta-catenin showed nuclear and membranous staining in a large subset of lesional cells. The Ki-67 proliferative index was 10% and PHH3 showed rare mitotic figures. Subsequent biopsies of the mass disclosed similar histological and immunohistochemical findings. Molecular analysis of the tumor and comparator sample identified a hotspot missense variant in CTNNB1 (p.T41I). No other medically meaningful sequence variants or gene fusions were identified in the tumor or germline. The patient is regularly monitored by MRI and shows no significant change in residual tumor four months after debulking.

Conclusion: We describe a case of a mature-appearing skeletal muscle neoplasm with CTNNB1 mutation in an infant with benign clinical behavior to date. The conjunction between the histological appearance, immunohistochemical staining profile, and molecular findings (CTNNB1 hotspot mutation) suggested a differential of rhabdomyoma, benign triton tumor/neuromuscular choristoma, and rhabdomyosarcoma. The relatively mature appearance of lesional skeletal muscle made a diagnosis of rhabdomyosarcoma unlikely; myogenin and myoD1 positivity is known to occur in developing and regenerating skeletal muscle as well as benign skeletal muscle tumors. Histologic features were most consistent with a benign tumor in the spectrum of fetal rhabdomyoma and benign triton tumor. Although CTNNB1 mutations

are commonly identified in rhabdomyosarcoma, they may also be identified in benign skeletal muscle tumors in young children.

Inflammatory leiomyosarcoma/histiocyte-rich rhabdomyoblastic tumor (ILMS/HRRMT) in the lung of an adolescent male

S Koo ¹, F Malik ²; ¹ St. Jude Children's Research Hospital, ² St. Jude Children's Research Hospital

Background: Histiocyte-rich rhabdomyoblastic tumor (HRRMT) is a distinctive rhabdomyoblastic neoplasm that morphologically and genetically overlaps with inflammatory leiomyosarcoma (ILMS). HRRMT usually presents in the extremities, is characterized by a dense histiocytic infiltrate intermixed with mildly pleomorphic spindled tumor cells that variably express skeletal muscle markers, and has a near-haploid genome. There are extremely rare reports of pulmonary tumors in young to middle aged adults with similar ILMS/HRRMT histology but with a non-rhabdomyoblastic/smooth muscle immunoprofile and diploid genome. We report a case of pediatric pulmonary ILMS/HRRMT.

Methods: A 15-year-old otherwise healthy male presented with cough and hemoptysis and was found on imaging to have a 6.2-cm mass in the right lower lobe of the lung. A right lower lobectomy was performed. Grossly, a 7.5-cm firm, bright yellow, circumscribed, lobulated mass was identified at the right lower lobe hilum undermining major bronchi. Immunohistochemistry, transcriptome sequencing, large gene sequencing panel, and copy number analysis by chromosomal microarray were performed.

Results: Histologically, the tumor was well-circumscribed and lobulated, pushing beneath the bronchial lining. It was comprised of fascicles of spindled and plump cells with pale eosinophilic, occasionally vacuolated cytoplasm resembling smooth muscle, with variable pleomorphism. Multinucleated Touton giant cells and small clusters of foamy histiocytes were scattered throughout the tumor with interspersed lymphocytes, eosinophils, and plasma cells. Mitoses were not readily identified. Immunohistochemical workup showed patchy positivity for desmin, cytokeratin CAM5.2, and cytoplasmic S100 in tumor cells. An extensive CD163, CD68, and Factor XIIIa-positive histiocytic infiltrate was present. SMA, myogenin, myoD1, SOX10, HMB45, Melan-A, CD1a, ALK, and BRAF V600E were negative. Transcriptome sequencing was negative for recurrent fusion transcripts. Gene sequencing panel and copy number analysis results are pending. The distinctive histologic appearance, rich histiocytic infiltrate, and desmin positivity supported a diagnosis of HRRMT but without a rhabdomyoblastic phenotype, similar to other reported cases in the lung.

Conclusion: We present an ILMS/HRRMT-like neoplasm in the lung of an adolescent male, which to our knowledge is the first case in this population. These tumors have indolent behavior, with complete excision curative for the reported cases. Awareness of the clinical presentation and characteristic histologic appearance of this tumor enables distinction from diagnostic pitfalls, including inflammatory myofibroblastic tumor, histiocytic neoplasm, or leiomyosarcoma. Additional molecular characterization, including copy number analysis (currently pending), will aid in further clarifying the relationship between ILMS/HRRMT-

like tumors of the extremity and lung.

Angiomatoid Fibrous Histiocytoma with ALK expression mimicking a lipoma, a case report.

M Shaheen J Davis, I González; Indiana University

Background: Angiomatoid fibrous histiocytoma (AFH) is a rare neoplasm predominantly occurring in the subcutaneous tissue of the extremity and is of an intermediate malignant potential. It has a wide age of presentation, but most cases occurred in the first two decades of life. Given its rarity, it can be a diagnostic challenge. Here we present an unusual case with diffuse and strong cytoplasmic ALK expression.

Methods: We describe a case of Angiomatoid fibrous histiocytoma (AFH) with ALK expression. Clinical, radiographic, operative and histopathologic data were retrospectively collected from the electronic medical records.

Results: An 8-year-old girl presented with a painless lump on her upper back. The mass was moveable and firm mimicking a lipoma on physical exam. Ultrasound demonstrated a 2.4 x 1.0 x 0.8 cm complex solid and cystic subcutaneous mass in the mid upper back, and intraoperatively the mass was subcutaneous and reaching the underlying fascia. Grossly, the mass had a lobulated yellow-gray cut surface. Sections showed a well-circumscribed lesion with a fibrous pseudocapsule and an accompanying dense lymphoplasmacytic infiltrate in a vaguely lobular pattern mimicking a nodal architecture; however, no sinuses were identified. These nodules were composed of ovoid histiocytoid tumor cells with scant to moderate eosinophilic cytoplasm and a vesicular nucleus with occasional prominent nucleoli. Several mitotic figures were seen including some atypical forms. At the periphery of the nodules some of the tumor cells had a more epithelioid-like appearance and focal pleomorphism. Rare areas of necrosis were also seen. Immunohistochemically, the tumor cells showed diffuse and strong cytoplasmic ALK staining and a weak membranous CD99 staining. EMA was positive in a subset of the epithelioid-like cells, and Desmin was focally and weakly positive. CD68, CD163, SMA, S100, AE1/AE3, CD20, CD3 and CD30 were negative in tumor cells.

Conclusion: The morphologic features and the immunohistochemical profile support the diagnosis of angiomatoid fibrous histiocytoma (AFH). ALK expression in AFH particularly with the antibodies D5F3 and 5A4 is well known and is an important potential diagnostic pitfall.

Early T-cell Precursor Lymphoblastic Leukemia Recurring with Substantial Antigenic Drift as an Adnexal Mass

C Sande ¹, S Bohling ², K Chisholm ²; ¹ Seattle Children's Hospital, ² Seattle Children's Hospital

Background: Early T-cell precursor lymphoblastic leukemia (ETP-ALL) is a subtype of T-lymphoblastic leukemia characterized by unique immunophenotypic and genomic features indicating early T cell differentiation. We report a 17-year-old female, who initially presented with ETP-ALL and later developed a T-cell neoplasm with dramatic antigenic drift, found to be clonally related to her original neoplasm.

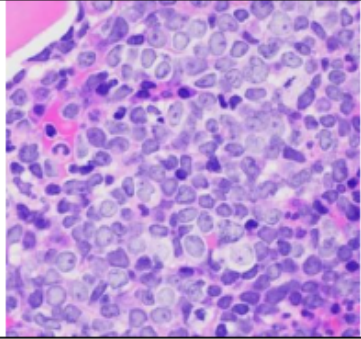
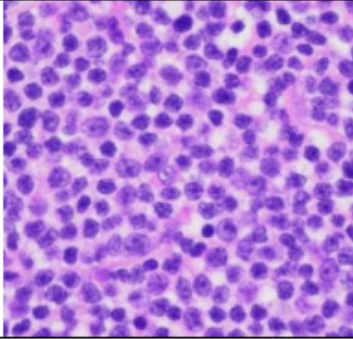
Methods: Diagnostic (blood and marrow) and relapse specimens (pelvic tumor) were evaluated. Testing modalities included routine H&E and immunohistochemical staining, flow cytometry, immunoglobulin (IGH) and T-cell receptor (TCR) clonality by next-generation sequencing (NGS), and NGS panel targeting malignancy associated genes.

Results: The patient presented with a 3-month history of progressive lymphadenopathy, fatigue, early satiety, and night sweats. Initial work-up revealed diffuse lymph node enlargement on CT, anemia, and leukocytosis with 70% circulating blasts. A bone marrow aspirate showed 90% involvement. Flow cytometry demonstrated the following immunophenotype for the blasts: cytoplasmic CD3+(dim), CD5+(partial), CD7+(bright), HLA-DR+(partial), CD11b+, CD33+(partial), CD2-, surface CD3-, CD1a-, CD8-, CD13-, CD117-, MPO-, and TdT-, supporting the diagnosis of ETP-ALL (see Table). She underwent treatment following Children's Oncology Group protocol AALL0434, achieving negative measurable residual disease (MRD) at mid consolidation. At 19 months, she presented with acute on chronic right lower quadrant pain. MRI showed an 8 cm solid mass adjacent to the right ovary, ascites, omental and sigmoid colon thickening, a soft tissue deposit along the rectosigmoid bowel, and bilaterally enlarged pelvic lymph nodes. Tissue biopsy showed a T-cell neoplasm with multiple immunophenotypic differences compared to her prior ETP-ALL: cytoplasmic CD3+, CD2+, CD7+(subset), CD8+(dim), CD56+(mildly increased), CD117+, HLA-DR-, CD11b-, CD33-, CD5-, surface CD3-, CD1a-, CD13-, MPO-, and TdT- (see Table). Staging bilateral bone marrow aspirates and core biopsies showed partial involvement by this population. Comparative TCR and IgH NGS clonality studies identified identical dominant TCRG (n=2) and IGH (n=1) sequences in both the patient's diagnostic bone marrow and subsequent adnexal mass, supporting relapse of her original disease with marked immunophenotypic changes. NGS identified the same NOTCH1, IL7R, and ETV6 mutations present at diagnosis as well as shared copy number variants (CNVs); several new mutations and CNVs were also identified in the pelvic mass (see Table), suggesting disease progression. Despite salvage chemotherapy and radiation, she ultimately succumbed to her disease 2.5 months after recurrence.

Conclusion: Given the marked differences in immunophenotype, the possibility of a second de novo T-cell neoplasm was considered. However, the genetic findings supported a

recurrence and progression of the patient's original ETP-ALL, demonstrating the potential for ETP-ALL to recur as a solid tumor with striking antigenic drift.

Table 1: Summary of Key Diagnostic Features

	Initial Presentation	Recurrence
Specimen	Blood and bone marrow	Adnexal mass
Bone marrow involvement	90% (right core biopsy)	30% (right core biopsy)
Morphology (H&E, 400x original magnification)		
Immunophenotype		
CD34	Negative	
CD38	Positive (Heterogeneous)	Positive (Uniform)
CD45	Positive (Dim)	Positive (Normal)
CD117	Negative	Positive
HLA-DR	Partial Positive (Heterogeneous)	Negative
TdT	Flow Negative; IHC Partial Positive	Negative
CD19	Partial Positive (Heterogeneous)	Negative
Cytoplasmic CD79a	Partial Positive (Heterogeneous)	Negative
CD1a	Negative	
CD2	Negative	Positive (Mildly Increased)
Surface CD3	Negative	
Cytoplasmic CD3	Positive (Dim)	Positive (Normal)
CD4	Negative	
CD5	Partial Positive (Heterogeneous)	Negative
CD7	Positive (Increased)	Partial Positive (Heterogeneous)
CD8	Negative	Positive (Dim)
CD56	Negative	Positive (Mildly Increased)
TIA1	Negative	Positive
CD11b	Positive (Heterogeneous)	Negative
CD13	Negative	
CD33	Partial Positive (Heterogeneous)	Negative
Cytoplasmic MPO	Negative	
NGS (Pathogenic)	<p><i>NOTCH1</i> p.V1721M <i>NOTCH1</i> p.S2329Efs*25 <i>IL7R</i> p.S246delinsKRGR <i>ETV6</i> p.R418G</p>	
		<p><i>ATM</i> p.L427* <i>PMS2</i> c.2174+1G>A</p>
NGS (CNV)	<p>Loss of portions of 1p, 6p, 7q (<i>EZH2</i>), 8q, 9p (homozygous <i>CDKN2B</i> and portion of <i>CDKN2A</i>), 12p (<i>ETV6</i>), 21q (last 2 exons of <i>RUNX1</i>)</p>	
	Loss of portion of 7p (single copy majority of <i>DHAC9</i>)	<p>Loss of portion of 7p (biallelic majority of <i>DHAC9</i> plus more telomeric genes); Loss of portions of 4q (<i>PDGFRA</i>, <i>KIT</i>) and 5q; Gain of 11p (<i>HRAS</i>, <i>CDKN1C</i>), 15, 17q (<i>STAT5B</i>)</p>
Clonality testing	Identical <i>TCRG</i> and <i>IGH</i> clones	

Chronic granulomatous disease with abnormal RBCs: a manifestation of contiguous genomic deletion

N Uddin ¹, A Sengupta ², J Park ², C Wysocki ³; ¹ Department of Pathology, University of Texas Southwestern Medical Center / Children's Health, Dallas, Texas, ² Department of Pathology, University of Texas Southwestern Medical Center / Children's Health, Dallas, Texas, ³ Department of Pediatrics, University of Texas Southwestern Medical Center / Children's Health, Dallas, Texas

Background: We describe a rare case of primary immunodeficiency with abnormal red blood cells (RBCs). Genomic testing revealed a single underlying genomic etiology that guided the management and established the prognosis.

Methods: The patient was a 2-year-old male. He presented initially with recurrent perianal abscesses and a fistula for which he received surgical treatment. Prior to his current presentation his only other medical issue was an ear malformation. 13 months after his surgical treatment for the fistula, he was admitted with daily fever and progressive cervical lymphadenopathy. His mother reported that for the last year he had fevers 1-2 times per month, facial rash, and mouth blisters; these symptoms lasted a week each time. Symptomatic management had been provided. His current presentation was notable for bilateral cervical lymphadenopathy confirmed by CT scan. All infectious disease evaluations (EBV and CMV PCRs, and blood cultures) were negative. Of note, his CBC showed acanthocytes. Excisional biopsy of a left cervical lymph node was performed, and a primary immunodeficiency workup was initiated. A 527 gene panel for immunodeficiencies and cytopenia was obtained. A chromosomal microarray (CMA) was also performed as part of the genetic evaluation.

Results: The lymph node showed necrotizing granulomatous inflammation. All special stains for infectious agents were negative, as were microbial cultures. The immunological workup showed an abnormal neutrophil oxidative burst test. The gene panel showed hemizygous deletion of the entire CYBB gene. CMA demonstrated a pathogenic, 1.118 Mb, hemizygous interstitial Xp21.1p11.4 deletion involving PRRG1, XK, CYBB, and DYNLT3 genes [arr[GRCh37] Xp21.1p11.4(36,734,682_37,853,020)x0]. This deletion involved the entire XK and CYBB genes, as a contiguous gene deletion. Subsequently, blood group testing showed K (kell) negative blood group. Taken together, these findings are consistent with McLeod syndrome associated with X-linked chronic granulomatous disease (CGD).

Conclusion: CGD is a disorder of the NADPH oxidase system resulting in phagocyte functional defects due to inability to generate superoxide anion. It manifests as recurrent bacterial and fungal infections. Most commonly (> 66%) it is due to X-linked CYBB gene (at Xp21.1) aberrations. CGD can also be autosomal recessive. McLeod Syndrome is due to XK gene (at Xp21.1) variants; it is characterized by the absence of the red blood cell Kx antigen, weak expression of Kell antigens, acanthocytosis, elevated serum creatine kinase levels, compensated hemolysis, and late onset neuropsychological symptoms. Xp21.1p11.4 is a gene rich region and can be involved in contiguous gene deletions which can manifest depending

on the genes involved. Only 7 cases have been reported so far. The management and prognosis depend on the genes involved. Our patient is receiving prophylactic antibiotics and undergoing a workup for bone marrow transplant. To mitigate the risk of hemolysis, which may occur with peri-transplant transfusion of K⁺ RBCs, autologous RBC units are being collected prior to the bone marrow transplant. The XK deletion increased the complexity of bone marrow transplant for this patient. He does not have any neurological symptoms yet.

Pediatric papillary thyroid carcinoma with STRN::ALK fusion with morphologic features suggestive of cribriform-morular carcinoma: a rare diagnostic challenge

K Wang J Shabbir, F Balarezo, K Glomski; Hartford Hospital

Background: Papillary thyroid cancer (PTC) is the most prevalent endocrine tumor in children. Although pediatric PTC cases are more likely to present with larger tumors, regional lymph nodes and/or distant metastases compared to adult patients, they carry a better prognosis. Genetic sequencing advancements have revealed several genetic alterations considered “driver mutations” in pediatric thyroid carcinoma. While most cases of thyroid carcinoma demonstrate alterations in RET and BRAF genes, other genetic lesions have been described. This report presents one of the youngest patients diagnosed with papillary thyroid carcinoma carrying a rare STRN::ALK fusion, which also demonstrates cribriform-morular features and presents a diagnostic and management challenge.

Methods: Patient clinical information was extracted from electronic medical record, and the immunochemistry (IHC) stainings and molecular testing were performed following standard protocols.

Results: A 6-year-old female presented with gradually enlarging neck mass over 6 months with occasional pain. The mass was tender and firm on palpitation. Initial thyroid function tests revealed increased TSH level, while free T4 was normal. Thyroid ultrasound revealed a lobulated, solid, vascular and heterogeneous mass measuring up to 2.9 cm in the anterior cervical midline, with microcalcifications and bilateral cervical lymphadenopathy. Surgical resection of the neck mass revealed cribriform, papillary, solid and trabecular areas with squamoid morules. Focal classical PTC features were observed. IHC studies showed positive TTF1 and PAX8, and negative CDX2 for tumor cells. Cells in the squamoid morules were p63 positive, raising a morphologic differential of cribriform morular PTC (CM-PTC). However, beta-catenin IHC, typically observed in a nuclear pattern within CM-PTC, was not present. Genetic analysis revealed a STRN::ALK fusion. Due to the high risk of recurrence associated with STRN::ALK fusion, the patient received radioiodine therapy, with no recurrence observed 13 months since the initial diagnosis. In the absence of an APC mutation (typically identified in CM-PTC), screening colonoscopy was not recommended.

Conclusion: ALK fusions-driven thyroid cancers are rare and are associated with more aggressive clinical behavior. STRN::ALK fusions are more common in poorly differentiated thyroid carcinomas compared to the EML4::ALK fusion. In light of this, FISH utilizing ALK break-apart probes may show limitations in predicting clinical behavior (and arguing for NGS Fusion assay utilization). ALK inhibitors have shown therapeutic benefits in other types of cancer driven by ALK fusions, which may be considered in the setting of recurrence. This case represents one of the youngest reported STRN::ALK PTC and raises the potential morphologic overlap with CM-PTC, a mimic with important clinical implications.

A case of congenital disseminated malignant rhabdoid tumor, mimicking a vascular lesion

K Wang F Balarezo; Hartford Hospital

Background: Malignant rhabdoid tumor (MRT) is a rare and aggressive tumor primarily affecting children under 3 years of age. It typically occurs in the central nervous system (CNS, ~65%) and kidney (~35%); cases in various soft tissue sites have been reported. Due to its rarity and aggressiveness, the overall survival rate remains below 50%. Here we present a case of congenital MRT of the right forearm clinically thought to represent a congenital vascular lesion.

Methods: Patient clinical information was extracted from electronic medical record, and the immunochemistry (IHC) stainings and molecular testing were performed following standard protocols.

Results: During prenatal ultrasound at 37-1/7 week gestation, the baby was found to have a right forearm soft tissue mass not present in prior exams. Clinically and radiologically, it was thought to represent a vascular lesion. The baby was delivered via Cesarean section, and MRI revealed an 8.7 cm heterogeneous mass enveloping the radius and ulna, along with multiple lesions in the liver. No lesions were seen on CNS or kidneys. Subsequently, the forearm mass was resected. Histologically, the lesion exhibited polygonal cells with eosinophilic cytoplasm, large eccentric nuclei, prominent nucleoli, necrosis, moderate pleomorphism and high mitotic rate. IHC showed loss of INI-1 nuclear expression in tumor cells. Additionally, the tumor cells were positive for EMA and CD56, with a few CK AE1/3 and SALL4-positive cells. Desmin, myogenin, CD34, S100, chromogranin, synaptophysin and TFE3 were negative; SMARCA4 and H3K27 were retained. Based on morphology and IHC, the diagnosis of extrarenal MRT was established, and confirmed by NGS showing SMARCB1 gene deletion. Placental examination showed no involvement by MRT. The differential diagnosis based on clinical/radiologic findings included epithelioid hemangioendothelioma (EHE) and epithelioid angiosarcoma. Both entities are positive for endothelial markers such as CD34. Histologically, EHE is composed of medium-sized epithelioid cells and spindled endothelial cells, within myxohyaline stroma. Epithelioid angiosarcoma, a variant of angiosarcoma, displays round/polygonal epithelioid cells with abundant eosinophilic cytoplasm, vesicular nuclei, and prominent nuclei. Most cases of EHE are characterized by WWTR1-CAMTA1 gene fusion, and angiosarcomas show genetic heterogeneity.

Conclusion: Congenital MRT is an aggressive malignancy with a poor prognosis, often considered a fatal disease. Most MRT involve SMARCB1 or SMARCA4 mutation, which is necessary for diagnosis according to the new WHO classification. Differentiating MRT from other soft tissue sarcomas poses challenges, underscoring the importance of histopathology and IHC in conjunction with clinical and radiologic findings. Given the rarity of MRT, its poor prognosis and need for prompt treatment, we present this case of congenital

disseminated MRT to contribute to the case pool for future mechanistic studies.

Vein of Galen Malformation: An In-Depth Analysis through Autopsy Findings

J Suddock¹, M Harrell², P Zamiara², C Guardado³, A Dharmadhikari², J Ji², J Cotter², L Wang², D Hawes²; ¹ University of Southern California/Los Angeles General Medical Center, Los Angeles, CA, ² Children's Hospital Los Angeles, Los Angeles, CA, ³ Valley Children's Hospital, Fresno, CA

Background: Vein of Galen malformations (VOGMs) are uncommon vascular anomalies of venous channels responsible for draining cerebral blood. These aneurysmal dilations, characterized by direct connections of arteries to the venous system, typically originate during embryogenesis, leading to a complex pathophysiologic state. Therapeutic interventions, such as coil embolization, aim to occlude anomalous vascular connections and ameliorate aberrant hemodynamics. Autopsy findings hold significant value, providing insights into the pathophysiology of VOGMs and contributing to a more refined understanding of the underlying mechanisms and potential therapeutic targets.

Methods: A consented, unrestricted autopsy was conducted on a three-month-old boy with a coil embolized VOGM, cardiac failure, and persistent pulmonary hypertension. The autopsy encompassed external and internal examinations and was supplemented by a dedicated neuropathologic assessment of the formalin-fixed brain and spinal cord. Chromosomal microarray analysis was performed and interpreted on an antemortem peripheral blood sample.

Results: External examination revealed anomalous features including cleft lip, hypertelorism, and congenital dermal melanocytosis. Internal examination disclosed myocardial fibrosis, cardiac biventricular and bi-atrial dilation, and asymmetric bi-ventricular and interventricular septal hypertrophy. Patent foramen ovale and patent ductus arteriosus were also present. The lungs exhibited intra-alveolar hemorrhage, arterial hypertrophy, and hemosiderin-laden macrophages, consistent with persistent pulmonary hypertension. Other findings included hepatomegaly, splenomegaly, and ascites. Neuropathologic examination revealed an intact VOGM with coil embolization, accompanied by marked cerebral vascular congestion and hydrocephalus. Antemortem chromosomal microarray detected an 849kb copy number gain of uncertain significance in chromosomal region 8p23.2, partially involving the 3' end of the CSMD1 gene.

Conclusion: The autopsy findings are congruent with a diagnosis of VOGM. The high-flow state of the malformation and the resulting vascular congestion likely induced cardiac dilation, hypertrophy, and persistent pulmonary hypertension, making the heart prone to failure. Hydrocephalus emerged from increased venous pressure and altered blood flow, which disrupted the balance of cerebrospinal fluid production and absorption, a condition further exacerbated by physical obstruction of the VOGM at the aqueduct. Additionally, the detected copy number gain in 8p23.2, involving CSMD1, offers compelling molecular insights. Genetic variants involving CSMD1 have been linked to variable neurodevelopmental conditions; however, the association's precise nature in the context of

VOGM remains an area for continued exploration.

Blue Rubber Bleb Nevus Syndrome with Multisystem Organ Involvement: A Case Report and Immunohistochemical Characterization

P Rungsiprakarn ¹, D Adams ², A Britt ², A Dewitt ², A Viaene ², L Finn ², L Surrey ², P Kreiger ²; ¹ Children's Hospital of Philadelphia, ² Children's Hospital of Philadelphia

Background: Blue rubber bleb nevus syndrome (BRBNS) is a rare venous malformation syndrome involving skin, gastrointestinal tract (GI), and other organs caused by somatic mutations in TEK (TIE2). Aberrant immunohistochemical (IHC) expression of lymphatic endothelial markers (D2-40 and Prox-1) within malformed veins in BRBNS has been previously described in cutaneous, GI, and hepatic sites. We describe a case of a neonate with extensive cutaneous and multisystem organ involvement (GI, heart, brain, oropharynx, bladder) with immunohistochemical characterization by site.

Methods: Clinical information was obtained by standard chart review. Pathology reports, genomic reports, histologic and IHC sections were reviewed.

Results: A 33-week gestational age neonate was born with a prenatally diagnosed enlarging cardiac mass and multiple blue-hued cutaneous lesions. Biopsy of the left foot lesion at 1 day of age showed thin-walled engorged vascular channels consistent with venous malformation. At 2 weeks of age, cardiac mass resection was performed due to mass effect and impaired cardiac output. Operatively, the vascular mass was attached to the anterior and lateral epicardial surfaces of the left heart. Histologic examination showed variably sized vessels with variably thin to thick walls containing fibrous tissue and smooth muscle, consistent with venous malformation. The patient expired post-operatively since the remaining myocardium was severely dysfunctional leading to hypotension. Autopsy revealed venous malformations involving skin (scalp, face, chest, back, extremities, abdomen, ventral left foot), brain, heart, oropharynx, small and large bowel, and bladder. Immunohistochemistry showed vascular lesions to be uniformly CD31 positive and D2-40 negative; Prox-1 was only expressed in cutaneous lesions. CD34 expression was diffuse in the heart lesion and present in a subset of vessels (variable) at other sites (Table 1). Genomic testing of the patient's left foot tissue showed two pathogenic somatic variants in cis within TEK c.[2690A>T; 2753G>A], p.[Tyr897Phe; Arg918His]. No variants were identified in the blood sample.

Conclusion: We report a pediatric case of BRBNS with severe multisystem organ involvement. Although aberrant lymphatic endothelial expression has been reported in BRBNS at cutaneous, gastrointestinal, and hepatic sites, we found it only in cutaneous lesions. This attests to the variability of the disorder and demonstrates that aberrant lymphatic endothelial immunohistochemical expression is not a means to distinguish BRBNS from other venous malformations at visceral sites.

Sites	CD31	CD34	D2-40	Prox-1
Brain	Pos	Variable	Neg	Neg
Heart	Pos	Pos	Neg	Neg
Skin, subcutis	Pos	Weak to Neg	Neg	Pos
Skin, dermis	Pos	Weak to Neg	Neg	Weak to Neg
Oropharynx	Pos	Variable	Neg	Neg
Small intestine	Pos	Variable	Neg	Neg
Large intestine	Pos	Variable	Neg	Neg
Bladder	Pos	Weak to Neg	Neg	Neg

Pediatric Angiosarcoma Masquerading as a Lymphatic Malformation in an Autopsy Case: A Rare Case Providing Insight Into Possible Etiologies for Disease Natural History

J Pierce J Goldstein, Y Shui; UCLA

Background: The patient was a 10 year-old male with no significant past medical history who presented to an outside urgent care clinic for evaluation of new onset difficulty breathing. Based on similar symptoms in siblings an infectious etiology was initially diagnosed. The patient's symptoms continued to worsen despite antibiotic therapy. He was eventually taken to an outside hospital where a pleural effusion was identified. A therapeutic thoracentesis revealed a chylous effusion. Further imaging for lymphatic leaks revealed what appeared to be a posterior mediastinal lymphatic anomaly. Subsequently the patient continued to have high volume bloody effusions and was sent to UCLA for higher level of care. Despite high level ICU care and multiple thoracic duct glue embolization procedures, the patient continued to have very large bloody chest tube output. The patient experienced multiple organ system failure and passed away after a lengthy hospital stay . The parents consented to a full medical autopsy.

Methods: The pediatric autopsy was performed following UCLA protocol. Multiple immunostains were performed by the UCLA immunohistochemistry lab including CD68, Keratin AE1/3, CD1A, Langerin, CD31, CD34, ERG, Fli-1, D2-40, S100, CD45, PU.1, Ki67, Myogenin, MyoD1, HHV8, CD3, CD19, cKIT, TdT, and CD30. In house Pan-cancer panel NGS sequencing was performed on Formalin Fixed, Paraffin-Embedded (FFPE) tissue by the UCLA molecular pathology laboratory using tumor and matched normal (liver).

Results: Autopsy examination revealed a diffusely infiltrative, non-mass-forming, process in the thorax which initially was masked by, and mimicked, severe hemothorax. The process was found to involve both hilar regions of the lungs, trachea, bronchi, pericardium, thymus, distal esophagus, diaphragm and posterior mediastinum including the embolized thoracic duct and ligamentum flavum. Additional discoloration was seen on the serosa of the sigmoid colon and in the grey white matter junction of the brain. Microscopic evaluation of the lesion revealed a diffusely infiltrative process composed of epithelioid cells with high nuclear to cytoplasmic ratio, nuclear pleomorphism, large nucleoli, and frequent mitotic forms including markedly atypical figures. Architecturally the cells ranged from discohesive to vaguely vascular in pattern with extravasated red blood cells as a common finding. Perineural invasion was another common finding at multiple sites. Brain and colonic metastasis were present. Use of immunohistochemistry reveal the cells to be vascular in origin (CD31, Fli-1, ERG, and D2-40 positive) with a high ki-67 proliferation index. In-house molecular testing revealed a somatic NF1 mutation.

Conclusion: This case represents an extremely rare pediatric case of widely metastatic epithelioid angiosarcoma arising from or mimicking a central lymphatic vascular malformation. The diagnosis was made at autopsy and represents an unusual presentation of

this tumor which usually manifests which cutaneous or mass forming lesions which allow for diagnosis and treatment. The unknown etiology of this lesion presents opportunity for discussion of conditions such as Stewart-Treves Syndrome and reports of angiosarcoma developing in pediatric patients in the setting of neurofibromatosis.

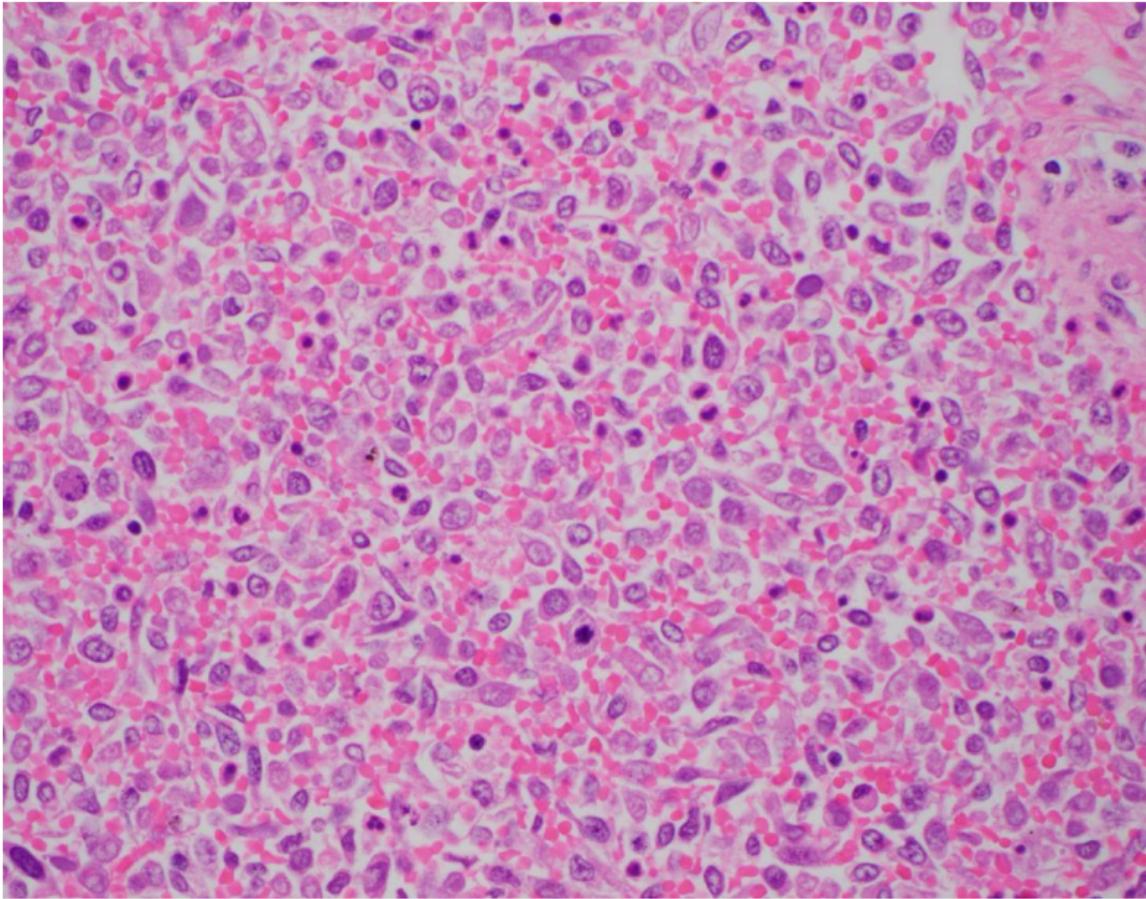


Figure 1: Lesional cells involving the mediastinum. Discohesive epithelioid cells with high N:C ratio, nuclear pleomorphism, frequent atypical mitosis and karyorrhectic debris in a background of extravasated RBCs mimic a leukemic infiltrate.

A Novel TEK::GAB2 Gene Fusion identified in a Pediatric Angiosarcoma of Soft Tissue

Z Sandoval ¹, J Bhutada ², B Pawel ², R Schmidt ², N Shillingford ², L Wang ², M Warren ², S Zhou ²; ¹ Baylor College of Medicine, Children's Hospital Los Angeles, ² Children's Hospital Los Angeles

Background: Angiosarcoma is a rare malignant vascular neoplasm that predominantly affects adults and the elderly, with exceedingly rare occurrences in children. Angiosarcomas exhibit genetic heterogeneity, often characterized by complex karyotypes. Upregulation of genes associated with angiogenesis and vascular-specific receptor tyrosine kinases, such as TEK, is commonly observed. Additionally, a subset of cases, typically found in younger patients, is linked to CIC gene abnormalities. The GAB2 gene encodes an intracellular adaptor protein that functions downstream of tyrosine kinase receptors in signal transduction, transmitting signals to downstream signaling pathways upon ligand binding to surface receptors. GAB2 has been identified as an oncogene in various cancer types.

Methods: The tumor samples were subjected to microscopic examination using H&E staining and immunohistochemical analysis. Ancillary techniques such as chromosomal microarray, targeted next-generation sequencing (NGS) panel (OncoKids), and exome capture RNA sequencing analysis for the detection of gene fusions were employed.

Results: A previously healthy 17-year-old female presented with acute onset left hip pain. MRI revealed a 22 cm heterogeneously enhancing mass, likely originating from the left iliacus muscle, extending through the left femoral canal, and involving the left iliopsoas muscle. Histologic examination of the tumor biopsy demonstrated an infiltrative, hemorrhagic tumor composed of areas of vasoformative proliferation exhibiting ramifying channels lined by atypical spindle to epithelioid cells with abundant eosinophilic cytoplasm, alternating with sheet-like arrangements of atypical spindle to epithelioid cells in a fibromyxoid background. Mitotic activity was increased. Multiple foci of tumor necrosis and hemorrhage were identified. Tumor cells were strongly positive for CD31, CD34, phosphorylated S6 ribosomal protein (p-S6RP) and cyclin D1, weakly to moderately positive for TFE3, and negative for AE1/AE3, EMA and Glut-1. Chromosomal microarray analysis did not reveal any pathogenic copy number aberrations, and the OncoKids panel showed no clinically significant variants. Further investigation using RNA sequencing identified a novel in-frame gene fusion between the TEK and GAB2 genes, which was confirmed by RT-PCR followed by Sanger sequencing. This fusion event resulted in a hybrid fusion protein encoded by the 5' portion of the TEK gene (exons 1-22 of 23 total exons) and the 3' portion of the GAB2 gene (exons 6-10 of 10 total exons). This recombination protein is likely a driver molecule contributing to tumorigenesis in this particular tumor.

Conclusion: To the best of our knowledge, the TEK::GAB2 gene fusion has not been previously reported in angiosarcoma or other tumors. Our study expands the molecular spectrum of pediatric angiosarcoma, shedding light on the involvement of this fusion in

tumorigenesis.

DNA Methylation Profiling Using Diff-Quik Stained Touch Preparation Slide Resolves Diagnostic Dilemma in Pediatric Sarcoma Case With Limited Diagnostic Material

I Gelarden¹, P Chou²; ¹ Lurie Children's Hospital, ² Lurie Children's Hospital

Background: Pediatric sarcomas represent a heterogeneous group of neoplasms often showing overlapping morphologic, immunophenotypic, and molecular features, which can present diagnostic challenges. DNA methylation profiling of brain and soft tissue tumors has recently led to the discovery of distinct entity-specific methylation signatures, which have been diagnostically useful in confirming or resolving challenging or equivocal diagnoses. While methylation profiling is promising technology, it comes with specific challenges specifically from limited specimens.

Methods: We present a challenging case of a pediatric sarcoma sent to us for consultation. The patient is a 19-year-old female with no significant past medical history who presented with a 7.5 cm mass within the left semitendinosus and biceps femoris muscles. Ultrasound core needle biopsy was performed at an outside institution with rapid onsite evaluation using touch preparations of core needle biopsy material. Routine H&E and immunohistochemical stains were performed. These include cytokeratin AE1/AE3, Desmin, S100, and INI-1. No additional formalin-fixed, paraffin embedded tissue remained for ancillary testing. A touch preparation slide was sent for DNA methylation profiling using a validated-microarray-based test.

Results: Histologic sections demonstrated a malignant neoplasm composed of sheets of rhabdoid to epithelioid cells with abundant eosinophilic cytoplasm, eccentric nuclei, and prominent nucleoli in a background of hemorrhage and necrosis. Tumor cells were diffusely AE1/AE3 positive with patchy positivity for S100. Desmin was negative, and INI-1 showed loss of nuclear expression. A diagnosis of INI-1 deficient malignancy was made with differential including proximal type epithelioid sarcoma, myoepithelial carcinoma, and extrarenal malignant rhabdoid tumor. Due to the strong S100 positivity, a diagnosis of myoepithelial carcinoma was favored. Methylation profiling revealed the highest probability of epithelioid sarcoma methylation class with a score of 0.61, with unsupervised clustering analysis (t-SNE) showing closest distance to epithelioid sarcoma methylation class with 2.473. When using the separate DKFZ classifier (Koelsche et al) a score of 0.99 was obtained. Overall, the findings confirmed the diagnosis of epithelioid sarcoma.

Conclusion: Classification of pediatric sarcomas can be difficult. Epithelioid sarcoma classically does not show S100 positivity by immunohistochemistry. Rare cases reported with this immunophenotype usually show only weak positivity. Because a subset of myoepithelial carcinomas can also demonstrate loss of nuclear INI-1 immunopositivity, resolving this differential diagnosis can be challenging if not impossible without ancillary studies such as methylation profiling. In cases where other diagnostic material is exhausted, cytology preparation slides can be used to obtain genetic material for important ancillary studies.

Heterotopic Mesenteric Ossification: A Rare Entity...For How Long?

K Liu L Parsons; Medical College of Wisconsin

Background: Firearm-related injuries in the pediatric population have significantly increased in recent years. With this increase and the associated surgical interventions/complications, pediatric pathologists are likely to encounter entities that are important to recognize as benign. Heterotopic mesenteric ossification (HMO) - the abnormal formation of benign bone tissue within the mesentery – is one such entity. First described in 1983, about 75 cases have been reported with only a handful in patients under 18 by an unknown mechanism. HMO often presents as a small bowel obstruction or is discovered incidentally. It may be morphologically concerning for osteosarcoma; therefore, recognizing this entity as benign is crucial. With increasing pediatric injuries related to gun violence, is HMO going to be more frequently encountered? We report a case of HMO in a pediatric patient to raise awareness of this entity and its management challenges.

Methods: A 16-year-old male with no medical history presented to the hospital after a gunshot wound to the abdomen. They underwent emergency surgery to repair his colon. Three weeks later, he underwent abdominal closure and ileostomy revision with a portion of small bowel submitted to us.

Results: Gross examination revealed a small segment of bowel and a 1.2 cm tan, semi-firm mesenteric area. Microscopically, the area displayed bone formation with surrounding osteoblasts at the periphery within the mesenteric soft tissue (figure 1), consistent with HMO.

Conclusion: HMO is abnormal formation of benign bone tissue within the mesentery. Patients are mostly male, have a history of previous surgery and/or trauma, and often present with symptoms of small bowel obstruction or it is discovered incidentally. Less than 5 cases are in pediatric patients. The exact mechanism is unknown, but is thought to be a reactive phenomenon. It has occurred 11 days to up to 30 years after the initial surgery/injury. Surgery is the treatment for symptomatic patients, though recurrence has been reported. Prophylaxis with diphosphonates and radiation therapy have been tried with unclear success. Due to its rarity, the diagnosis requires a high index of suspicion. Radiologists may mistake the ossification as an oral contrast leak for example. An awareness of this condition could prevent a missed diagnosis and inappropriate management. Clues for the pathologist include a gritty sensation while sectioning. HMO may have concerning features such as frequent mitotic figures. However, a lack of nuclear atypia and atypical mitotic figures should favor a diagnosis of HMO. Our case is a classic presentation of a rare entity in a pediatric patient after firearm trauma and surgery. A grossly visible semi-firm area was a clue for HMO and was confirmed on histology with reactive bone formation without atypical features (figure 1). Due to the potential of delayed presentation and recurrence, further research should follow-up on previously attempted prophylaxis. If HMO is suspected, the clinical team needs to be aware of its long-term complications, treatment, and potential prophylaxis. With the increase in firearm-related injuries in the pediatric population, HMO may become increasingly

common, which provides increased incentive for recognition of this entity.

